Physics – Uspekhi **43** (5) 453 – 491 (2000)

REVIEWS OF TOPICAL PROBLEMS

PACS numbers: 36.40.Vz, 36.40.Wa, **61.46.+w**, **85.42.+m**

Cluster plasma

B M Smirnov

DOI: 10.1070/PU2000v043n05ABEH000722

Contents

Abstract. Properties of cluster plasma are considered, the term implying that clusters and small particles present in a plasma are involved in effective growth and evaporation processes. Instability against such processes arises both in uniform and nonuniform cluster plasmas. The charging of clusters and small particles is analyzed. The properties of an arc plasma are studied along with cluster nucleation and radiation processes proceeded in it. Arc plasma presents an opportune medium for the transformation of an atomic vapor into a cluster beam, and cluster plasma is also an effective light source. Methods for cluster beam generation are presented and a cluster generation technique using afterglow plasmas is discussed. Relaxation, cluster charging, electric and transport processes in an afterglow cluster plasma are analyzed.

1. Introduction

A plasma with a disperse phase is a weakly ionized gas containing small particles or clusters, with the latter being capable of influencing some properties of the plasma. Such a plasma may be divided into several types including aerosol plasma, dusty plasma and cluster plasma. Aerosol plasmas exist in the Earth's atmosphere, and the properties of these plasmas differ depending on the altitude above the Earth's surface and the character of particle formation [1, 2]. At low altitudes, charged particles in the atmosphere are formed from atmospheric mist, from dust transported from the Earth's surface, and may be products of chemical and combustion processes on the Earth's surface. Because these particles can be charged, they determine the atmospheric conductivity, and therefore influence electric phenomena in the Earth's atmosphere.

Particles of dusty plasma are stable and their charge is usually determined by electron and ion attachment processes, so that these particles are negatively charged. An example of a dusty plasma is an ionized gas which is formed in the channel of a magnetohydrodynamic generator using a solid fuel. Then soot particles are present in the products of combustion, and they can be ionized due to the high temperature or may acquire a negative charge due to attachment of electrons. The charge of soot particles can be used for extracting them from the flow of gaseous products of combustion. Dusty plasma is observed in interstellar clouds; it is produced in the course of star and planet formation, and also as a result of the interaction of planetary rings with planetary magnetospheres, as occurs with Jupiter, Saturn and Uranus [3 – 5]. Sometimes a laboratory dusty plasma is called 'colloidal plasma' [5] by analogy with liquid colloids. In this case particles may contain the total negative charge of the plasma [5, 6]. An example of a laboratory dusty plasma is provided by the 'dusty plasma crystals' that arise when stable negatively charged particles are trapped by radio-frequency or glow gas

B M Smirnov Institute for High Temperatures, Russian Academy of Sciences, Izhorskaya ul. 13/19, 127412 Moscow, Russian Federation
Tel. (7-095) 190 42 22
E-mail: smirnov@orc.ru

Received 18 January 2000, revised 21 February 2000
Uspekhi Fizicheskikh Nauk **170** (5) 495 – 534 (2000)
Translated by B M Smirnov; edited by A Radzig

discharges and form crystal structures there, giving rise to specific phenomena in the dusty plasma [5, 7–15]. Such a dusty plasma is of fundamental interest for the following reasons. Firstly, study of the self-organization of this plasma, giving rise to the formation of a dusty-plasma crystal, widens our understanding of self-organizing systems and allows us to model some phenomena in such systems, in particular, phase transitions. Secondly, the negative charge of solid dielectric particles in this plasma reaches 10^3-10^6e [13–15], where e is the electron charge. Due to the giant charge of dielectric particles, the condition of strong coupling may be realized in this plasma in spite of the large distances between particles. This allows one to use this plasma for modelling a plasma with strong coupling (or nonideal plasma) [16, 17].

In contrast to a dusty plasma, the particles or clusters of a cluster plasma under consideration can be destroyed or formed in processes involving their atoms [18]. In particular, in the case when clusters are charged, like cluster charges do not allow contact between clusters in the course of their evolution. Hence, the processes of cluster growth and destruction are determined by processes involving vapor atoms and proceed according to the scheme

$$\mathrm{M}_n + \mathrm{M} \longleftrightarrow \mathrm{M}_{n+1}\,, \tag{1.1}$$

where M is a metal atom, and M_n is a cluster consisting of n atoms.

A charge of the cluster in a gas-discharge plasma can be either positive or negative depending on the processes which establish the charge equilibrium in the plasma. In order to increase the cluster charge, a unipolar plasma from a corona discharge is used. In this review we shall consider the properties of a quasi-neutral cluster plasma.

2. Properties of cluster plasma

2.1 Cluster instability in a homogeneous vapor

We use the liquid drop model for a liquid cluster, so that the cluster is assumed to be similar to a spherical liquid drop with the density of a macroscopic system. Within the framework of this model, the rate constant of atom attachment to a cluster surface is equal to [19]

$$v_n = Nv\sigma_n\,, \tag{2.1}$$

where N is the atom number density, v is the average atom velocity, and σ_n is the cross section of atom attachment to a cluster consisting of n atoms. If we assume that each contact of an incident atom with the cluster surface leads to attachment, this cross section is $\sigma_n = \pi r_n^2$, where $r_n = r_{\mathrm{W}} n^{1/3}$ is the cluster radius, and r_{W} is the Wigner–Seitz radius. In this approximation, formula (2.1) takes the form

$$v_n = Nk_0\, n^{2/3}\,, \qquad \text{where} \qquad k_0 = \sqrt{\frac{8T}{\pi m}}\,\pi r_{\mathrm{W}}^2\,. \tag{2.2}$$

Here T is the gaseous temperature, and m is the atomic mass. Values of the parameters r_{W} and k_0 for some elements are given in Table 1.

Let us analyze the equilibrium of a cluster with an atomic vapor, assuming that the properties of the cluster surface are similar to those of the surface of a corresponding macroscopic system. The equilibrium near the latter surface occurs at the saturation vapor pressure when the atom number density is equal to $N_{\mathrm{sat}}(T)$, where T is the vapor temperature. The temperature dependence of this quantity has the form

$$N_{\mathrm{sat}}(T) \sim \exp\left(-\frac{\varepsilon_0}{T}\right),$$

where ε_0 is the binding energy for surface atoms. The identical equilibrium for a cluster leads to the following expression for the atom evaporation rate v_{ev}^n from the surface of a cluster consisting of n atoms [19, 20]:

$$v_{\mathrm{ev}}^n = v_n\,\frac{N_{\mathrm{sat}}}{N}\,\exp\left(-\frac{\varepsilon_n - \varepsilon_0}{T}\right), \tag{2.3}$$

where ε_n is the binding energy for surface cluster atoms. In fact, this relation expresses the principle of detailed balancing

Table 1. Parameters† of large liquid clusters based on the data from Ref. [21].

Element	T_{m}, K	T_{b}, K	r_{W}, A	k_0	ε_0, eV	p_0, 10^5 atm	A, eV	ΔH_{f}, eV	$\varepsilon_0/\Delta H_{\mathrm{f}}$
Ti	1941	3560	1.67	5.82	4.89	300	3.2	4.91	0.99
V	2183	3680	1.55	4.86	4.9	46	3.7	5.34	0.90
Fe	1812	3023	1.47	4.18	3.83	11	3.0	4.32	0.89
Co	1768	3200	1.45	3.96	4.10	3.5	3.1	4.41	0.93
Ni	1728	3100	1.44	3.70	4.13	47	2.9	4.46	0.93
Zr	2128	4650	1.85	5.18	6.12	52	3.8	6.31	0.97
Nb	2750	5100	1.68	4.23	7.35	360	4.5	7.47	0.98
Mo	2886	4912	1.60	3.78	6.3	59	4.5	6.82	0.92
Rh	2237	3968	1.55	3.42	5.42	7.7	3.8	5.78	0.94
Pd	1828	3236	1.58	3.50	3.67	4.4	2.9	3.92	0.94
Ta	3290	5731	1.68	3.30	8.1	250	4.7	8.12	1.00
W	3695	5830	1.60	2.73	8.59	230	4.7	8.82	0.97
Re	3459	5880	1.58	2.64	7.36	63	5.3	7.99	0.92
Os	3100	5300	1.55	2.52	7.94	230	4.7	8.16	0.94
Ir	2819	4700	1.58	2.60	6.44	130	4.9	6.93	0.93
Pt	2041	4098	1.60	2.65	5.6	170	3.6	5.87	0.95
Au	1337	3129	1.65	2.80	3.65	12	2.5	3.80	0.96
U	1408	4091	1.77	2.93	4.95	5.4	3.8	5.53	0.93

† T_{m} is the melting point of a metal; T_{b} is its boiling point; the Wigner–Seitz radius r_{W} is defined by formula $r_{\mathrm{W}} = (3m/4\pi\rho)^{1/3}$; the rate constant of atom attachment to a cluster k_0 is given by formula (2.2) and relates to a temperature of 2000 K, being measured in units 10^{-11} cm^3 s^{-1}; the saturation vapor pressure near the melting point is $p_{\mathrm{sat}}(T) = p_0 \exp(-\varepsilon_0/T)$; ΔH_{f} is the enthalpy of conversion of a solid into a monatomic gas at the pressure 1 atm and temperature 298 K, and the parameter A characterizes the cluster surface energy according to formula (2.6).

for processes involving the attachment of atoms to the cluster surface and evaporation of atoms from its surface.

If the cluster plasma under consideration is in thermodynamic equilibrium, the balance of attachment and evaporation events for atoms leads to the equation

$$f_{n-1}v_{n-1} = f_n v_{\mathrm{ev}}^n ,$$

where f_n is the size distribution function of clusters. Thus, under equilibrium conditions we have

$$\frac{f_{n-1}}{f_n} = \frac{N_{\mathrm{sat}}}{N} \exp\left(-\frac{\varepsilon_n - \varepsilon_0}{T}\right) . \tag{2.4}$$

From this, it follows that the equilibrium cluster distribution function has a minimum at a critical cluster size when

$$\exp\left(\frac{\varepsilon_0 - \varepsilon_n}{T}\right) = \frac{N}{N_{\mathrm{sat}}} = S , \tag{2.5}$$

where S is the degree of supersaturation of the vapor.

The character of the cluster size dependence for the atomic binding energy ε_n is different for solid and liquid cluster states. The solid cluster state is characterized by so-called magic numbers [22–24], which are the numbers of cluster atoms at which the cluster structures are completed. Maximum values of the atomic binding energies relate to fully occupied cluster structures and, correspondingly, to magic numbers of cluster atoms. In the case of the liquid state, the size dependence ε_n is monotonic, thus leading to the classical character [25–28] of the cluster growth when the bulk condensation of a vapor is determined mostly by the evolution of the size distribution function of clusters near its minimum.

Figure 1 displays the equilibrium size dependence of the function (2.5) for these aggregate states of clusters. In the case of the liquid state, this function goes a minimum for the critical cluster size. In both cases the size distribution function of clusters grows when one moves from the critical cluster size to large and small clusters. This means that clusters include a minority of atoms under equilibrium conditions when the atoms are found mostly in a condensed macroscopic system or in an atomic gas. Hence, clusters contain the most part of atoms only under nonequilibrium conditions when the atomic system undergoes transition from a gas to a condensed system. Note that the growth process of liquid clusters proceeds continuously whereas, as follows from Fig. 1, the growth of solid clusters takes place by jumps and returns, and there is a large probability to observe magic cluster numbers at any given instant. Correspondingly, the typical time of cluster growth for solid clusters is significantly more than for liquid clusters.

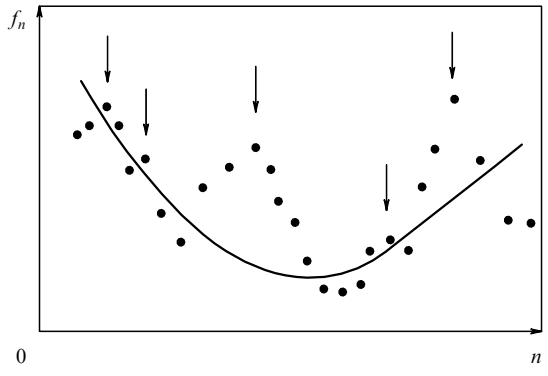

Figure 1. The equilibrium size distribution function for a solid (•) and liquid (full line) cluster. Arrows show the cluster magic numbers.

Along with the violation of stable size distribution for clusters in a uniform plasma, this analysis shows the different behavior of solid and liquid clusters in a dense buffer gas. For large liquid clusters, the total atomic binding energy E may be separated into volume and surface parts, giving the formula

$$E = \varepsilon_0 n - An^{2/3} . \tag{2.6}$$

Here n is the number of cluster atoms, ε_0 is the sublimation energy per atom in a macroscopic system; the second term in the right-hand side of this relation corresponds to the surface energy, and this formula is an expansion of the cluster energy over a small parameter $\sim n^{-1/3}$. Parameters of this formula for large liquid clusters near the melting point are given in Table 1. Along with the specific atomic binding energy ε_0 for the liquid state, this table contains the values of ΔH_{f}, the specific enthalpy for conversion of a solid into a monatomic gas at a pressure of 1 atm and temperature of 298 K. Note that the quantities ε_0 and ΔH_{f} characterize the atomic binding energy under different conditions. Evidently, the quantity ΔH_{f} is greater than ε_0, because it includes also the fusion heat and the energy of heating of the solid up to the melting point. But for strong bonds, as is the case for the metals under consideration, this difference is not large. Hence, though the ratio $\varepsilon_0/\Delta H_{\mathrm{f}}$ is less than unity, it is close to unity. The average value of this ratio for the elements included in Table 1 is equal to 0.94 ± 0.03.

Presence of magic numbers allows one to distinguish the solid cluster state from the liquid one. As an example of this, Fig. 2 shows mass spectra of sodium clusters obtained using the near-threshold photoionization of clusters at different temperatures [29, 30]. When a cluster melts, the spectrum structure disappears. This figure shows the size dependence of the cluster melting point. Note that the melting point of bulky sodium is 371 K.

2.2 Chemical equilibrium and chemical regeneration in cluster plasma

A cluster plasma can exist only under certain conditions. First, clusters or small particles of plasma must not be destroyed in collisions with charged or neutral plasma particles, so the plasma temperature has to be restricted. Second, the energy of plasma electrons must be enough to support the plasma. These requirements may be fulfilled for clusters of heat-resistant metals. Due to their high boiling temperatures, clusters of these metals can exist under conditions when a stable plasma is supported under the action of external electric fields. But if a metal vapor is present in a discharge plasma, its atoms or clusters may attach to the walls of the discharge tube. In order to prevent such metal consumption, it is convenient to activate the regeneration process [31]. Then the metal is introduced into the plasma in the form of a chemical compound which is found in the gaseous state at low temperatures and its decomposition leads to the formation of clusters at higher temperatures. In this way one can avoid the attachment of the metal to cold walls.

Probably, the first cluster plasma was created in experiments by Scholl et al. [31–34] in a cluster light source. The

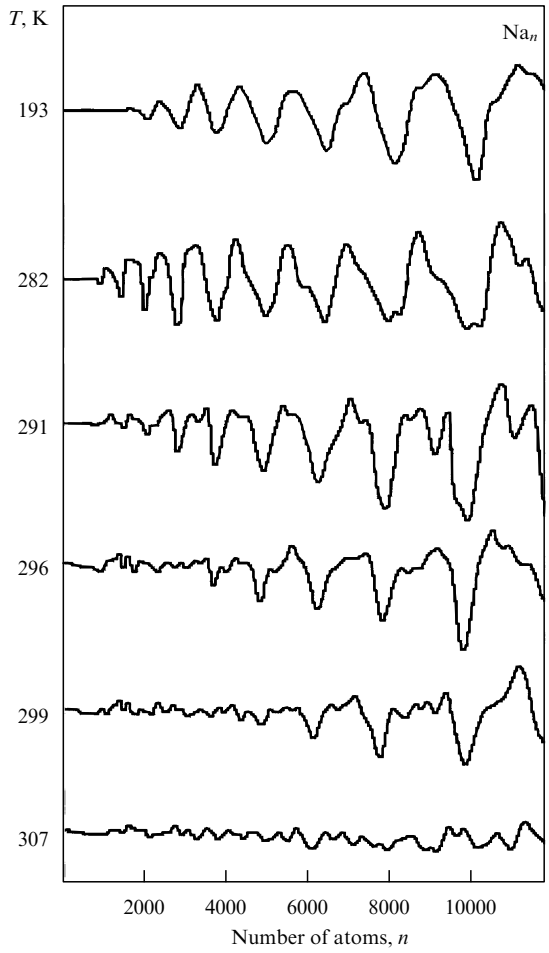

Figure 2. Mass spectra of sodium clusters, resulting from near-threshold photoionization [29, 30]. Disappearance of magic numbers at heating testifies to the melting of clusters of relevant sizes. Each oscillation in the spectrum of a solid cluster corresponds to one atomic shell. Variation of the number of atomic shells from 6 to 14, i.e. the number of cluster atoms from 923 to 10179, leads to an increase in the cluster melting point from (288 ± 4) to (303 ± 3) K.

scheme of this device is given in Fig. 3 together with processes in this plasma. The source of the plasma is a microwave discharge of frequencies 2.3 – 2.5 GHz and the power of about 100 W. This microwave discharge creates a plasma in a dense vapor inside a quartz vessel which typically has a volume of about 0.25 cm^3. This quartz vessel is located inside the microwave resonator cavity and receives the microwave power through a coupled antenna, as shown in Fig. 3. The microwave discharge supports the temperature at the center of the vessel near 4000 – 5000 K, which is optimal for the cluster plasma and its use as a light source.

The processes in this vessel are represented in Fig. 3 in the case when molecules of WO_2Br_2 are added to a dense buffer gas (Ar) with the admixture of CsBr, which provides for the ionization of the mixture. Molecules of WO_2Br_2 are evaporated from the walls completely at a wall temperature of 1000 K. At temperatures above 2500 K, these molecules are destroyed and tungsten clusters are formed at higher temperatures. These clusters are effective radiators, and Fig. 4 gives the spectrum of radiation emitted by this cluster plasma, which is determined mostly by cluster radiation at temperatures about 3500 K. The chemical regeneration in these cluster lamps is observed with various heat-resistant metals and their compounds such as Re_2O_7, OsO_4, MoO_2X_2, TaX_5, $TaOX_5$, NbX_5, $NbOX_3$, HfX_4, ZrX_4, and TiX_4, where X is a halogen atom. This list testifies to the universal character of the chemical regeneration process.

Below, we shall take for this purpose a compound MX_k, where M is the metal atom, X is the halogen atom, k is an integer. We now can find the criteria which provide the above distribution of components in the arc plasma. The chemical equilibrium for the gaseous compound corresponds to the scheme

$$MX_k \longleftrightarrow M + kX\,. \tag{2.7}$$

Let us introduce the binding energy ε_X per halogen atom, so that the total binding energy of atoms in the compound MX_k is $k\varepsilon_X$. Along with reactions (2.7), the equilibrium between metal atoms and clusters according to reactions (1.1) occurs. Introducing ε_M — the binding energy per atom for a bulky metal, we have the following rough criterion for the existence of the above chemical compound at low temperatures:

$$\varepsilon_M < k\varepsilon_X\,. \tag{2.8}$$

From the chemical equilibrium of MX_k, one can estimate the typical temperature T_1 at which this compound decomposes into atoms, and from the chemical equilibrium of clusters M_n one can find the typical temperature T_2 at which clusters are transformed into atoms, viz.

$$T_1 = \frac{\varepsilon_X}{\ln(N_0/[X])}\,, \qquad T_2 = \frac{\varepsilon_M}{\ln(N_0/[M])}\,. \tag{2.9}$$

Here [X] denotes the total number density of free and bound atoms X, N_0 is a typical atomic quantity, and [M] is the total number density of free and bound metal atoms. Evidently, clusters exist in the temperature range [35]

$$T_1 < T < T_2\,. \tag{2.10}$$

One can determine the temperature T_2 of decomposition of clusters more precisely using the formula

$$[M] \sim N_{sat}(T_3)\,, \tag{2.11}$$

where $N_{sat}(T_3)$ is the atomic density in a saturated vapor at the temperature T_3. We denote this temperature as T_3, though according to definition it should coincide with the temperature T_2. Evidently, if $[X] \sim [M]$, the possibility of existence of clusters corresponds to the criterion

$$\varepsilon_X < \varepsilon_M\,. \tag{2.12}$$

The data in Table 2 were obtained on the base of results from Ref. [21] and they allow one to ascertain the conditions defining the existence of metallic clusters in a plasma. The corresponding variables ε_X and ε_M we denote as ΔG_X and ΔG_M if they are obtained on the base of free Gibbs thermodynamic potentials, and also as ΔH_X and ΔH_M if they are determined on the base of enthalpies. One can see a shift in temperatures T_1, T_2 in the second case — when they are given in parentheses — by ~ 200 K. The accuracy in determining the temperatures for cluster existence is estimated at about 100 – 200 K, as follows from comparison of the values of T_2 and T_3 which must be identical. Thus, insertion of some metallic compounds into an arc plasma may lead to the formation of metallic clusters in some arc region, and these cases are marked in the table by symbol +.

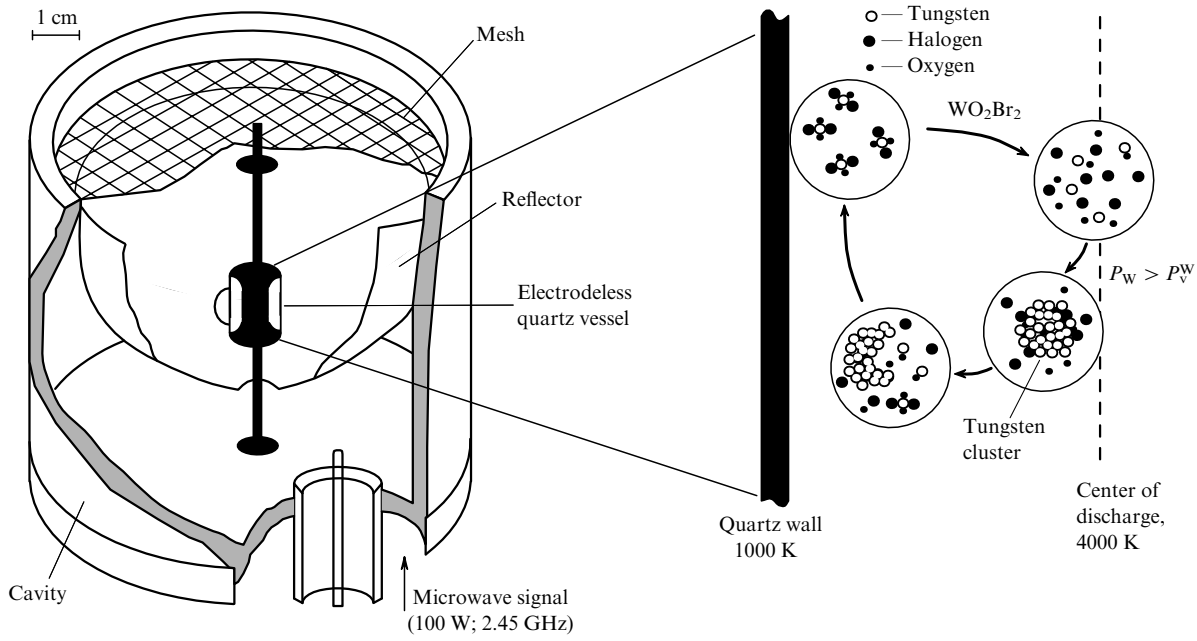

Figure 3. The layout of a cluster lamp using a microwave discharge, and the processes involving tungsten clusters inside the plasma [31].

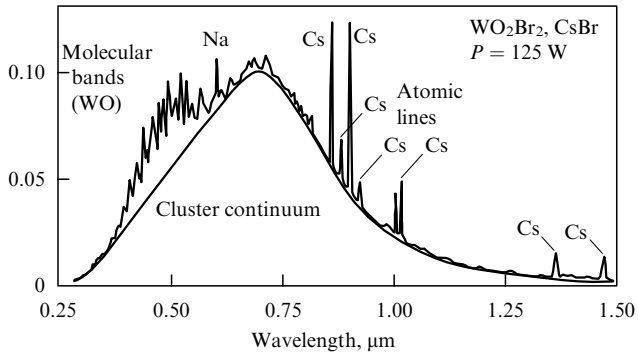

Figure 4. A typical emission spectrum of a cluster lamp of Fig. 3, which includes a continuous spectrum of clusters, spectral lines of radiative transitions in the cesium atom and the molecular bands of the WO molecule [31].

The cluster plasma can be used in producing cluster lamps, for generation of large clusters and also for extraction of heat-resistant metals from their gaseous or volatile compounds. These applications are enhanced due to the cluster instability [35] which develops due to the low mobility of large clusters and the high rate of atomic attachment to clusters. As a result, all the metal is collected in the cluster region of the gas discharge in the form of clusters.

2.3 Cluster instability in an inhomogeneous vapor

Thus, a uniform cluster plasma is unstable, and the processes of cluster growth and cluster evaporation lead to the transformations of clusters into an atomic vapor or a condensed macroscopic system depending on the temperature. One can expect this instability to disappear in an inhomogeneous plasma with a temperature gradient. In this case, clusters grow in a cold plasma region and evaporate in a hot plasma region. A flux of clusters from a cold region to a hot one establishes an equilibrium. This equilibrium corresponds to a stationary spatial distribution of clusters and the atomic vapor, and the typical cluster size is determined by the cluster growth time, which is the transport time of clusters from a cold region to a hot one.

But this scheme is not realized for real metallic vapors in a dense buffer gas due to the so-called cluster instability [35]. This instability results from the cluster-size dependence of both the rate of cluster growth and the cluster diffusion coefficient in the buffer gas. In order to analyze this instability, we now study the fate of an individual cluster located in a cold region. In this region, the cluster evaporation process is not significant, so that the cluster size n (the number of cluster atoms) varies in time due to the process of atomic attachment to a cluster:

$$\frac{\mathrm{d}n}{\mathrm{d}t} = k_0 n^{2/3} N\,, \tag{2.13}$$

and the right-hand side of this equation is the rate of atomic attachment which is given by formula (2.2). Concurrent with the cluster growth, a probe cluster moves away from the initial point due to the diffusive motion in the buffer gas. The distance z that the cluster is moved from the initial point in the temperature gradient direction is determined by the probe cluster diffusion and is given by the equation

$$\frac{\mathrm{d}\overline{z^2}}{\mathrm{d}t} = 2D_n\,, \tag{2.14}$$

where an average is taken over possible positions of the cluster, and D_n is the diffusion coefficient in the buffer gas for a cluster consisting of n atoms. We use the cluster-size dependence for the diffusion coefficient $D_n = D_0/n^{2/3}$, and in the Chapman – Enskog approximation we have [36, 37]

$$D_0 = \frac{3}{8\sqrt{2\pi}\, r_W^2 N_a} \sqrt{\frac{T}{m}}. \tag{2.15}$$

Here r_W is the Wigner – Seitz radius, m is the mass of a buffer gas atom, N_a is the number density of atoms of the buffer gas,

Table 2. Parameters of some compounds of heat-resistant metals at the initial number density of the molecules $[MX_k] = 1 \times 10^{16}$ cm^{-3} [44].

Compound	ΔG_X, eV	ΔG_M, eV	ΔH_X, eV	ΔH_M, eV	T_1, 10^3 K	T_2, 10^3 K	T_3, 10^3 K	Cluster existence
$HfCl_4$	—	6.0	4.2	6.4	(2.4)	3.0(3.2)	3.15	+
HfF_4	—	6.0	6.3	6.4	(3.5)	3.0(3.2)	3.15	−
$SnBr_4$	—	2.8	3.2	3.1	(1.8)	1.4(1.6)	1.73	−
$SnCl_4$	2.1	2.8	2.6	3.1	1.2(1.5)	1.4(1.6)	1.73	+
$ThCl_4$	—	5.8	4.7	6.2	(2.6)	3.0(3.1)	3.12	+
ThF_4	6.2	5.8	6.5	6.2	3.5(3.6)	3.0(3.1)	3.12	−
$TiBr_4$	3.0	4.4	3.2	4.9	1.7(1.8)	2.2(2.5)	2.28	+
$TiCl_4$	3.5	4.4	3.8	4.9	2.0(2.1)	2.2(2.5)	2.28	+
UCl_4	3.8	5.1	4.1	5.5	2.1(2.3)	2.6(2.8)	2.73	+
UF_4	5.7	5.1	5.9	5.5	3.2(3.3)	2.6(2.8)	2.73	−
VCl_4	3.0	4.7	3.3	5.3	1.7(1.8)	2.4(2.7)	2.40	+
VF_4	—	4.7	4.4	5.3	(2.5)	2.4(2.7)	2.40	−
$ZrCl_4$	4.3	5.9	4.8	6.3	2.4(2.7)	3.0(3.2)	3.08	+
ZrF_4	6.5	5.9	6.9	6.3	3.6(3.9)	3.0(3.2)	3.08	−
$NbCl_5$	3.3	7.1	3.6	7.5	1.8(2.0)	3.6(3.8)	3.41	+
NbF_5	5.2	7.1	5.5	7.5	2.9(3.1)	3.6(3.8)	3.41	+
VF_5	4.1	4.7	4.4	5.3	2.3(2.5)	2.4(2.7)	2.40	+
IrF_6	2.2	6.4	2.5	6.9	1.2(1.4)	3.2(3.5)	3.15	+
MoF_6	3.9	6.3	4.2	6.8	2.2(2.4)	3.2(3.4)	3.19	+
UCl_6	3.0	5.1	3.3	5.5	1.7(1.8)	2.6(2.8)	2.73	+
UF_6	4.7	5.1	5.0	5.5	2.6(2.8)	2.6(2.8)	2.73	−
WCl_6	—	8.4	3.0	8.8	(1.7)	4.2(4.4)	4.04	+
WF_6	4.5	8.4	4.9	8.8	2.5(2.7)	4.2(4.4)	4.04	+

Table 3. Parameters describing diffusion of large clusters in argon as a buffer gas at $T = 1000$ K. The reduced diffusion coefficient is given by formula (2.15) for $T = 1000$ K, and Λ is given by formula (2.17).

Element	D_0, cm^2 s^{-1}	$\Lambda\sqrt{N_0 N}$, 10^{15} cm^{-2}
Ti	0.91	1.59
V	1.05	3.51
Fe	1.17	2.13
Co	1.20	2.22
Ni	1.22	2.31
Zr	0.74	1.52
Nb	0.90	1.85
Mo	0.98	2.05
Rh	1.05	2.23
Pd	1.01	2.16
Ta	0.90	2.19
W	0.98	2.42
Re	1.01	2.49
Os	1.05	2.60
Ir	1.01	2.51
Pt	0.98	2.45
Au	0.93	2.32
U	0.81	2.11

T is the gaseous temperature. Table 3 gives the values of D_0 for some metallic clusters in argon with the standard number density of atoms $N_a = 2.7 \times 10^{19}$ cm^{-3} and at the gaseous temperature $T = 1000$ K.

Thus, we have the equation for cluster displacement from the initial point in a cold plasma region of the form

$$\frac{d\overline{z^2}}{dn} = \frac{2D_0}{k_0 n^{4/3} N}, \tag{2.16}$$

where N is the number density of free atoms of the metal vapor in the buffer gas. It follows from this equation that clusters move more slowly as they increase in size. For a large cluster, the mean value of the distance squared $\overline{z^2}(t)$ at the end of the process is

$$\overline{z^2}(\infty) = \frac{\Lambda^2}{n^{1/3}}, \qquad \Lambda^2 = \frac{6D_0}{k_0 N}. \tag{2.17}$$

and a large cluster remains in the cluster region. Because $D_0 \sim 1/N_a$, we have $\Lambda \sim 1/\sqrt{N_a N}$, i.e. the quantity $\Lambda\sqrt{N_a N}$ does not depend on the density of the buffer gas. Table 3 contains the values of this quantity at $T = 1000$ K for argon as the buffer gas. From data of this table, for typical values $N_a \sim 10^{19}$ cm^{-3}, and $N \sim 10^{13} - 10^{15}$ cm^{-3} we have $\Lambda \sim 0.01 - 0.1$ cm. This means that there is cluster instability under real laboratory conditions.

Neglecting the diffusive motion of large clusters in a cluster plasma, we consider the cluster growth processes as follows. There is local thermodynamic equilibrium between clusters and the atomic vapor at each point, which results from the processes of evaporation of clusters and attachment of atoms to their surfaces. In the limit of large cluster sizes, the number density of free metal atoms tends to the saturation vapor density at a given temperature. The temperature gradient in the buffer gas ∇T, which is supported in the plasma, creates a gradient of the concentration of metal atoms, which is equal to

$$\nabla N = \frac{\varepsilon_0}{T^2} N \nabla T,$$

and the increase in the atomic number density is directed towards the cold region. As a result, the flux of free metal atoms is directed towards the cold region, where atoms attach to clusters. Therefore, clusters evaporate in a hot region, and the atoms formed take part in the growth of clusters in a cold region. Finally, metal atoms gather in a cold gas-discharge region, forming clusters there. Thus, as a result of the above processes a metal is concentrated in a cold region of a nonuniform plasma.

Let us estimate the depth of penetration of the atomic flux into the cluster plasma under favorable conditions for cluster growth, when one can neglect the cluster evaporation in a cold region. The atomic flux into a cold region is given by

$$j = -D_a \nabla N = -D_a N \frac{\varepsilon_0}{T^2} \nabla T,$$

where D_a is the diffusion coefficient of metal atoms in the buffer gas. The rate of atomic attachment to clusters is

determined by the cluster-size balance equation (2.13), and the depth l of penetration of free atoms into a cold region is

$$l = \frac{j}{k_0 n^{2/3} N_{\rm cl} N} = \frac{D_{\rm a}}{k_0 N_{\rm b}} \frac{\varepsilon_0}{T} \frac{\nabla T}{T} n^{1/3} . \qquad (2.18)$$

Here, $N_{\rm cl}$ is the number density of clusters, $N_{\rm b} = nN_{\rm cl}$ is the total number density of bound atoms in clusters, and n is the average number of cluster atoms. It is of importance that the regime under consideration satisfies the criterion

$$N_{\rm b} \gg N . \qquad (2.19)$$

This means that the majority of metal atoms are bound in clusters, so that the number density of free atoms is small compared to the number density of bound atoms. This condition corresponds to intense nucleation processes in the plasma and ensures that metal atoms gather in a narrow region of the plasma at the end.

For a numerical estimate, we shall consider argon as a buffer gas at pressure 1 atm and $T = 3700$ K. This temperature exceeds slightly the melting point of tungsten, and the diffusion coefficient $D_{\rm a}$ of tungsten atoms in argon under these conditions may be set $10\,{\rm cm^2\,s^{-1}}$. We also take the total number density of bound tungsten atoms in a cold region to be $N_{\rm b} = 1 \times 10^{16}$ cm^{-3}. Note that the number density of free tungsten atoms at this temperature and saturation vapor pressure is 6.4×10^{13} cm^{-3}, and the equilibrium number density of free tungsten atoms near clusters of an average size $n = 10^3$ is equal to 1.4×10^{14} cm^{-3}. For this cluster size and laboratory values of the temperature gradient $\nabla T/T \sim 1$ cm^{-1}, we obtain in this case $l \sim 0.005$ cm.

This transport process involving free atoms which are in equilibrium with clusters leads to redistribution of the latter in space. If clusters occupy a region of size Δx, i.e. in this region the condition (2.10) is fulfilled, a noticeable atom transport into this region proceeds during a typical time τ, which is estimated by

$$\tau \sim \frac{N_{\rm b}}{N} \frac{\Delta x^2}{D_{\rm a}} \frac{T}{\varepsilon_0} \frac{T}{\Delta T} , \qquad (2.20)$$

where $\Delta T = T_2 - T_1$, so that $\nabla T \approx \Delta T/\Delta x$. Taking $\Delta x \sim 1$ cm, we find that under the above conditions $\tau \sim 1$ s. This process leads to the redistribution of bound atoms in a region occupied by clusters. Thus, for this regime of transport processes, when the majority of atoms become bound and collect in a cold plasma region, it is required that, on the one hand, the vapor pressure is relatively small, so that the criterion (2.19) is fulfilled, and, on the other hand, compounds of metal atoms and halogen atoms are not formed at these temperatures.

2.4 Stability of charged clusters

Along with evaporation, a large charged cluster can be destroyed under the action of internal electric fields. This problem is actual for liquid dielectric particles, and below we shall consider instabilities of liquid clusters as a result of the interaction of their charges. We assume the cluster to be similar to a liquid charged drop, so that its destruction is determined by the Rayleigh instabilities of a charged liquid drop [38]. For the case of the Rayleigh instability, the cluster surface tension energy $4\pi r^2\gamma$ prevents the drop from decaying due to the Coulomb interaction $Z^2e^2/(2r)$ of cluster charges. Here r is the drop radius, Z is the drop charge expressed in electron charges e, and γ is the surface tension. Here we assume drop charges to be distributed uniformly over the drop surface.

The Rayleigh instability gives rise to the separation of a drop into two identical drops due to large deformations or the decay of a drop owing to small drop vibrations. Below, we shall restrict our consideration to drop decay due to small deformations whose threshold has the form [38]

$$Z^2e^2 = 16\pi\gamma r^3 . \qquad (2.21)$$

This criterion corresponds to the case where the charge is distributed uniformly over the drop surface and we assume the Poisson coefficient to be zero, so that a deformation in one direction does not create deformations in other ones. Notice that clusters that are stable with respect to this criterion can be found unstable with respect to large deformations, i.e. these clusters are in a metastable state.

Let us consider clusters with a short-range interaction of atoms or molecules, where the cluster binding energy is determined mostly by interaction of nearest neighbors. In this situation the solid cluster has the close-packed structure, and an internal atom is surrounded by its 12 nearest neighbors. Then we have for the cluster radius $r = r_{\rm W} n^{1/3}$, where $r_{\rm W} = [3m/(4\pi\rho)]^{1/3}$ is the Wigner–Seitz radius, m is the atom mass, ρ is the density of an atomic macroscopic system, n is the number of drop atoms, and the surface energy is represented in the form $4\pi r^2\gamma = An^{2/3}$, where A is the specific surface energy of the cluster (see Table 1). These parameters for clusters of rare gases are given in Table 4; they were compiled on the base of data presented in Ref. [15]. Using these parameters, the criterion (2.21) can be represented in the form

$$n_{\rm cr}(Z) = \frac{Z^2e^2}{4Ar_{\rm W}} . \qquad (2.22)$$

Here $n_{\rm cr}(Z)$ is the critical size of the cluster starting from which the cluster of the charge Z is stable with respect to small deformations. The values of $n_{\rm cr}/Z^2$ are also given in Table 4. Note that there are different versions of the Rayleigh instability [13, 15–17] depending on the instability character, the distribution of charges in the drop, the Poisson coefficient of the drop and its polarizability. It is convenient to represent formula (2.22) in the form

$$n_{\rm cr}(Z) = C \frac{Z^2e^2}{4Ar_{\rm W}} . \qquad (2.23)$$

Let us require that this formula fits experimental data. Then, comparing this formula with the measured values of $n_{\rm cr}$ for krypton and xenon [39–43] with $Z = 2$–4, where the measurements are reliable, we get $C = 0.8 \pm 0.1$. Using this value of the coefficient C, one can find the critical cluster size

Table 4. Parameters of rare-gas clusters.

Gas	$r_{\rm W}$, A	A, meV	$n_{\rm cr}/Z^2$
Ne	1.74	15.3	135
Ar	2.08	53	33
Kr	2.15	73	23
Xe	2.40	97	15

at a given charge. As a result of the statistical treatment of the data, which follow from formula (2.23) with $C = 0.8$ and parameters of this formula according to Table 1, we obtain

$$\frac{n_{\rm cr}(Z)}{Z^2} = 0.5 \pm 0.1\,. \tag{2.24}$$

It follows from formula (2.24) that the problem of the electric stability of metallic clusters is not so sharp as it is for rare-gas clusters. Indeed, in the latter case the energy per bond is relatively small, which leads to destruction of charged clusters of rare gases at relatively weak internal electric fields. For metallic clusters, and the more so for clusters of transient metals, where the binding energy per bond is relatively high, this effect is not so significant.

3. Charging of clusters and small particles in plasma

3.1 Charging due to transport processes involving plasma particles

Small particles or clusters located in a weakly ionized gas acquire a charge as a result of attachment of electrons and negative or positive ions to them. For this reason, small particles in a gas are charged, and their behavior differs from the behavior of neutral atomic particles. In particular, aerosols, i.e. small particles in the atmosphere, are usually charged, so their fall under the action of gravity creates the Earth's electric charge and the electric fields in the atmosphere. Hence, small water particles in the atmosphere determine the character of electrical phenomena in the atmosphere and near the Earth's surface.

Small particles can emit electrons at high temperatures, but at low temperatures their charge results from attachment of electrons and ions to them. This process leads to formation of chemical bonds between charged atomic particles on the surface of a small particle and can proceed through several intermediate stages. For example, dissociative attachment of electrons to dielectric particles can proceed via formation of free negative ions. These negative ions later attach to the surface due to collisions with gaseous atoms or molecules. When positive ions in the plasma attach to the surface of a small particle, they can recombine on the surface with negative charges. The character of such recombination depends on the type of the particle's material. In the case of a metallic particle, electrons can move through the entire particle volume, and the attachment of a positive ion to a metallic particle decreases by one the total number of particle electrons. This means the charge exchange of a positive ion on a small metallic particle, so that one electron transfers from the small particle to the positive ion. In collisions with a negative ion, a weakly bound electron of the negative ion transfers to the small metallic particle as a result of their contact. Thus, the charging of a small metallic particle in a plasma proceeds through the interaction of positive or negative ions on the particle's surface with an electron subsystem.

In the case of a dielectric small particle, attachment of positive and negative ions to its surface leads to formation of bound states of ions at some points on the particle's surface. We call these points active centers. As this takes place, the bound states of positive and negative ions can exist simultaneously on the particle's surface. Diffusion of these bound ions across the particle surface leads to their recombination. Thus, though the recombination of positive and negative charges on the surface of a metallic particle differs from that on the surface of a dielectric particle, these processes are identical from the standpoint of fluxes of charges onto the particle's surface because opposite charges recombine at the end. Hence, below we shall not distinguish recombination of charges on the particle's surface for metallic and dielectric small particles.

We start with the charging of a spherical particle, when its radius r exceeds the mean free path λ of atoms in the gas:

$$r \gg \lambda\,. \tag{3.1}$$

Under this condition, the charging of a small particle as a result of attachment of electrons or ions to its surface is hampered by their motion towards the particle. Below we shall evaluate the currents of plasma ions towards the particle, when the ion motion is determined by their diffusion in a gas and their drift under the action of the electric field of a charged particle. We introduce the boundary conditions according to which the number density of ions equals zero on the particle's surface and tends to the equilibrium value at large distances from the particle in a plasma. Taking the particle's charge to be Z, we get for the current I of positive ions towards the particle at a distance R from it the following relationship:

$$I = 4\pi R^2 \left(-D_+ \frac{{\rm d}N}{{\rm d}R} + K_+ EN\right) e\,.$$

The first term corresponds to ion diffusive motion, the second term to ion drift motion, N is the current number density of ions, D_+, K_+ are the diffusion coefficient and the mobility of positive ions, respectively, e is the ion charge (usually it is equal to an electron charge), and $E = Ze/R^2$ is the strength of the electric field created by the particle. Using the Einstein relationship $D_+ = eK_+/T$, where T is the gaseous temperature, we obtain for the positive ion current onto the particle's surface the following expression

$$I = -4\pi R^2 D_+ e \left(\frac{{\rm d}N}{{\rm d}R} - \frac{Ze^2 N}{TR^2}\right).$$

This relationship can be considered as the equation for the ion number density. Taking into account that ions do not recombine in the bulk, we find that the ion current is independent of R. Solving this equation with the boundary condition $N(r) = 0$, we obtain

$$\begin{aligned} N(R) &= \frac{I}{4\pi D_+ e} \int_r^R \frac{{\rm d}R'}{(R')^2} \exp\left(\frac{Ze^2}{TR'} - \frac{Ze^2}{TR}\right) \\ &= \frac{IT}{4\pi D_+ Ze^3} \left[\exp\left(\frac{Ze^2}{Tr} - \frac{Ze^2}{TR}\right) - 1\right]. \end{aligned}$$

Using the fact that at large R the ion number density tends to the equilibrium value N_+ in a plasma far from the particle, we arrive at the following expression for the ion current [45]

$$I_+ = \frac{4\pi D_+ N_+ Ze^3}{T\{\exp[Ze^2/(Tr)] - 1\}}\,. \tag{3.2}$$

This formula is called the Fuks formula. The latter can be generalized to other geometric forms of the particle. Then the

ion current onto the particle surface is equal to

$$I_+ = \frac{4\pi D_+ N_+ Ze^3}{T\{\exp[Ze^2/(CT)] - 1\}} ,$$

where C is the particle capacity. For a spherical particle $C = r$ and this formula is transformed into (3.2).

Formula (3.2) describes a positive ion current if the particle charge has the same sign. In order to obtain the expression for negative ion current, it is necessary to perform substitution in this formula: $Z \to -Z$, and the parameters of positive ions must be replaced by the parameters of negative ions. Then we have for the negative ion current toward the particle:

$$I_- = \frac{4\pi D_- N_- Ze^3}{T[1 - \exp(-Ze^2/Tr)]} . \tag{3.3}$$

Equalizing the currents of positive and negative ions in a plasma, we shall find the equilibrium particle charge. This gives for a quasi-neutral plasma ($N_+ = N$):

$$Z = \frac{rT}{e^2} \ln \frac{D_+}{D_-} . \tag{3.4}$$

Thus, the particle acquires a positive charge if $D_+ > D_-$, i.e. positive ions have a greater mobility than negative ones. Notice that this formula is valid for an individual particle under the condition

$$r \gg \frac{e^2}{T} , \tag{3.5}$$

when $Z \gg 1$. In this case the capture of one ion does not alter the particle's potential significantly. Thus, as this takes place the particle charge induces a certain potential which equalizes the currents of positive and negative ions. Note that the above formulas are valid under the condition (3.1). At room temperature, criterion (3.5) takes the form $r > 0.06$ μm, and for atmospheric air $\lambda = 0.1$ μm.

Formulas (3.2) and (3.3) for currents of ions onto an absorbing sphere may be used in the limit $Z \to 0$ for determination of the diffusive flux J of neutral particles onto the surface of an absorbing sphere:

$$J = \frac{I_+}{e} = 4\pi D_+ N_+ r . \tag{3.6}$$

This formula is known as the Smoluchowski formula. In the other limit, $Ze^2/(rT) \gg 1$, formula (3.3) is transformed into the Langevin formula [46]

$$I_- = \frac{4\pi Ze^3 D_- N_-}{T} = 4\pi Ze^2 K_- N_- . \tag{3.7}$$

Notice that formulas (3.2) and (3.3) for ion currents may be combined by introducing the reduced variable $x = |Z|e^2/(rT)$, so that we have

$$I = \begin{cases} \dfrac{I_0 x}{\exp(x) - 1} , & Ze^2 > 0 , \\ \dfrac{I_0 x}{1 - \exp(-x)} , & Ze^2 < 0 , \end{cases} \qquad \lambda \ll r . \tag{3.8}$$

Here, I_0 is given by the Smoluchowski formula (3.6), which corresponds to atomic attachment to the neutral particle: $I_0/e = 4\pi DNr$, where N is the number density of atoms, and D is the diffusion coefficient of atoms in a gas. In particular, in the limiting case $x \gg 1$ it is transformed into the Langevin formula

$$I = 4\pi K N_0 Ze^2 ,$$

where $K = eD/T$ is the mobility of ions in a gas, N_0 is the mean number density of ions.

Formulas (3.2) and (3.3) for currents of positive and negative ions include the ion temperature which originated in these formulas via the Einstein relation. Therefore, formula (3.3) can be used for the current of electrons onto the particle surface if the energy distribution function of electrons is not Maxwellian. In this formula, $T_e = eD_e/K_e$ is used as an effective electron temperature T_e, where K_e, D_e are the mobility and diffusion coefficient of electrons in a gas. In particular, it is valid for a particle located in a glow discharge, where the distribution function of electrons over velocities differs from the Maxwellian distribution function. Correspondingly, the particle charge in this case is equal to

$$Z = r \frac{D_e}{eK_e} \ln \frac{K_e}{K_+} . \tag{3.9}$$

For a more general form of the particle, this charge is given by

$$Z = C \frac{D_e}{eK_e} \ln \frac{K_e}{K_+} ,$$

where C is the particle's capacity, which coincides with its radius for a spherical particle. In an equilibrium plasma where the Maxwellian distribution functions of electrons and ions are characterized by an identical temperature, this formula transforms to formula (3.4).

Due to its charge, the particle has an electric potential with respect to the plasma where it is located. This potential is equal to

$$\varphi_0 = \frac{Ze}{C} = \frac{T}{e} \ln \frac{D_-}{D_+} .$$

It is seen that the potential energy $e\varphi_0$ corresponding to ions on the particle's surface is of the order of the ion thermal energy T. This follows from the nature of the process, which requires the equality of currents of positive and negative ions onto the particle's surface.

If the criterion opposite to (3.1) is fulfilled, the particle charge results from individual collisions of plasma ions and electrons with this charged particle. For simplicity, we assume that each contact of a colliding ion or electron with the particle surface leads to transfer of its charge to the particle. Next we assume the particle radius to be large enough for collisions to feature a classical character. This allows us to express the currents of ions and electrons onto the particle surface through classical cross sections for their attachment to a charged particle.

Because the distance of closest approach r_0 of classical particles is connected with the impact parameter ρ of their collision by the relation [47]

$$1 - \frac{\rho^2}{r_0^2} = \frac{Ze^2}{r_0 \varepsilon} ,$$

where ε is the collision energy in the center-of-mass system, we have that the cross section of ion collision with the particle's surface under these conditions is defined as

$$\sigma = \pi r^2 \left(1 - \frac{Ze^2}{r_0 \varepsilon}\right).$$

When $Z > 0$, i.e. the charges of the particle and ions have the same sign, account must be taken of the fact that if $\varepsilon \leqslant Ze^2/r_0$, then the cross section equals zero, because in this case the potential energy of repulsion of the particle and a colliding ion exceeds their kinetic energy near the particle's surface. From this it follows that the rate constant of contact between a colliding ion and the particle after averaging over the ion energies with the aid of the Maxwellian distribution function for ions is written as

$$k = \langle v\sigma \rangle = k_0 \exp\left(-\frac{|Z|e^2}{rT}\right),$$

where r is the particle's radius, and $k_0 = \pi r^2 \sqrt{8T/(\pi m)}$. In the case of attraction of the particle to an ion, the averaged rate constant of this collision is given by

$$k = k_0 \left(1 + \frac{|Z|e^2}{rT}\right).$$

Introducing the dimensionless parameter $x = |Z|e^2/(rT)$ and the probability ξ that the ion transfers its charge to the particle as a result of their contact, we combine the above formulas for the rate of ion attachment to the particle and finally obtain [48]

$$J = \xi k_0 N_i \begin{cases} 1 + x\,, & Ze^2 < 0\,, \\ \exp(-x)\,, & Ze^2 > 0\,. \end{cases} \tag{3.10}$$

This formula is valid in the limit $\lambda \gg r$.

Let us consider the charging of clusters in an equilibrium plasma with identical temperatures of electrons and ions, as occurs in an afterglow plasma. The current density of electrons attaching to the particle's surface in this regime is

$$j_{\text{at}} = N_{\text{e}} \sqrt{\frac{T}{2\pi m_{\text{e}}}} \exp\left(-\frac{|Z|e^2}{rT}\right), \tag{3.11a}$$

where m_{e} is the electron mass, Z is the particle's charge expressed in electron charges, r is the particle radius, and we assume that each contact of an electron with the particle's surface leads to the electron attachment. Assuming fulfillment of the criterion

$$\frac{|Z|e^2}{rT} \gg 1\,,$$

we have for the current density of ions j_+ onto the particle surface:

$$j_+ = \sqrt{\frac{T}{2\pi M}}\, N_{\text{i}}\, \frac{|Z|e^2}{rT}\,, \tag{3.11b}$$

where M is the ion mass, N_{i} is the number density of positive ions, and $N_{\text{i}} = N_{\text{e}}$ for the quasi-neutral plasma. Equalizing these current densities, we get for the particle's charge under this regime of particle charging the following expression:

$$x = \ln\left(\frac{1}{x}\sqrt{\frac{M}{m_{\text{e}}}}\right), \qquad |Z| = x\,\frac{r_{\text{W}} n^{1/3} T}{e^2}\,, \tag{3.12}$$

where r_{W} is the Wigner – Seitz radius. Table 5 gives the solution of this equation for an inert buffer gas with atomic positive ions, and for the case when nitrogen plays the part of the buffer gas and its plasma contains N_2^+ ions. Table 6 includes the reduced equilibrium charge $Z/n^{1/3}$ of metallic particles in an argon plasma with Ar^+ ions at temperature $T = 1000$ K.

Table 5. The solution of equation (3.12).

Buffer gas	He	Ne	Ar	Kr	Xe	N_2
x	3.26	3.90	4.17	4.47	4.65	4.03

One can combine the above results when the criterion (3.1) is valid or the opposite relation between these parameters takes place. For this purpose, we shall consider first the limiting case $\lambda \gg r$ with a general boundary condition on the particle's surface: $N(r) = N_1 \neq 0$. Using expression (3.10) for the current near the particle's surface, we shall find the ion number density in an intermediate region where it varies from the value N_1 near the particle's surface up to the value N_i far from the particle. Repeating the operations that we used when deducing formula (3.2), we arrive at

$$\begin{aligned} N(R) - N_1 &= \frac{I}{4\pi e D_{\text{i}}} \int_r^R \frac{\mathrm{d}R'}{(R')^2} \exp\left(\frac{Ze^2}{TR'} - \frac{Ze^2}{TR}\right) \\ &= \frac{IT}{4\pi D_{\text{i}} Ze^3} \left[\exp\left(\frac{Ze^2}{Tr} - \frac{Ze^2}{TR}\right) - 1\right]. \end{aligned}$$

Employing the second boundary condition $N(\infty) = N_i$, we obtain for the ion current

$$I = \frac{4\pi D_{\text{i}} (N_{\text{i}} - N_1) Ze^3}{T\left[\exp(Ze^2/Tr) - 1\right]}\,.$$

Taking the boundary value $N = N_1$ for the ion number density at the particle's surface, we get the following expression for the ion current:

$$I = \left(\frac{1}{I_>} + \frac{1}{I_<}\right)^{-1}, \tag{3.13}$$

where the ion current $I_>$ corresponds to the case $\lambda \gg r$ and is given by formula (3.8), while the ion current $I_<$ corresponds to the opposite relation between the mean free path of ions in a gas and the particle radius, namely, $I_< = eJ$, where J is given by formula (3.10). Formula (3.13) transforms to formula (3.8) in the limit $I_> \gg I$, and to formula (3.10) for the opposite relation between these currents. Thus, formula (3.13) includes any relationships between the problem parameters. Notice that the ratio of these currents is estimated as

$$\frac{I_<}{I_>} \sim \frac{\xi r}{\lambda}\,.$$

The above expressions for currents of ions and electrons onto the surface of a charged particle allow us to determine the rate of establishment of the charge equilibrium for the

particle. Let us determine this quantity for a plasma including ions whose diffusion coefficients D_+, D_- are close, i.e. $\Delta D = |D_+ - D_-| \ll D$. Introducing the mean diffusion coefficient of ions $D = (D_+ + D_-)/2$ and using formula (3.9), we obtain the following expression for the equilibrium particle charge

$$Z_0 = \frac{rT}{e^2}\frac{\Delta D}{D}\,.$$

The charging of the particle is defined by an equation of the form

$$\frac{\mathrm{d}Z}{\mathrm{d}t} = \frac{I_- - I_+}{e}\,,$$

where Z is a current particle's charge. Subject to the initial condition $Z(0) = 0$ and using formulas (3.2), (3.3) for the charging currents, we have

$$\frac{\mathrm{d}Z}{\mathrm{d}t} = \frac{4\pi N_0 e^2 Z}{T}\left[D_- - D_+\exp\left(\frac{Ze^2}{Tr}\right)\right]\left[\exp\left(\frac{Ze^2}{Tr}\right) - 1\right]^{-1},$$

where N_0 is the average number density of ions in a plasma. Because $Z_0e^2/(Tr) = \Delta D/D \ll 1$ and $Z \leqslant Z_0$ in the course of charging of the particle, one can expand the above equation in a series in powers of a small parameter $Ze^2/(Tr)$. Then the equation of charging takes the form

$$\frac{\mathrm{d}Z}{\mathrm{d}t} = \frac{Z_0 - Z}{\tau}\,,$$

where

$$\frac{1}{\tau} = \frac{4\pi N_0 e^2 D}{T} = 2\pi\Sigma\,. \tag{3.14}$$

Here $\Sigma = N_0 e(K_+ + K_-) = 2N_0e^2D/T$ is the coefficient of conductivity of the plasma.

The solution of the above equation with the initial condition $Z(0) = 0$ is written as

$$Z = Z_0\left[1 - \exp\left(-\frac{t}{\tau}\right)\right].$$

It is seen that the typical time of establishing the equilibrium charge does not depend on the particle radius.

Though the topic of this review is the cluster plasma, these results for charging of particles are also valid for other types of a plasma containing particles or clusters, in particular, for a dusty and aerosol plasma. For example, from this one can determine the mobility K of a large particle which is located in the atmospheric air. According to the Einstein relation, it is expressed through the particle's diffusion coefficient D by

$$K = \frac{ZeD}{T}\,.$$

Under the criterion (3.1), the particle's charge (3.9) is proportional to its radius r, and $D \sim 1/r$. From this it follows that the mobility of a large particle in the atmospheric air does not depend on its size. Taking the ratio of the ion diffusion coefficients $D_+/D_- \approx 0.8$ which corresponds to atmospheric air of typical humidity, we find the limiting value $K = 1.8 \times 10^{-5}\ \mathrm{cm^2\ (V\ s)^{-1}}$ under the condition $r \gg \lambda$.

In the problem under consideration, we touched with three parameters of size dimensionality: r, e^2/T, λ. From this follows six different regimes for the particle's charging depending on the relation between these parameters. Briefly, in the case when the charging results from attachment of positive and negative plasma ions or positive ions and electrons to the particle, the character of the process is as follows. In the case $r \gg \lambda$, the particle's charging process is limited by the motion of ions in a gas and is determined by the diffusion of ions in a gas and the drift of ions. The particle charge may be large if $r \gg e^2/T$; and it can only be unity in the case $r \ll e^2/T$. With the proviso that $r \ll \lambda$, the process of the particle charging proceeds via pair collisions between plasma ions or electrons and the particle, and its charge can be large for $r \gg e^2/T$. In all the cases we assume $r \gg a_0$, where a_0 is the Bohr radius, and under this condition collisions involving the probe particle have a classical character.

3.2 The charge distribution function of particles in plasma

In addition to the above analysis of particle charging in a dense gas, we below shall find the charge distribution function of small particles. Let us introduce the distribution function f_z of small particles over charges, so that $N_\mathrm{p} f_z$ is the number density of particles of a charge ze, and N_p is the total number density of small particles. Then the normalization condition has the form

$$\sum_z f_z = 1\,,$$

and the kinetic equation for the distribution function is

$$f_z(J_{z,z+1} + J_{z,z-1}) = f_{z-1}J_{z-1,z} + f_{z+1}J_{z+1,z}\,,$$

where J_{ml} is the reaction rate, i.e. the probability per unit time for the particle charge to change from me to le as a result of attachment of ions. This kinetic equation takes into account the fact that the change in the particle charge as a result of an elementary process of ion attachment can only be one, the left-hand side of this equation accounts for loss of particles of a charge ze, and the right-hand side of this equation takes into account the formation of such particles.

On the basis of formulas (3.2), (3.3), we have the following expressions for rates of charging

$$J_{z,z+1} = \frac{4\pi D_+ N_0 r z x}{\exp(zx) - 1}\,, \qquad J_{z,z-1} = \frac{4\pi D_- N_0 r z x}{1 - \exp(-zx)}\,,$$

where $x = e^2/rT$, N_0 is the number density of ions of each sign far from the particles, and the other notations were explained above. Thus, we have the following kinetic equation for the distribution of small particles over charges:

$$\frac{\left[D_+ + D_-\exp(zx)\right]zx}{\exp(zx) - 1} f_z = \frac{D_+(z-1)x}{\exp\left[(z-1)x\right] - 1} f_{z-1} + \frac{D_-(z+1)x}{\exp\left[(z+1)x\right] - 1} f_{z+1}\,. \tag{3.15}$$

In the limiting case $x \gg 1$, the average particle's charge is small, and particles are mostly neutral. Then from the set of equations (3.15) it follows for the probability f_2, if we assume $f_3 \ll f_2$, that

$$\frac{f_2}{f_1} = \frac{D_+\left[\exp(2x) - 1\right]}{2\left[D_+ + D_-\exp(2x)\right]\left[\exp(x) - 1\right]} = \frac{D_+}{2D_-}\exp(-x)\,,$$

i.e. f_z with $z \geqslant 2$ are exponentially small. The same relation holds for $z \leqslant -2$. Thus, we can restrict our consideration to

neutral and single-charged particles which give the main contribution to the total number of particles. Under this assumption, we obtain from the set of equations (3.15):

$$\frac{f_1}{f_0}=\frac{D_+\left[\exp(x)-1\right]}{\left[D_++D_-\exp(x)\right]x}=\frac{D_+}{D_-x}\,,$$

$$\frac{f_{-1}}{f_0}=\frac{D_-\left[\exp(x)-1\right]}{\left[D_-+D_+\exp(x)\right]x}=\frac{D_-}{D_+x}\,,$$

and in this limiting case $f_0\approx 1$. The average charge of particles equals

$$\bar{z}=f_1-f_{-1}=\frac{D_+^2-D_-^2}{D_+D_-x}\,.$$

In particular, if $D_+-D_-=\Delta D\ll D_+$, this formula gives $\bar{z}=2\Delta D/(Dx)$.

In the case of a large particle of size $r\gg\lambda$, the average particle's charge is large according to formula (3.9). We now determine the distribution function of small spherical particles over charges if they are located in a quasi-neutral plasma under the restrictions $r\gg\lambda$, $r\gg e^2/T$. Considering f_z to be a continuous function of the particle's charge and introducing the variable $y=zx$, we have a normalization condition of the form

$$\int_{-\infty}^{\infty}f(y)\,\mathrm{d}y=x\,.$$

Then the kinetic equation (3.15) takes the form

$$-f(y)\left[D_+F(y)+D_-G(y)\right]+f(y-x)D_+F(y-x)$$
$$+f(y+x)D_-G(y+x)=0\,,$$

where

$$F(y)=\frac{y}{\exp(y)-1}\,,$$

$$G(y)=F(-y)=\exp(y)F(y)=\frac{y}{1-\exp(-y)}\,.$$

Let us expand the equation in a series in powers of a small parameter x. As a result we get

$$-D_+x\,\frac{\mathrm{d}}{\mathrm{d}y}\left[f(y)F(y)\right]+D_-x\,\frac{\mathrm{d}}{\mathrm{d}y}\left[f(y)F(y)\exp(y)\right]$$
$$+D_+\,\frac{x^2}{2}\,\frac{\mathrm{d}^2}{\mathrm{d}y^2}\left[f(y)F(y)\right]$$
$$+D_-\,\frac{x^2}{2}\,\frac{\mathrm{d}^2}{\mathrm{d}y^2}\left[f(y)F(y)\exp(y)\right]=0\,.$$

Restricting ourselves to linear terms, we obtain the equation

$$\frac{\mathrm{d}}{\mathrm{d}y}\left[\left(\frac{D_+}{D_-}-\exp(y)\right)f(y)F(y)\right]=0\,.$$

The solution of which has the form

$$f=\frac{C\left[\exp(y)-1\right]}{\left|D_+/D_--\exp(y)\right|}\,.$$

We see that the distribution function becomes infinite at

$$z=\frac{1}{x}\ln\frac{D_+}{D_-}\,,$$

which corresponds to the average particle's charge defined by formula (3.4).

Accounting for terms of the next order in a power expansion over a small parameter, we reduce the kinetic equation to the form

$$\frac{\mathrm{d}}{\mathrm{d}y}\left[\left(\frac{D_+}{D_-}-\exp(y)\right)f(y)F(y)\right]$$
$$-\frac{x}{2}\,\frac{\mathrm{d}^2}{\mathrm{d}y^2}\left[\left(\frac{D_+}{D_-}+\exp(y)\right)f(y)F(y)\right]=0\,. \qquad (3.16)$$

First we consider the case $D_+=D_-$, when the average particle charge is zero and the distribution function is symmetric about the reflection with respect to y, i.e. $f(y)=f(-y)$. Then the kinetic equation is written in the form

$$\frac{\mathrm{d}}{\mathrm{d}y}\left[yf(y)\right]+\frac{x}{2}\,\frac{\mathrm{d}^2}{\mathrm{d}y^2}\left[\frac{\exp(y)+1}{\exp(y)-1}\,yf(y)\right]=0\,.$$

Integration of this equation gives

$$yf(y)+\frac{x}{2}\,\frac{\mathrm{d}}{\mathrm{d}y}\left[\frac{\exp(y)+1}{\exp(y)-1}\,yf(y)\right]=C_1\,.$$

From the symmetry of the distribution function, $f(y)=f(-y)$ we have $C_1=-C_1=0$. Integrating this equation yields

$$f(y)=\frac{C}{2}\,\frac{\exp(y)-1}{\exp(y)+1}\exp\left[-\frac{2}{x}\left(2\ln\frac{1+\exp(y)}{2}-y\right)\right],$$

where the constant of integration C is the normalization constant of the distribution function. One can see that for $x\ll 1$ the main contribution to the normalization of the distribution function gives $y\sim\sqrt{x}\ll 1$. Expanding this expression in small y and using the normalization condition, we reduce the distribution function to the form

$$f(y)=\sqrt{\frac{1}{2\pi x}}\,\exp\left(-\frac{y^2}{2x}\right).$$

From this it follows that the probability for the particle to have a charge ze is given for $x\ll 1$ and $zx\ll 1$ by

$$f_z=\sqrt{\frac{x}{2\pi}}\,\exp\left(-\frac{zx^2}{2}\right). \qquad (3.17)$$

Here we shall consider the kinetic equation in the general case $D_+\neq D_-$. Let us introduce the parameter $y_0=\ln(D_+/D_-)$ and recast equation (3.16) in the range $|y-y_0|\ll 1$. In these new variables the kinetic equation (3.16) assumes the form

$$\frac{\mathrm{d}}{\mathrm{d}y}\left[(y-y_0)f(y)\right]+y\,\frac{\mathrm{d}^2f}{\mathrm{d}y^2}=0\,.$$

The normalized solution to this equation is

$$f(y)=\sqrt{\frac{1}{2\pi x}}\,\exp\left[-\frac{(y-y_0)^2}{2x}\right],$$
$$|y-y_0|\ll 1\,,\qquad x\ll 1\,. \qquad (3.18)$$

Note that the normalization of the distribution function for $x \ll 1$ is determined by just this range of the variable $|y - y_0| \ll 1$.

Along with the equilibrium charge distribution function of particles, the above analysis allows us to describe the evolution of the charge distribution function. We now analyze the evolution of the particle's charge in the simplest case $D = D_+ = D_-$. In doing so the kinetic equation takes the following form

$$\frac{\partial f}{\partial t} = 4\pi D N_0 r x \left[\frac{\partial (yf)}{\partial y} + x \frac{\partial^2 f}{\partial y^2} \right],$$

where N_0 is the number density of ions of each charge sign far from the particle. Multiplying this equation by y^2 and integrating the result over dy, we obtain

$$\frac{\mathrm{d}\overline{y^2}}{\mathrm{d}t} = -\frac{2}{\tau}(\overline{y^2} - x),$$

where the typical time for the establishment of the equilibrium charge distribution function is

$$\tau = \frac{T}{4\pi N_0 D e^2}. \tag{3.19}$$

The solution of the above equation is

$$\overline{z^2} = x\left[1 - \exp\left(-\frac{2t}{\tau}\right)\right].$$

This solution describes the character of the establishment of equilibrium for the charge distribution function of particles, and τ is a typical time of this process.

3.3 Ionization equilibrium for clusters in plasma

Above we considered the kinetic regime of charging of clusters or small particles in a plasma as a result of their collisions with plasma ions and electrons and under conditions when this process depends weakly on the character of the interaction of an attaching ion or electron with a cluster or particle. Apart from these charging processes, other processes may be responsible for cluster charging, and Fig. 5 lists these processes. Ionization of clusters by electron impact, recombination of electrons with positively charged clusters, and thermoemission of electrons from the cluster surface are additional charging processes for excited clusters in a plasma. When analyzing these processes, it is necessary to take into account the different character of these processes for small metallic and dielectric clusters. In the case of metallic clusters, electrons move freely over the entire volume of the cluster or small particle, so that the ionization equilibrium of metallic particles is similar to that of atoms and molecules. The ionization equilibrium in metallic clusters is determined by the equality of the fluxes of released and attached electrons. For large and hot metallic clusters, the flux of released electrons as a result of ionization of the particle corresponds to the thermoemission flux from the metallic surface, so that the temperature of internal electrons is responsible for this equilibrium.

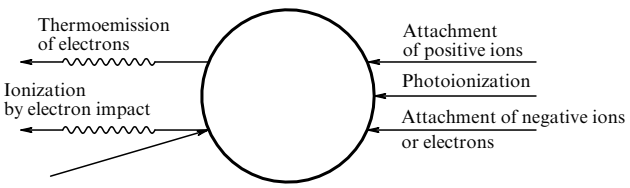

Figure 5. The processes of the cluster charging in a plasma.

Usually, the ionization potential of small particles is lower than that of the corresponding atoms and molecules. Therefore, ionization of small metallic particles occurs at relatively low electron temperatures or typical electron energies at which ionization of atoms or molecules is absent. As a result, small metallic particles located in a plasma can give a contribution to the formation of free electrons. Next, metallic particles and clusters emit electrons to and accept them from the surrounding plasma, and they can be positively or negatively charged. At high electron temperatures, metallic particles or clusters have a positive charge, while at low temperatures they are negatively charged. The character of the ionization equilibrium for a dielectric particle is different. Each dielectric particle or cluster has on its surface traps for electrons that we call active centers. Electrons are captured by these centers, and this leads to formation of negative ions located at certain points on the particle's surface. The ionization equilibrium relevant to dielectric particles in a plasma corresponds to the equilibrium of these bound negative ions and free plasma electrons. Though electrons can transit between neighboring active centers, this process proceeds slowly. The ionization equilibrium in this case results from detachment of bound negative ions from the particle's surface by electron impact and capture of free electrons by active centers on the particle's surface.

Thus, there are various processes involving clusters and small particles located in a plasma. At high temperatures, ionization of metallic particles and clusters can result from collisions of internal electrons. This leads to the formation of fast internal electrons which may be released from the cluster's surface. This process corresponds to the thermoemission of electrons from a surface of a macroscopic system. In parallel with this process, attachment of plasma electrons to the cluster establishes the charge equilibrium. As a result, metallic particles or clusters are positively charged at high temperatures owing to the electron thermoemission. At low temperatures, they are charged negatively. Usually dielectric particles are charged negatively, because their ionization potential greatly exceeds the electron affinity.

Notice that the charge equilibrium due to ionization and recombination processes takes place if the mean free path of electrons and ions significantly exceeds the particle size, i.e. the criterion opposite to (3.1) is fulfilled. In addition, the ionization processes are noticeable at not very low electron and particle temperatures, and the ionization equilibrium for charged clusters results from their collisions with electrons:

$$\mathrm{A}_n^{+Z+1} + \mathrm{e} \leftrightarrow \mathrm{A}_n^{+Z}. \tag{3.20}$$

These processes account for the interaction of a metallic particle or cluster with plasma electrons, so that the metallic particle absorbs and emits electrons. For simplicity, we assume the temperatures of free and bound electrons to be identical. Then the probability $P_Z(n)$ for a cluster consisting of n atoms to have a charge Z is determined by the Saha formula [2, 49]

$$\frac{P_Z(n) N_\mathrm{e}}{P_{Z+1}(n)} = 2\left(\frac{m_\mathrm{e} T_\mathrm{e}}{2\pi\hbar^2}\right)^{3/2} \exp\left[-\frac{I_Z(n)}{T_\mathrm{e}}\right], \tag{3.21}$$

where T_e is the electron temperature, m_e is the electron mass, N_e is the electron number density, and $I_Z(n)$ is the ionization potential of the cluster consisting of n atoms and having a charge Z.

Note that because the number density of the internal electrons in metallic clusters greatly exceeds that of the plasma electrons, the third particle in the recombination process (3.20) is a bound electron. Moreover, internal electrons can be responsible for release of initially bound electrons. Thus, if the temperatures of internal and plasma electrons are different, the Saha formula is valid, but the electron release in the equilibrium (3.20) is determined by processes involving internal cluster electrons.

Let us consider the case of a large cluster where

$$r \gg \frac{e^2}{T_e} .$$

Since the equilibrium (3.20) between the free electrons and bound electrons of a metallic cluster corresponds to a large mean free path of electrons in the plasma in comparison with the cluster radius, the interaction energy of a removed electron and a charged cluster must be included in the ionization potential of this cluster. The ionization potential $I_Z(n)$ of a large charged cluster ($n \gg 1$) differs from that of the neutral cluster $I_0(n)$ by the energy that is consumed as a result of the electron removal from the cluster's surface to infinity. Hence, we have

$$I_Z(n) - I_{Z-1}(n) = \frac{Ze^2}{r} .$$

From this it follows that

$$I_Z(n) = \frac{Z^2 e^2}{2r} + I_0(n) , \tag{3.22}$$

where $I_0(n)$ is the ionization potential of a neutral cluster.

Substituting this relation into formula (3.21), one can reduce it to the form of the Gauss formula in the limiting case $Z \gg 1$. We get

$$\frac{P_Z}{P_{Z-1}} = A \exp\left(-\frac{Ze^2}{rT_e}\right) , \tag{3.23}$$

where

$$A = \frac{2}{N_e}\left(\frac{m_e T_e}{2\pi\hbar^2}\right)^{3/2} \exp\left(-\frac{I_0}{T_e}\right) .$$

Then one can represent formula (3.23) in the form

$$\frac{P_Z}{P_0} = A^Z \exp\left(-\frac{Z^2 e^2}{2rT_e}\right) .$$

Expanding this expression near the maximum of the function $\ln P_Z(n)$, one can reduce it to the Gauss formula

$$P_Z(n) = P_{\bar{Z}}(n) \exp\left[-\frac{(Z-\bar{Z})^2}{2\Delta^2}\right] , \tag{3.24}$$

where the mean cluster charge $\bar{Z}$ and the width of the distribution function Δ are given by

$$\bar{Z} = \frac{rT_e}{e^2}\left\{\ln\left[\frac{2}{N_e}\left(\frac{m_e T_e}{2\pi\hbar^2}\right)^{3/2}\right] - \frac{I_0(n)}{T_e}\right\} , \qquad \Delta^2 = \frac{rT_e}{e^2} . \tag{3.25}$$

This formula is valid if $\Delta \gg 1$, which is fulfilled for large clusters. Note that this formula corresponds to the definition of the mean cluster charge $\bar{Z}$ through the relation $P_{\bar{Z}}(n) = P_{\bar{Z}+1}(n)$.

The cluster ionization potential in the limit $n \to \infty$ tends to the work function of the metal, and assuming $I_0(n)$ to be a continuous function of n, we have for a large cluster:

$$I_0(n) = W + \frac{\text{const}}{n^{1/3}} .$$

For a large metallic cluster, the constant in this formula (in units e^2/r_W) is equal to 1/2 [50, 51] or 3/8 [52–54] for different versions of the theory. In the same manner, we have for the const in the expression for the electron affinity of a large cluster the value $-1/2$ or $-5/8$ depending on the relevant version of the theory. According to a more in-depth theoretical analysis [55–57] and experimental data [58–61], these constants depend on the cluster material. In particular, Fig. 6 gives the size dependence for the ionization potential and electron affinity of aluminium clusters. Below we shall use a simplified method to determine this constant, assuming the above expression to be valid even for the atom ($n = 1$). This gives $\text{const} = I_0(1) - W$, where $I_0(1)$ is the atomic ionization potential, and the similar expression we shall use for the cluster electron affinity. Then employing formula (3.25) we have for the average cluster charge when it is positive:

$$\bar{Z} = \frac{T_e r}{e^2}\left\{\ln\left[\frac{2}{N_e}\left(\frac{m_e T_e}{2\pi\hbar^2}\right)^{3/2}\right] - \frac{W}{T_e} - \frac{I_0(1)-W}{T_e\, n^{1/3}}\right\} . \tag{3.26}$$

A metallic cluster or particle located in a plasma can be charged positively or negatively depending on the relation between the fluxes of electrons emitted from the cluster surface and absorbed by this surface. An equilibrium number density of electrons corresponds to the case where the cluster charge is zero at a given electron temperature. If the number density of electrons exceeds this value, the cluster is charged negatively on average, and in the opposite case it has an average positive charge. Let us denote by N_+ the number density of positive single-charged clusters, and by N_- the number density of clusters of a unit negative charge.

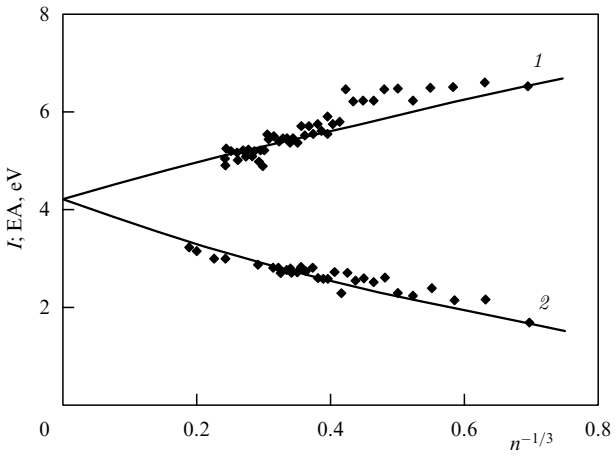

Figure 6. The size dependence of the ionization potentials of aluminium clusters (curve *1*) and the electron affinities of aluminium clusters (curve *2*) according to experimental (marks) and theoretical (curves) data [61].

Evidently, the sign of the mean cluster charge coincides with the sign of the quantity $\ln(N_+/N_-)$. In other words, if $N_+/N_- > 1$, the mean cluster charge is positive, and for $N_+/N_- < 1$ it is negative. Let us employ the Saha relation for determining the ratio between the number densities of positively charged N_+ and neutral N_0 clusters:

$$\frac{N_+ N_e}{N_0} = 2\left(\frac{m_e T_e}{2\pi\hbar^2}\right)^{3/2} \exp\left[-\frac{I_0(n)}{T_e}\right],$$

where N_e is the electron number density, and $I_0(n)$ is the ionization potential of a neutral cluster consisting of n atoms. In the same way one can express the ratio between the number densities of neutral and negatively charged clusters through the cluster electron affinity.

Let us connect the cluster ionization potential with the atomic ionization potential $I_0(1)$ and the work function W of the corresponding surface as was done above. By the same method we connect the cluster electron affinity with the electron affinity EA of the atom and the work function W. Then we get

$$\frac{N_+}{N_-} = \zeta^2 \exp\left(-\frac{\Delta}{T_e n^{1/3}}\right),$$

where

$$\zeta = \frac{2}{N_e}\left(\frac{m_e T_e}{2\pi\hbar^2}\right)^{3/2} \exp\left(-\frac{W}{T_e}\right), \qquad (3.27)$$

and $\Delta = I_0(1) + \mathrm{EA} - 2W$. Table 6 contains the parameters of this formula and the characteristic temperature T_* at which $N_+ = N_-$. Thus, a metallic cluster is positively charged at high temperatures, and negatively charged at low temperatures. As a demonstration of this fact, Fig. 7 gives the average charge of tungsten clusters in a plasma as a function of the cluster temperature, and also the cluster temperature T_* at which this cluster becomes neutral on average, i.e.

$$\ln\zeta(T_*) = \frac{\Delta}{2T_e n^{1/3}}.$$

Table 6. Parameters† of charged metallic clusters.

Element	I, eV	W, eV	EA, eV	Δ, eV	T_*, 10^3 K	$\bar{Z}/n^{1/3}$
Ti	6.82	3.92	0.08	−0.96	2.51	0.084
V	6.74	4.12	0.52	−0.98	2.63	0.078
Fe	7.90	4.31	0.15	−0.57	2.75	0.074
Co	7.86	4.41	0.66	−0.30	2.82	0.073
Ni	7.64	4.50	1.16	−0.20	2.87	0.072
Zr	6.84	3.9	0.43	−0.53	2.51	0.093
Nb	6.88	3.99	0.89	−0.21	2.57	0.085
Mo	7.10	4.3	0.75	−0.75	2.74	0.081
Rh	7.46	4.75	1.14	−0.90	3.00	0.078
Pd	8.34	4.8	0.56	−0.70	3.04	0.080
Ta	7.89	4.12	0.32	−0.03	2.65	0.085
W	7.98	4.54	0.82	−0.28	2.90	0.081
Re	7.88	5.0	0.2	−1.92	3.12	0.080
Os	8.73	4.7	1.1	0.43	3.01	0.078
Ir	9.05	4.7	1.56	1.21	3.03	0.080
Pt	8.96	5.32	2.13	0.45	3.38	0.081
Au	9.23	4.30	2.31	2.94	2.85	0.083

† I is the atomic ionization potential; W is the metal work function; EA is the atom electron affinity; $\Delta = I + \mathrm{EA} - 2W$; T_* is the temperature when the number densities of positively and negatively charged clusters are equalized at the average cluster size $n = 1000$ and the electron number density $N_e = 10^{13}$ cm^{-3}, and $\bar{Z}$ is the average cluster negative charge at temperature 1000 K with argon as the buffer gas if the cluster charging is determined by processes of attachment of electrons and positive ions to the cluster.

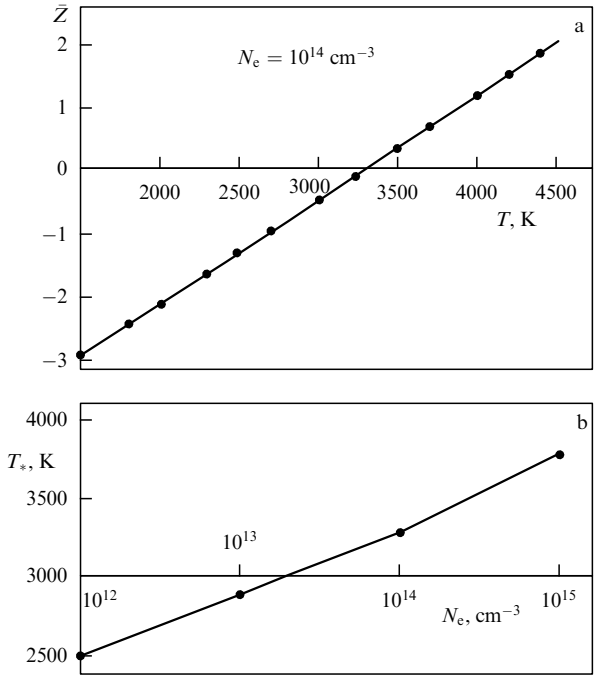

Figure 7. Dependence of the mean charge of a tungsten cluster consisting of $n = 1000$ atoms on the electron temperature in a plasma with the number density of electrons $N_e = 10^{14}$ cm^{-3} (a), and the electron number density dependence of the electron temperature at which this cluster charge is zero (b).

From formula (3.26) it follows that the basic dependence of the cluster charge on its size is $\bar{Z} \sim n^{1/3}$, and the coefficient of proportionality depends on the cluster temperature. In the limit of large clusters, this formula can be represented in the form

$$\bar{Z} = z n^{1/3}(T_e - T_*), \qquad z = \frac{W r_W}{e^2 T_*}, \qquad (3.28)$$

where r_W is the Wigner–Seitz radius, and T_* is the electron temperature at which the cluster charge is zero. Notice that the parameter z depends on the electron number density through the variable T_*.

The number density of electrons N_e in formulas (3.26)–(3.28) leans upon a free parameter which does not depend on cluster characteristics. Now we consider another case when this quantity is determined by the ionization of clusters. This is realized at a high density of clusters. We shall consider the case when $T > T_*$, and the number density of electrons results from their thermoemission from the cluster surface. Assuming the plasma to be quasi-neutral, we have $N_e = \bar{Z} N_{cl}$, where $\bar{Z}$ is the average cluster charge, and N_{cl} is the number density of clusters. The balance of rates per unit volume for the processes of thermoemission of electrons and attachment of electrons to clusters takes the form

$$\nu_{em} N_{cl} n^{2/3} = N_e N_{cl} k_e n^{2/3},$$

where v_{em} is the rate of the electron thermoemission process, $k_e = (8T_e/\pi m_e)^{1/2}\pi r_W^2$ is the reduced rate constant of electron–cluster collisions. From this we have for the average cluster charge

$$\bar{Z} = \frac{v_{em}(T)}{k_e N_{cl}} . \tag{3.29}$$

It follows from this formula that clusters tend to be neutral at low temperatures and large densities of clusters.

We now can find the charge distribution for negatively charged metallic clusters if the temperatures of internal and free electrons are identical. The cluster radius is small compared to the mean free path of electrons, and the Coulomb interaction of an electron with the cluster charge on its surface greatly exceeds the electron thermal energy. Assume the identical character of electron thermoemission for charged and neutral metallic clusters.

As above, the balance of reaction rates for formation and destruction of negatively charged metallic clusters has the form

$$N_{-Z}N_e\pi r^2\overline{\left(v - \frac{2Ze^2}{rm_e v}\right)} = N_{-(Z+1)}4\pi r^2\,\frac{em_eT_e^2}{2\pi^2\hbar^2}\exp\left(-\frac{EA}{T_e}\right),$$

where the bar means averaging over electron velocities. Here we assume that the electron release proceeds near the cluster's surface, and hence it is determined by the electron affinity EA of the neutral cluster. The cluster field accelerates the released electron and removes it from the surface. Therefore, the difference in the electron thermoemission process for clusters of different charges is observed far from the cluster's surface.

In the limit $Ze^2/r \gg T_e$, the above formula takes the form

$$\frac{N_{-Z}N_e}{N_{-(Z+1)}} = 2\left(\frac{m_eT_e}{2\pi\hbar^2}\right)^{3/2}\exp\left(-\frac{EA}{T_e}\right)\exp\left(-\frac{Ze^2}{rT_e}\right).$$

Note that Z in this formula is a positive quantity. A low rate constant of electron attachment to a strongly, negatively charged cluster does not allow for a metallic cluster to have very high negative charge in a rarefied ionized gas.

Let us find the charge of a negatively charged metallic cluster on the basis of the above formula. We shall define the average cluster charge to be $-(Z+1/2)$ if $N_{-Z} = N_{-(Z+1)}$. Then the above formula yields

$$\bar{Z} = \frac{1}{2} + \frac{rT_e}{e^2}\ln\frac{1}{\zeta} \tag{3.30}$$

for the average negative charge $-\bar{Z}$ of a metallic cluster, where the quantity ζ is defined by formula (3.27). It is seen that a metallic cluster can have large negative charge at high electron temperatures, large cluster sizes or small number densities of electrons when $\zeta \ll 1$. Because we neglect here the formation of positive ions, this formula differs from formula (3.27) near $\zeta \sim 1$.

3.4 Ionization processes involving metallic clusters

Above we considered the ionization equilibrium for a metallic cluster or particle, which is established as a result of ionization and recombination processes. Now we consider the character of ionization processes in detail, which allows us to analyze the regimes of cluster charging when this equilibrium is violated. First we evaluate the density of electric current from a large metallic surface by leaning upon the equilibrium between this process and the process of electron attachment to the surface, proceeding in a surrounding plasma.

We assume that particles containing n atoms are located in a hot gas, and electrons are emitted into this gas from the particle surfaces. In the limit of large particles, the parameter $Ze^2/(rT_e)$ becomes small. Taking the formulas (3.25), (3.26) to the limit $Z \to 0$, $n \to \infty$, we obtain

$$N_e = 2\left(\frac{m_eT_e}{2\pi\hbar^2}\right)^{3/2}\exp\left[-\frac{I_0(n)}{T_e}\right]$$

for the equilibrium number density of free electrons near the particle surface. We take into account in this case that the electron temperature T_e coincides with the particle temperature T, i.e. the temperature of free and bound electrons is the same. Correspondingly, from the equality between the currents of attached and emitted electrons, for the density of current emitted from a large surface of this metallic particle we get

$$i = eN_e\sqrt{\frac{T_e}{2\pi m_e}} = \frac{em_eT_e^2}{2\pi^2\hbar^2}\exp\left(-\frac{W}{T_e}\right), \tag{3.31}$$

where $N_e\sqrt{T_e/(2\pi m_e)}$ is the flux of electrons attached if the probability of attachment as a result of the electron's contact with the surface is close to unity. Next, we replaced in this formula the ionization potential of a large metallic particle by the work function W of the corresponding metallic surface. This formula is called the Richardson–Dushman formula and describes the thermoemission current from a hot metallic surface.

It is convenient to rewrite the Richardson–Dushman formula (3.31) for the thermoemission current density in the form

$$i = A_R T_e^2\exp\left(-\frac{W}{T_e}\right), \qquad A_R = \frac{em_e}{2\pi^2\hbar^3}, \tag{3.32}$$

and the Richardson parameter A_R according to formula (3.32) is equal to 120 A $(\text{cm}^2\,\text{K}^2)^{-1}$. Table 7 contains values of this parameter for some real metals.

In order to understand the nature of the thermoemission process at hand, we shall evaluate the thermoemission current from a metallic surface using the properties of a metallic plasma inside the particle. We assume the metallic plasma to be similar to a degenerate electron gas, and that the

Table 7. Parameters of the electron current for thermoemission of metals [21, 62]; i_b is the electron current density at the boiling point, and T_b is the metal boiling point.

Metal	A_R, A $(\text{cm}^2\,\text{K}^2)^{-1}$	W, eV	T_b, K	i_b, A cm^{-2}
Ba	60	2.49	1910	600
Cs	160	1.81	958	0.045
Cu	60	4.4	2868	4.6
Mo	51	4.3	5070	8.8×10^4
Nb	57	4.0	5170	2.1×10^5
Pd	60	4.8	3830	240
Re	720	5.0	5870	2.3×10^6
Ta	55	4.1	5670	3.3×10^5
Th	70	3.3	4470	2.2×10^5
Ti	60	3.9	3280	750
W	75	4.5	5740	2.8×10^5
Y	100	3.3	3478	3.5×10^3
Zr	330	3.9	4650	2.4×10^5

distribution function of electrons over momenta is given by the Fermi – Dirac formula

$$f(\mathbf{p})\,\mathrm{d}\mathbf{p} = \frac{2\mathrm{d}\mathbf{p}}{(2\pi\hbar)^3}\left[1+\exp\left(\frac{\varepsilon-\mu}{T}\right)\right]^{-1}.$$

Here, $\mathbf{p} = m_\mathrm{e}\mathbf{v}$ is the electron momentum, $\mathbf{v}$ is the electron velocity, $\varepsilon = p^2/(2m_\mathrm{e})$ is the electron kinetic energy, and $\mu = \varepsilon_\mathrm{F}$ is the chemical potential or the Fermi energy for this distribution. The electron is liberated if its kinetic energy in the direction toward the metal surface exceeds the quantity $\varepsilon_\mathrm{F} + W$, where W is the metal's work function. Hence, the flux of electrons released from the metal surface is equal to $\int v_x f(\mathbf{p})\,\mathrm{d}\mathbf{p}$, where the integral is taken over velocities of electrons satisfying the inequality $m_\mathrm{e}v_x^2/2 \geqslant \varepsilon_\mathrm{F} + W$, and v_x is the component of the electron velocity normal to the surface.

Notice that because $W \gg T$, one can neglect unity compared to the exponent in the denominator of the Fermi – Dirac formula, so that it takes the form of the Boltzmann formula. In this case, the number density of electrons in the momentum interval from $\mathbf{p}$ up to $\mathbf{p} + \mathrm{d}\mathbf{p}$ and in the energy range $\varepsilon - \mu \gg T$ is given by

$$f(\mathbf{p})\,\mathrm{d}\mathbf{p} = \frac{2\mathrm{d}\mathbf{p}}{(2\pi\hbar)^3}\exp\left(-\frac{\varepsilon-\mu}{T}\right).$$

Using cylindrical coordinates $\mathrm{d}\mathbf{p} = 2\pi p_\rho\,\mathrm{d}p_\rho\,\mathrm{d}p_x$ and $\varepsilon = p_x^2/(2m_\mathrm{e}) + p_\rho^2/(2m_\mathrm{e})$, we obtain for the flux of released electrons

$$j = 2\pi m_\mathrm{e}T\int\frac{m_\mathrm{e}v_x\,\mathrm{d}v_x}{4\pi^3}\exp\left(-\frac{m_\mathrm{e}v_x^2}{2T}+\frac{\mu}{T}\right) = \frac{m_\mathrm{e}T^2}{2\pi^2\hbar^3}\exp\left(-\frac{W}{T}\right).$$

Considering that the electron current density $i = ej$, we find that this expression coincides with (3.32). Thus, we obtained identical results for the electron thermoemission current densities both from the equilibrium of a metal surface with a surrounding plasma and from the evaporation of bound electrons from an internal metallic plasma modelled by a degenerate electron gas. Note that the energy spectrum of electrons released as a result of thermoemission is described by the factor $\sim\exp(-\varepsilon/T)$, as follows from the above formulas. In reality, along with this spectrum, a resonant tail is observed in the electronic spectrum [63, 64], which is determined by the cluster electronic structure. The resonant structure of the electronic spectrum, which is defined by positions of cluster electronic levels, is more essential for the photoabsorption electronic spectrum (see, for example, Refs [65 – 69]).

We now ascertain the role of internal and plasma electrons in cluster ionization. Release of electrons from the surface of a metallic particle or cluster is determined by two processes — thermoemission of electrons and cluster ionization by plasma electrons. Below we shall find the contribution of these processes to the release of bound electrons from a metallic cluster. If the temperature of internal electrons is not equal to the temperature of free electrons, the thermoemission current of electrons from the surface of a metallic cluster is determined by the cluster temperature, while the current of electrons released due to cluster ionization by the plasma electrons is defined by the electron temperature of the plasma. Below we shall estimate the role of plasma electrons in ionization of a metallic cluster.

We take a simple model for the interaction of electrons with a metal surface, according to which the surface effective potential has the form of rectangular walls in a space region, and the depth of this potential well is W, the metal's work function. For collisions of plasma electrons with internal ones we use the Thomson model of pair collisions. Within the framework of this model, the internal electron energy is zero at collision with an incident electron, and interaction with surrounding electrons and ions is absent in the course of collisions between the plasma and internal electrons. The energy ε of an incident electron satisfies the relation $\varepsilon \sim T_\mathrm{e} \ll W$, where T_e is the temperature of the plasma electrons. Penetrating the metal region, this electron obtains the energy $\varepsilon + W$. The collision cross section resulting in that a plasma electron transfers to an internal electron an energy in the interval from $\Delta\varepsilon$ to $\Delta\varepsilon + \mathrm{d}\Delta\varepsilon$ is given by the Rutherford formula

$$\mathrm{d}\sigma = \frac{\pi e^4}{\varepsilon+W}\,\frac{\mathrm{d}\Delta\varepsilon}{\Delta\varepsilon^2}.$$

An incident electron is captured by the metal surface if the energy transfer to an internal electron exceeds ε but does not exceed W, so that both colliding electrons are closed in the metal potential well. Hence, the rate constant of this process is

$$k_\mathrm{cap} = \int f(\varepsilon)\,\mathrm{d}\varepsilon\int_\varepsilon^W \mathrm{d}\sigma.$$

Here $f(\varepsilon)$ is the Maxwellian distribution function of plasma electrons, which is normalized to unity. Introducing $x = \varepsilon/T_\mathrm{e}$, we have

$$f(\varepsilon)\,\mathrm{d}\varepsilon = 2\pi^{-1/2}x^{1/2}\exp(-x)\,\mathrm{d}x.$$

From this it follows

$$k_\mathrm{cap} = \frac{\pi e^4}{WT_\mathrm{e}}\sqrt{\frac{8T_\mathrm{e}}{\pi m_\mathrm{e}}}$$

for the effective rate constant of capture of a plasma electron due to its collision with an internal electron of the metal surface, if we take into account $T_\mathrm{e} \ll W$.

Let us compare this rate constant with that of the ionization process affecting internal electrons under action of plasma electrons, which is given within the framework of the Thomson model by the formula

$$k_\mathrm{ion} = \int_W^\infty f(\varepsilon)\,\mathrm{d}\varepsilon\int_W^\varepsilon \mathrm{d}\sigma = \frac{\pi e^4}{W^2}\sqrt{\frac{8T_\mathrm{e}}{\pi m_\mathrm{e}}}\exp\left(-\frac{W}{T_\mathrm{e}}\right) = k_\mathrm{cap}\,\frac{T_\mathrm{e}}{W}\exp\left(-\frac{W}{T_\mathrm{e}}\right). \qquad (3.33)$$

Note that release of an internal electron takes place if the energy obtained by this electron exceeds W, but does not exceed the energy of the incident electron ε, so that both colliding electrons leave the metal potential well. Next, since the cluster temperature is relatively small, the thermal energy of internal electrons does not influence this process.

From this it follows that the ionization rate constant is small compared to that of electron capture, because $W \gg T_\mathrm{e}$.

We shall obtain the cluster equilibrium charge from the equality between the rate of thermoemission of internal electrons and the rate of capture of plasma electrons. Because the rate of capture of plasma electrons is large compared to the rate of release of internal electrons in collisions with plasma electrons, the cluster ionization process due to plasma electrons turns out to be weak compared to the thermoemission process. Hence, plasma electrons do not influence the charge equilibrium of metallic clusters.

Let us analyze now the character of recombination of free electrons with a small metallic particle. Above we considered various conditions for the charging of a small particle. If the particle radius r is large compared to the mean free path λ of ions and electrons in the buffer gas where the particle is located, the charging process is determined by collisions of ions and electrons with gaseous atoms. This proceeds at large distances from the particle's surface compared to λ, so that the character of interaction of electrons and ions with the particle's surface is not essential for the charging process. Hence, the particle's charge is determined by plasma parameters only, and the character of the charging process is identical both for metallic and dielectric particles.

In the case $\lambda \gg r$, the character of charging of a particle is determined by processes near the particle's surface and is different for dielectric and metallic particles. At high temperatures, metallic particles have a positive charge due to the electron thermoemission process. At low temperatures, the charging process is determined by attachment of electrons and positive ions to the particle's surface, and this process is identical in character for metallic and dielectric particles.

Considering the charge equilibrium for a charged metallic particle of small size, we assumed the processes of electron evaporation and electron attachment to be similar to those for a neutral metallic particle. We now find the correction to the average particle charge due to the difference between the electron attachment cross sections for charged and neutral metallic particles. In the equilibrium conditions (3.20), we have the following equality between the rates of formation and destruction of particles of a given charge:

$$N_{Z+1} N_e k_{at} = N_Z \, 4\pi r^2 i \,.$$

Here, N_Z is the number density of metallic particles having a charge Z, r is the particle's radius, k_{at} is the rate constant of electron attachment to a particle of a charge $Z+1$, and i is the thermoemission current density. According to the definition, we have

$$\frac{N_Z}{N_{Z+1}} = \frac{P_Z}{P_{Z+1}} \,,$$

where P_Z is the probability for a particle to have a charge Z.

We first consider the charge equilibrium for a neutral particle, when the rate constant of electron attachment is given by formula (2.2). Using formula (3.32) for the thermoemission current density and replacing in this formula the metal's work function W with the cluster ionization potential I, we obtain from the above balance equation:

$$\frac{N_{Z+1} N_e}{N_Z} = 2\left(\frac{m_e T_e}{2\pi\hbar^2}\right)^{3/2} \exp\left(-\frac{I}{T_e}\right) . \tag{3.34}$$

This is the Saha formula (3.21) for the charge distribution of particles.

Now let us take into account the particle charge in the electron attachment process. Accounting for the Coulomb interaction between an electron and particle, which is modelled by a spherical liquid drop, we have for the rate constant of this process

$$k_{at} = \pi r^2 \overline{\left(v + \frac{2Ze^2}{r m_e v}\right)} \,,$$

where the over-line means an average over electron velocities v. Using the Maxwellian velocity distribution function of electrons, we obtain

$$\frac{N_{Z+1} N_e}{N_Z} = \left(1 + \frac{Ze^2}{r T_e}\right)^{-1} 2\left(\frac{m_e T_e}{2\pi\hbar^2}\right)^{3/2} \exp\left(-\frac{I}{T_e}\right)$$

from the equilibrium condition for the charging processes. It is seen that this formula coincides with the Saha formula in the limit $Ze^2/r \ll T_e$. Violation of this criterion leads to a decrease in the mean particle charge because the cross section of electron attachment to a positively charged particle increases. Note that we assumed an identical character for thermoemission of charged and neutral metallic particles.

3.5 Charging of dielectric particles in plasma

Above we discussed the different character of charging of metallic and dielectric particles in a plasma when the particle size is small in comparison with the mean free path of electrons and ions. In the case of metallic particles, the ionization equilibrium is established due to processes (3.20), so the recombination process involves free and bound electrons. In the case of dielectric particles, the ionization equilibrium results from the processes

$$\begin{aligned} &e + A_n^{-Z} \to \left(A_n^{-(Z+1)}\right)^{**} , \\ &\left(A_n^{-(Z+1)}\right)^{**} + A \to A_n^{-(Z+1)} + A \,, \\ &B^+ + A_n^{-(Z+1)} \to B + A_n^{-Z} \,, \end{aligned} \tag{3.35}$$

so an autodetachment state $\left(A_n^{-(Z+1)}\right)^{**}$ is quenched in collisions with surrounding atoms. Because the rate constant of pair attachment of an electron to a dielectric particle greatly exceeds the ionization rate constant of the particle by electron impact, this particle is charged negatively.

In contrast to metallic particles, the binding energies for active centers do not depend on particle size because the action of each center is concentrated in a small region of space. Evidently, the number of such centers is proportional to the area of the particle's surface, and for particles of micron size this quantity is large compared to that occupied by the ions captured. Hence, above and below we consider the regime of charging of a small dielectric particle as being far from the saturation of active centers. Then positive and negative charges can exist simultaneously on the particle's surface. They travel over the surface and can recombine there. Usually, the binding energy of electrons in negative active centers falls in the range $EA = 2-4$ eV, and the ionization potential needed for the production of positive active centers is of order $J_0 \approx 10$ eV. Hence, a small dielectric particle has a negative charge in a weakly ionized gas.

Due to its charge Z, the particle obeys the electric potential $\varphi = Ze/r$ with respect to a surrounding plasma, where r is the particle's radius. If $e\varphi < EA$, the electronic state is stable, while in the case $e\varphi > EA$ an electron tunnel

transition is possible that leads to decay of the electronic state. Hence, an isolated charged particle may emits electrons until its charge exceeds the limiting value

$$Z_* = r\,\frac{\mathrm{EA}}{e^2}\,. \tag{3.36}$$

In particular, for a dielectric particle of radius $r = 1$ μm, when EA = 3 eV, this charge is $Z_* = 2 \times 10^3$, and the particle's electric potential is equal to 3 V.

Notice that for the regime under consideration the number of active centers is large in comparison with the occupied ones, i.e. with the particle's charge. This is valid for micron particles. In particular, the above numerical example corresponds to distances between neighboring charged centers of about 0.3 μm, which are larger by one or two orders of magnitude than the typical distance between neighboring active centers. One more condition is required in the case when the particle's negative charge exceeds Z_*. Then the bound states of captured electrons become autodetachment states and can decay as a result of tunnel electron transitions. In this case the rate of capture of electrons must exceed the rate of decay of autodetachment states, i.e. the lifetime of the autodetachment state must be fairly large.

Let us estimate the lifetime of the autodetachment state of a negatively charged center locating on the surface of a dielectric particle. Its decay results from the electron tunnel transition, and the probability per unit time for an electron penetration through the potential barrier has the following exponential dependence

$$\frac{1}{\tau} \sim \exp(-2S)\,, \qquad S = \int_r^{R_\mathrm{c}} \mathrm{d}R\,\sqrt{\frac{2m_\mathrm{e}}{\hbar^2}\left[\mathrm{EA} - U(r) + U(R)\right]}\,.$$

Here EA is the electron binding energy in the active center, $U(R) = Ze^2/R$ is the interaction potential of an electron with the Coulomb field of the particle if its distance from the particle's center is R, and R_c is the turning point, i.e.

$$R_\mathrm{c} = \frac{r}{1 - \mathrm{EA}/\varepsilon_0}\,,$$

where $\varepsilon_0 = Ze^2/r$. Thus we have

$$S = \frac{\pi}{2}\,r\,\sqrt{\frac{2m_\mathrm{e}}{\hbar^2}\,\frac{\varepsilon_0}{1 - \mathrm{EA}/\varepsilon_0}}\,. \tag{3.37}$$

Assuming ε_0 to be of the order of a typical atomic value, we obtain $S \sim r/a_0$, where a_0 is the Bohr radius. For small particles of micron sizes, we obtain a very high lifetime for the surface negative ions with respect to the electron tunnel transition. Hence, under real conditions a particle's charge can exceed the limiting value Z_* resulting from processes (3.35).

Let us determine the charge of a small dielectric particle that emerges from the equilibrium of this particle with a surrounding electron gas. This equilibrium is similar to the Langmuir isotherm for the equilibrium of a surface with a gas, when gaseous atoms or molecules are absorbed by the active centers on the surface. In this case, the equilibrium state is described by the scheme

$$\mathrm{A} + \mathrm{e} \longleftrightarrow \mathrm{A}^-\,, \tag{3.38}$$

where A denotes an active center of the surface, and A^- is a bound negative ion. Denoting the total number of active centers on the particle's surface by p and the electron binding energy by EA, we have from this equilibrium

$$\frac{(p - Z)N_\mathrm{e}}{Z} = g\left(\frac{m_\mathrm{e}T_\mathrm{e}}{2\pi\hbar^2}\right)^{3/2}\exp\left(-\frac{\mathrm{EA}}{T_\mathrm{e}}\right).$$

Here, N_e is the number density of free electrons, Z is the particle charge or the number of bound electrons in the active centers, and $g \sim 1$ is the combination of the statistical weights of an electron, active center, and bound negative ion. Below, for simplicity, we shall take $g = 1$. From this we have for the particle charge in the limit $Z \ll p$:

$$Z = N_\mathrm{e}\,p\left(\frac{2\pi\hbar^2}{m_\mathrm{e}T_\mathrm{e}}\right)^{3/2}\exp\left(\frac{\mathrm{EA}}{T_\mathrm{e}}\right). \tag{3.39}$$

Because the number of active centers on the surface is proportional to its area, we obtain

$$Z \sim n^{2/3}\,.$$

Since the particle's radius is $r \sim n^{1/3}$, the electric potential of a large dielectric particle is

$$\varphi \sim \frac{Ze}{r} \sim n^{1/3}\,.$$

Therefore, the interaction of surface electrons with the electric potential of a negatively charged dielectric particle may be responsible for the negative charge of the large particle.

Let us analyze the character of the detachment of the surface bound negative ions from a dielectric particle as a result of interaction with a surrounding plasma, providing the mean free path of electrons and ions in a gas is large compared to the particle size. In the first channel of this process, detachment of surface negative ions is determined by collisions with free electrons according to the scheme (3.38). Another mechanism for this process is determined by the charge exchange process involving positive ions of the plasma, when loss of a bound electron of the negative ion results from its transfer to the field of the positive ion. Let us compare the rates of detachment of surface negative ions due to these processes. The rate of detachment of a bound negative ion in collisions with electrons is estimated as

$$\nu_\mathrm{e} \sim Zv_\mathrm{e}\sigma_0\exp\left(-\frac{\varepsilon_0}{T_\mathrm{e}}\right)N_\mathrm{e}\,,$$

where $v_\mathrm{e} \sim \sqrt{T_\mathrm{e}/m_\mathrm{e}}$ is a typical electron velocity, where T_e is the electron temperature, m_e is the electron mass; σ_0 is of the order of the cross section of the negative ion, and ε_0 is the electron binding energy on the surface of the particle. There are two ways for the recombination of free positive ions with bound negative ions. Via the first one, a positive ion captures a weakly bound electron of a surface negative ion as a result of the charge exchange process. The rate constant of this recombination process is defined to an order of magnitude as

$$\nu_\mathrm{i} \sim Zv_\mathrm{i}\,\sigma_\mathrm{ex}N_\mathrm{i}\,,$$

where $v_\mathrm{i} \sim \sqrt{T/m_\mathrm{i}}$ is a typical ion velocity, so that T is the ion temperature, m_i is the ion mass; σ_ex is the cross section of the charge exchange process for an incident positive ion and a bound negative ion, and N_i is the number density of positive ions. Assuming $\sigma_\mathrm{ex} \sim \sigma_0$ and accounting for the plasma's

quasi-neutrality condition $N_i = N_e$, we obtain for $T_e > T$ that the criterion $v_e \gg v_i$ assumes the form

$$T_e \gg 2\varepsilon_0 \left[\ln\left(\frac{T_e}{T}\frac{m_i}{m_e}\right)\right]^{-1}. \tag{3.40}$$

From this it follows that formula (3.39) for the charge of a dielectric particle can be valid at high electron temperatures.

In the case of the second channel for the recombination of positive and bound negative ions, each contact between a positive ion and the particle's surface leads to ion attachment. Then recombination takes place as a result of the drift of a bound electron along the particle's surface. In this situation the rate of the recombination process for free positive and bound negative ions is equal to

$$\nu_i \sim \pi r^2 v_i N_i\,,$$

where r is the particle's radius. In that event detachment of bound negative ions as a result of capture of positive ions by the particle's surface is preferable.

Comparing the cases of strongly negatively charged metallic and dielectric particles, note that all the electrons of a metallic particle participate in the charging process, while in the event of a dielectric particle, electrons are captured by active centers independently. Hence, the negative charge of a dielectric particle may greatly exceed that of a metallic particle. A typical negative charge of a dielectric particle is of the order of the critical charge Z_* below which a stable surface negative ion exists. This charge is given by formula (3.36), while formula (3.30) for the charge of a negatively charged metallic particle can be represented in the form

$$\bar{Z} = Z_* + \frac{1}{2} + \frac{rT_e}{e^2}\ln\frac{1}{\chi}\,, \quad \text{where} \quad \chi = \frac{2}{N_e}\left(\frac{m_e T_e}{2\pi\hbar^2}\right)^{3/2}. \tag{3.41}$$

Since

$$\frac{1}{\chi} \ll N_e a_0^3 \ll 1\,,$$

where a_0 is the Bohr radius, we have

$$Z_* - \bar{Z} \gg 1$$

for a strongly negatively charged metallic particle located in an ionized gas.

Thus, the character of cluster charging and its charge equilibrium with a surrounding plasma are determined by the processes of thermoemission of electrons from the cluster surface and collision processes which establish the cluster charge. These processes and possible regimes of cluster charging are given above.

4. Processes in cluster plasmas

4.1 Cluster growth in cluster plasmas

The growth of clusters in a cluster plasma proceeds via an atom attachment to the cluster and inverse processes which are characterized by the scheme (1.1), and also by a coagulation process according to the scheme

$$\mathrm{M}_{n-m} + \mathrm{M}_m \to \mathrm{M}_n\,. \tag{4.1}$$

For coagulation, evolution of the size distribution function f_n is described by the Smoluchowski equation [70]

$$\frac{\partial f_n}{\partial t} = -f_n \int k(n,m) f_m \,\mathrm{d}m + \frac{1}{2}\int k(n-m,m) f_{n-m}\, f_m \,\mathrm{d}m\,. \tag{4.2}$$

Here, $k(n-m,m)$ is the rate constant of the process (4.1), the multiplier $1/2$ accounts for the fact that collisions of clusters consisting of $n-m$ and m atoms are present in the equation twice, and the distribution function is normalized as $\int f_n \,\mathrm{d}n = N_{cl}$, where N_{cl} is the number density of clusters. If the rate constant of cluster association does not depend on cluster size, the Smoluchowski equation has a simple solution $f_n(t) \sim \exp(-n/\bar{n})$ [71, 72], where the average cluster size is introduced as

$$\bar{n} = \frac{N_b}{N_{cl}} \tag{4.3}$$

and N_b is the total number density of bound atoms in clusters. In this situation the average cluster size varies as [71, 72]

$$\bar{n} = \frac{N_b k_{as} t}{2}\,, \tag{4.4}$$

if one resorts to the definition (4.3) of the average cluster size. For large clusters or particles, when the condition (3.1) is fulfilled, the rate constant of cluster association does not depend on size, and this is realized for nucleation of particles in the Earth's atmosphere [73]. In the opposite case, when the typical cluster size is small in comparison with the mean free path of gaseous atoms, the rate constant of association of two clusters $k(n,m)$ of sizes n and m, which within the framework of the liquid drop model for clusters is the rate constant of their approach up to contact, is given by

$$k(n,m) = k_0 (n^{1/3} + m^{1/3})^2 \sqrt{\frac{n+m}{nm}}\,, \tag{4.5}$$

where k_0 is defined by formula (2.2).

Integrating the Smoluchowski equation (4.2), we now obtain

$$\frac{\mathrm{d}\bar{n}}{\mathrm{d}t} = k_0 N_b I \bar{n}^{1/6},$$

$$I = \frac{1}{2}\int_0^\infty\int_0^\infty (x^{1/3} + y^{1/3})^2 \sqrt{\frac{x+y}{xy}}\exp(-x-y)\,\mathrm{d}x\,\mathrm{d}y = 3.4\,, \tag{4.6a}$$

which leads to

$$\bar{n} = 3.5(N_b k_0 t)^{1.2}\,. \tag{4.6b}$$

According to numerical calculations [74], the coefficient in this formula is equal to 3.2 for the definition (4.3) of the average cluster size. Because this consideration relates to large clusters, the above formulas are valid under the condition

$$k_0 N_b t \gg 1\,. \tag{4.7}$$

Notice that cluster growth processes (1.1) and (4.1) are different in nature. First, the process (4.1) usually proceeds in one direction, whereas attachment and evaporation processes (1.1) balance out each other. Second, the process (4.1) is practically forbidden for charged clusters because the repulsion of clusters prevents them from approaching. Third, the

processes (1.1) proceed in a plasma containing an atomic vapor, whereas the process (4.1) is not concerned with the presence of an atomic vapor.

In the regime of cluster growth, when we start from an atomic vapor, the first stage in the transformation of an atomic vapor into a gas of clusters centers around the three-body process [19] which proceeds according to the scheme

$$2\mathrm{M} + \mathrm{A} \rightarrow \mathrm{M}_2 + \mathrm{A}\,, \tag{4.8}$$

where M is a metal atom, and A is an atom of the buffer gas. Correspondingly, the number density of diatomic molecules N_2 is determined by the balance equation

$$\frac{\mathrm{d}N_2}{\mathrm{d}t} = KN_{\mathrm{a}}N^2\,, \tag{4.9}$$

where K is the rate constant of the three-body process of interest, N_{a} is the number density of atoms of the buffer gas, and N is the number density of free atoms of a nucleating vapor. We assume that starting from diatomic molecules, the cluster growth process goes as a result of pair processes (1.1), (4.1). Then the diatomic molecules that form are the condensation nuclei for clusters. Provided that

$$KN_{\mathrm{a}}N\tau \ll 1\,,$$

formation of diatomic molecules does not influence the balance of metal atoms. Below we shall consider this regime of nucleation in order to estimate a typical time for the transformation of an atomic vapor into clusters.

According to equation (4.9), the number density of diatomic molecules formed in a time τ from the start of nucleation is estimated as

$$N_2 \sim KN_{\mathrm{a}}N^2\tau\,.$$

Then each molecule is a center of condensation at which a cluster grows with the rate constant (2.2), so that after a time τ a typical cluster size is

$$n \sim (k_0N\tau)^3\,.$$

The nucleation process is finished when all atoms are bound, viz.

$$N_2 n \sim N\,.$$

From this we find the typical time τ for the nucleation of an atomic vapor in the buffer gas and the typical cluster size n at this point in time:

$$\tau \sim \frac{1}{k_0N}\left(\frac{k_0}{KN_{\mathrm{a}}}\right)^{1/4}, \qquad n \sim (k_0N\tau)^3 \sim \left(\frac{k_0}{KN_{\mathrm{a}}}\right)^{3/4}. \tag{4.10}$$

Taking typical values of the parameters of this formula $k_0 \sim 10^{-11}$ cm^3 s^{-1}, $K \sim 10^{-33}$ cm^6 s^{-1}, $N_{\mathrm{a}} \sim 10^{18}$ cm^{-3}, we obtain $N\tau \sim 10^{12}$ cm^3 s and $n \sim 10^3$. Hence, large clusters are formed under such conditions.

Another regime of nucleation is realized when metal atoms are formed in the course of cluster growth, and the typical time τ_{ch} of formation of free atoms as a result of decay of molecules is large compared to an atomic lifetime with respect to their attachment to clusters. In this regime, like the case above, the first step of the nucleation process centers around formation of diatomic metal molecules in three-body collisions between metal atoms and the atoms of the buffer gas, and further these diatomic molecules become the nuclei of condensation for cluster growth. The set of balance equations describing this regime of cluster growth has the form

$$\frac{\mathrm{d}N}{\mathrm{d}t} = M - N_{\mathrm{cl}}k_0n^{2/3}N - KN^2N_{\mathrm{a}}\,,$$
$$\frac{\mathrm{d}N_{\mathrm{cl}}}{\mathrm{d}t} = KN^2N_{\mathrm{a}}\,, \qquad \frac{\mathrm{d}n}{\mathrm{d}t} = k_0n^{2/3}N\,,$$

where M is the rate of formation of free metal atoms as a result of molecular decomposition. The second equation is similar to equation (4.9), where we account for diatomic molecules acting as nuclei of condensation and being transformed into clusters later.

The ratio between the second and third terms in the right-hand side of the first equation is of the order of the current cluster size n and, since $n \gg 1$, one can neglect the third term. In this regime of cluster growth, the quantities N, N_{cl} grow during the first stage of the process. During the second stage, the number density of clusters does not vary, and that of free atoms drops. Denoting by $t_{\max}$ the time when the number density of free atoms reaches a maximum, we have for the parameters of this process:

$$t_{\max} \sim \frac{A^{1/8}}{\sqrt{Mk_0}}\,, \qquad N(t_{\max}) \sim Mt_{\max} \sim A^{1/8}\sqrt{\frac{M}{k_0}}\,,$$
$$N_{\mathrm{cl}} \sim A^{-5/8}\sqrt{\frac{M}{k_0}}\,, \qquad n(t_{\max}) \sim A^{3/4}\,, \tag{4.11a}$$

where

$$A = \frac{k_0}{KN_{\mathrm{a}}} \gg 1\,.$$

Thus, the following estimate for the rate of decay of molecules: $M \sim N_{\mathrm{b}}/\tau_{\mathrm{ch}}$ can be made, where N_{b} is the total number density of bound atoms in clusters when the nucleation process finishes, and τ_{ch} is a typical time of decay of molecules containing metal atoms. At the end of the nucleation process we are dealing with a typical cluster size

$$n \sim \frac{N_{\mathrm{b}}}{N_{\mathrm{cl}}} \sim A^{5/8}\sqrt{Mk_0}\;\tau_{\mathrm{ch}}\,. \tag{4.11b}$$

Thus, according to this analysis, two limiting regimes of nucleation of an atomic metal vapor in a buffer gas take place at different stages of nucleation. When criterion (4.7) is valid, clusters are mostly large but metal atoms themselves may be free or bound. Cluster growth proceeds due to processes (1.1) for free metal atoms and according to the scheme (4.1) when these atoms are bound in clusters. In the regime when the cluster growth is determined by attachment of free atoms to nuclei of condensation and a pair process of the cluster growth starts from diatomic molecules, the average cluster size is estimated on the base of formulas (4.10) or (4.11b) when all the atomic vapor is transformed into clusters. Thereafter the cluster growth is determined by cluster coagulation (4.1), and the average cluster size is given by formula (4.6b). Subject to the condition $N \gg N_{\mathrm{b}}$, the cluster growth is dictated by the processes (1.1), and in the other regime, when the opposite criterion $N \ll N_{\mathrm{b}}$ holds true, the

cluster growth proceeds according to the process (4.1). The character of cluster growth does not depend on the charge of clusters in the first case, whereas for clusters of an identical charge sign the coagulation process stops.

Concluding, the above analysis allows us to distinguish the following stages in the transformation of an atomic vapor located in a buffer gas into a gas of clusters. At the first stage of nucleation when atoms are mostly free, the process of formation of clusters is delayed due to three-body formation of diatomic molecules. The diatomic molecules formed become nuclei of condensation, and the subsequent growth of clusters from them proceeds fast. Therefore, when all the atomic vapor is transformed into clusters, the clusters formed are large. The second stage of the nucleation process, the coagulation process (4.1), proceeds until clusters become charged, and their charge prevents contacts between clusters. Then cluster growth proceeds through an atomic vapor which is in an equilibrium with the clusters. The interaction between the atomic vapor and the clusters leads to evaporation of small clusters and growth of large clusters. As a result, clusters grow and their number decreases. In this case the rate of cluster growth is lower than for the coagulation process, and the temperature dependence of this rate is sharp.

4.2 Properties of gas-discharge plasmas

For metallic clusters to exist in a gas-discharge plasma, a high density of the buffer gas is required. This condition is fulfilled in a high-pressure arc, and below we shall focus on this plasma. Clusters do not influence the electric parameters of this discharge, with the exception of the energy balance in a light source where the radiation of clusters can give a contribution to the plasma power. Hence, for this analysis of the arc positive column in a cylindrical tube we neglect the presence of clusters.

This plasma is characterized by a local thermodynamic equilibrium because of the high density of buffer gas and the slowness of transport processes. The electron concentration is high enough to cause an intense exchange of energy between electrons and allows us to introduce separately the electron T_e and gaseous T temperatures in this plasma. In the case of electron energy exchange as a result of elastic electron – atom collisions, this corresponds to the criterion

$$N_e \ll N \frac{m}{M} \frac{\sigma_{ea}}{\sigma_{ee}} ,$$

where m, M are the electron and atom masses, σ_{ea} is a typical cross section for electron – atom collisions, σ_{ee} is the same quantity for electron – electron collisions, and usually $\sigma_{ee} \gg \sigma_{ea}$. This regime of two-temperature plasma takes place at the degrees of ionization of discharge gases $N_e/N \gg 10^{-6} - 10^{-5}$, a condition that is usually fulfilled in high-pressure arc discharges.

Equally with the local thermodynamic equilibrium, the local ionization equilibrium

$$M \leftrightarrow M^+ + e$$

exits in this plasma, so that the electron N_e and atom N_a number densities are connected by the Saha formula [2, 49]

$$\frac{N_e^2}{N_a} = \frac{g_e g_i}{g_a} \left(\frac{mT_e}{2\pi\hbar^2}\right)^{3/2} \exp\left(-\frac{I}{T_e}\right) , \qquad (4.12)$$

where I is the atomic ionization potential, g_e, g_i, g_a are the statistical weights of an electron, ion and atom, correspondingly; we also assume the plasma to be quasi-neutral. Because of the high statistical weight of states of the continuous spectrum, viz.

$$\frac{(mT_e/2\pi\hbar^2)^{3/2}}{N_e}$$

in gas-discharge plasmas, a high degree of ionization is reached when

$$T_e \ll I . \qquad (4.13)$$

This criterion is satisfied well for gas-discharge plasmas, so that $T_e/I \sim 0.1$ for high-pressure discharge plasmas.

For the criterion of the local ionization equilibrium to be met, the typical time of electron recombination τ_{rec} has to be small compared to the time τ_{dr} of their drift to a plasma region with other number density. Let us take $\tau_{rec} = (K_e N_e^2)^{-1}$, where K_e is the rate constant of three-body electron – ion recombination, and $\tau_{dr} = r_0^2/(5.8 D_a)$, where r_0 is the radius of a cylindrical region occupied by the plasma, and D_a is the ambipolar diffusion coefficient of ions in the plasma. Then the criterion of the ionization equilibrium takes the form

$$\xi = \frac{\tau_{dr}}{\tau_{rec}} = \frac{K_e N_e^2 r_0^2}{5.8 D_a} \gg 1 . \qquad (4.14)$$

The three-body electron recombination rate constant is equal to $K_e = C/T_e^{9/2}$ [75], where $C = 2 \times 10^{-8}$ cm^6 K$^{9/2}$ s^{-1} [76]. In the case of a plasma of inert gases at high temperatures, ambipolar diffusion is determined by the resonant charge exchange process involving atomic ions. The cross section of this process varies weakly with the temperature. In particular, in the case of xenon for ion and gaseous temperatures in the order of thousands of kelvins, we have for the cross section of resonant charge exchange $\sigma_{res} = 110$ A^2, and for argon this quantity is equal to $\sigma_{res} = 59$ A^2. This gives the following expression for the ambipolar diffusion coefficient at such temperatures:

$$D_a N = d_0 \sqrt{\frac{T}{1000}} \left(1 + \frac{T_e}{T}\right) . \qquad (4.15)$$

Here, $d_0 = 2.6 \times 10^{18}$ cm^{-1} s^{-1} for argon and $d_0 = 7.6 \times 10^{17}$ cm^{-1} s^{-1} for xenon, and the temperatures are taken in kelvins. In the case of xenon, Table 8 gives the boundary values of the electron N_e^* and atom N_a^* number densities which follow from the relation $\xi = 1$ for a given electron temperature T_e and for the gaseous temperature $T = T_e/2$. The regime under consideration corresponds to conditions where $N_e \gg N_e^*$ and $N_a \gg N_a^*$. Because of the relation (4.12), this regime is also realized at $T_e > 4000$ K.

Table 8. Boundary values for the electron and atom number densities in xenon, when the local ionization equilibrium takes place.

T_e, 10^3 K	4	5	6	7	8
$N_a^* r_0$, cm^{-2}	2.4×10^{18}	1.1×10^{17}	1.4×10^{16}	3.4×10^{15}	1.2×10^{15}
$N_e^* \sqrt{r_0}$, cm$^{-5/2}$	2.5×10^{12}	2.1×10^{13}	9.0×10^{13}	2.1×10^{14}	6.2×10^{14}

Analyzing the electric properties of the plasma, we shall use the general formulas [77 – 79] for the drift velocity of electrons w_e and the difference between the electron T_e and

gaseous T temperatures in a weakly ionized gas:

$$w_e = \frac{eE}{T_e}\overline{\left(\frac{v^2}{v}\right)}, \qquad T_e - T = \frac{M}{3}\left(\frac{eE}{m}\right)^2 \frac{\overline{v^2/v}}{\overline{v^2 v}}, \tag{4.16}$$

where E is the electric field strength, an average is made over the Maxwellian distribution function of electrons, v is the electron velocity, and the rate of elastic electron–atom collisions is $\nu(v) = N_a v\sigma^*(v)$, where $\sigma^*(v)$ is the diffusion cross section of electron–atom collisions. These quantities depend on the electric field strength in the combination E/N_a, and the electron drift velocity at a given reduced electric field strength in the case of relation (4.12) differs from that in the limit of a small density of electrons. This was demonstrated in Ref. [80] for xenon.

It is convenient to write out formula (4.16) in the form

$$T_e - T = \frac{M}{6m}(eE\lambda_0)^2 F(T_e) \tag{4.17}$$

with $\lambda_0 = (\pi a_0^2 N)^{-1}$, where a_0 is the Bohr radius, and the function $F(T_e)$ for xenon as the buffer gas is presented in Fig. 8a. Because of the Ramsauer effect, this function has a maximum. This suggests that the stable regime of the plasma exists if $T > T_{cr}$, and $E > E_{cr}$. Indeed, Fig. 8b illustrates the graphical method for the solution of equation (4.17). From this it is inferred that at the limiting value of the electric field strength E_{cr}, the left-hand side of equation (4.17) as a function of T_e is a tangent to the curve described by the right-hand side of this equation. The point of tangency determines the critical values of the electric field strength and electron temperature. In particular, in the xenon case and for $T_e \gg T$ we have $T_{cr} = 2400$ K and $E_{cr}/N = 0.003$ Td [80].

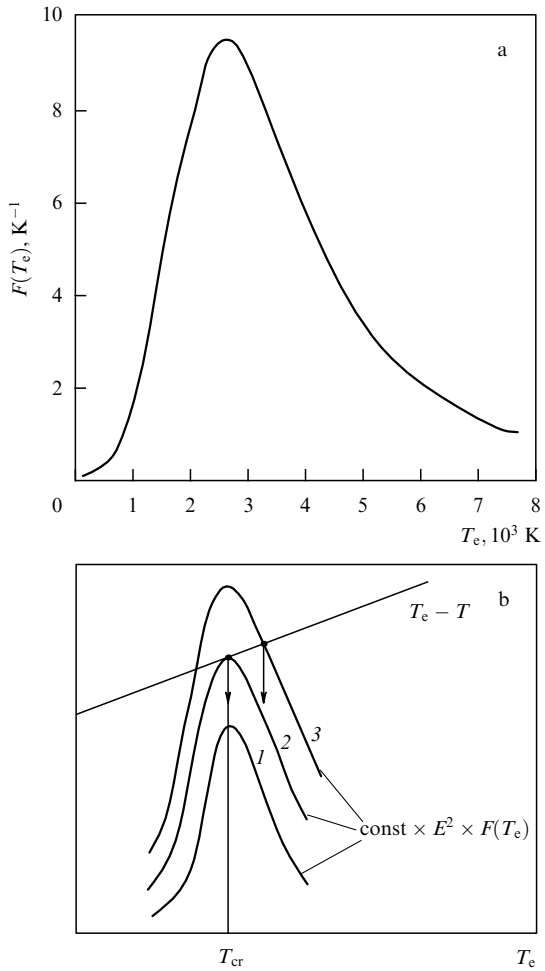

Figure 8. The function described by formula (4.17) for the example of xenon (a), and a graphic solution of equation (4.17) for the electron temperature (b). Arrows indicate the resultant electron temperatures, and T_{cr} is the minimum electron temperature.

The distribution of a plasma over the cross section of a discharge tube is governed by processes of heat balance in the plasma. We shall consider the regime of not very high currents, when the heat removal is determined by the thermal conductivity due to transport of atoms and electrons. The equation of the heat balance, known as the Elenbaas–Heller equation [81, 82], in this case has the form

$$\frac{1}{\rho}\frac{d}{d\rho}\left\{\rho\left[\kappa(T)\frac{dT}{d\rho} + \kappa_e(T_e)\frac{dT_e}{d\rho}\right]\right\} + p(\rho) = 0. \tag{4.18}$$

Here, ρ is the distance from the tube axis, $\kappa(T)$ and $\kappa_e(T_e)$ are the thermal conductivity coefficients for a gas and electrons in the plasma, and $p(\rho) = i(\rho)E = eEN_e(\rho)w$ is the specific power of heat release, where $i(\rho)$ is the electric current density. The first term in equation (4.18) corresponds to heat transport due to gaseous thermal conductivity, the second term describes heat transport due to electron thermal conductivity, and the third term corresponds to heat release as a result of the passage of the electric current through the plasma. This equation is responsible for the temperature distribution of an arc plasma over a discharge tube and hence it is of importance for the analysis of an arc plasma.

Because of the criterion (4.14) met for the considered regime of ionization equilibrium in the plasma, the plasma is concentrated for the most part in a tube region where the electron temperature differs only a little from its value on the axis. Then it is convenient to use a new variable

$$y = \frac{[T_e(0) - T_e(\rho)]I}{2T_e^2(0)}. \tag{4.19}$$

Because of the strong dependence of the electron number density on the electron temperature, which has the form $N(\rho) = N(0)\exp(-y)$, one can neglect the temperature dependences for other quantities, taking them at the tube center. Then $p(\rho) = p(0)\exp(-y)$, $\kappa_e \sim N_e \sim \exp(-y)$ and, introducing a new variable $x = \rho^2/r_0^2$, where r_0 is the tube radius, we reduce equation (4.19) to the form

$$\frac{d}{dx}\left\{x[\exp(-y) + \zeta]\frac{dy}{dx}\right\} - A\exp(-y) = 0 \tag{4.20}$$

with the following parameters which govern the plasma distribution over the tube cross section:

$$\zeta = \frac{\kappa(T)\alpha}{\kappa_e(T_e)}, \qquad A = \frac{p_0 r_0^2 I}{8T_e^2\kappa_e(T_e)}, \tag{4.21}$$

where

$$\alpha = \frac{dT(\rho)}{dT_e(\rho)} = \left[1 - (T_e - T)\frac{d\ln F(T_e)}{dT_e}\right]\left(\frac{2T_e}{T} - 1\right)^{-1}.$$

Equation (4.20) uses an additional condition $E = \text{const}$ fulfilled over the tube cross section and the temperature

dependence for the atom number density is $N \sim 1/T$. This consideration allows us to express the output parameters of the discharge plasma through the plasma parameters at the tube axis.

The analysis of equation (4.20) shows that plasma contraction — when the discharge current occupies only a part of the cross section of the discharge tube — takes place at small currents, so that heat transport is determined by gaseous thermal conductivity. At high currents when both heating and heat transport are determined by electrons, the electron current occupies the entire cross section of the discharge tube. In the limiting case of dominant gaseous thermal conductivity ($\zeta \gg 1$), the solution of equation (4.20) takes the form

$$N_e(\rho) = N_e(0)\exp(-y) = N_e(0)\left[1+\frac{\rho^2}{a^2}\right]^{-2},$$

$$a^2 = \frac{16T_e^2\kappa(T)\alpha}{p_0 I}. \qquad (4.22)$$

If the parameter a, which characterizes the size of the plasma region, is small compared to the tube radius r_0, contraction of the discharge takes place. Easy calculations give for the power of an arc discharge per unit length of the tube:

$$P = \int p_0 \exp(-y) 2\pi\rho \,\mathrm{d}\rho = \frac{16\pi T_e^2\kappa(T)\alpha}{I}.$$

This relationship establishes the connection between the discharge specific power and the plasma parameters at the center of a discharge tube. In the general event of both mechanisms of heat transport, this equation has the form [80, 83]

$$P = \frac{16T_e^2\kappa_e(T_e)(1+3.2\zeta)}{I}. \qquad (4.23)$$

Generally, the electric current radius ρ_0 can be introduced by the relation

$$\int N_e 2\pi\rho \,\mathrm{d}\rho = 1.36 N_e(0)\rho_0^2,$$

so that $\rho_0 = r_0$ in the Schottky case of small electric currents in a discharge tube. Accounting for both mechanisms of heat transport, we obtain in a general way for the plasma radius:

$$\rho_0^2 = \frac{12T_e^2\kappa_e(T_e)(1+3.2\zeta)}{p_0 I}. \qquad (4.24)$$

Equation (4.20) makes it possible to deduce one more convenient integral relation for a new variable

$$Z = \int^{T_e} \kappa_e(T_e')\,\mathrm{d}T_e' + \int^{T} \kappa(T')\,\mathrm{d}T' = \frac{2T_e^2}{I}\kappa_e(T_e) + \frac{T\kappa(T)}{1+\gamma},$$

where T, T_e are the gaseous and electron temperatures on the tube axis, respectively, $\gamma = \mathrm{d}\ln\kappa(T)/\mathrm{d}T$ (for xenon $\gamma = 0.7$ [84]). Twice integrating the heat balance equation (4.20) gives

$$Z = \int_0^{r_0} p(\rho)\rho\,\mathrm{d}\rho \ln\frac{r_0}{\rho} = \frac{2T_e^2}{I}\kappa_e(T_e) + \frac{T\kappa(T)}{1+\gamma}. \qquad (4.25)$$

This expression can be used for determination of plasma parameters.

The above relations and equations (4.16), (4.23)–(4.25) with $E = \mathrm{const}$ and $p = \mathrm{const}$ (p is the gas pressure) allow one to determine the parameters T, T_e, N, and N_e on the tube axis, the plasma size ρ_0 and the discharge current I. These relations must be supplemented by the relationship $E = \mathrm{const}$ and the equation of gas state $p = NT$. We shall demonstrate this capability in the limiting case when the heat removal is determined by the electron thermal conductivity, so that the electron current occupies the entire discharge tube. Then relation (4.25) takes the form

$$Z = 0.235 p_0 r_0^2 = \frac{2T_e^2}{I}\kappa_e(T_e),$$

where

$$p_0 = eEw_eN_e, \qquad \kappa_e(T_e) = \kappa_0\frac{N_e}{N_a}\sqrt{\frac{T_e}{1000}}$$

and $\kappa_0 = 1.23\ \mathrm{W\,(cm\,K)^{-1}}$. Together with the relations (4.13), (4.15) and the equation of gas state $p = N_a T$ we now have 4 equations for determining the quantities N_e, N_a, T_e, and T at a given E. Note that all the values are taken at the center of the discharge tube.

Some parameters of a xenon plasma are given in Fig. 9 [80]. Figure 9a displays the dependence of the gaseous

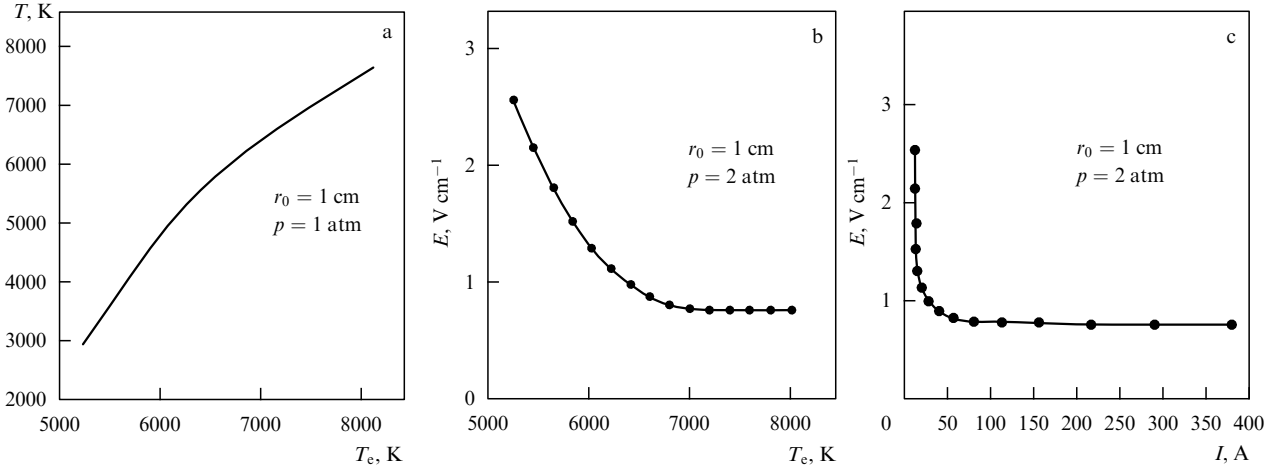

Figure 9. Relations between parameters of the positive column of the xenon arc discharge in a cylindrical tube of radius r_0 [80]: (a) connection between the gaseous and electron temperatures; (b) the electric field strength versus the electron temperature; (c) the electric field strength versus the electric current.

temperature on the electron temperature for the discharge regime considered. It is seen that an increase in the electron temperature leads to a decrease in the difference between the electron and gaseous temperatures [85]. Hence, in the limit of high temperatures or high discharge currents, the electron and gaseous temperatures of an arc plasma coincide. Figure 9b shows the electron temperature dependence for the electric field strength in the positive column, and Fig. 9c plots the current–voltage characteristic of this discharge. Notice that in the regime of high currents when $T_e = T$, the electric field strength is independent of the electron and gaseous temperatures (see Fig. 9b), and the increase in the discharge power is due only to an increase in the electron current (or in the electron number density).

Along with ionization of atoms of the buffer gas, at high electron temperatures ionization of a metal atomic vapor proceeds according to the scheme

$$M + e \longleftrightarrow M^+ + 2e\,.$$

Some of the atoms which are transformed into atomic ions do not take part in nucleation processes. In order to prevent ionization of metal atoms, it is necessary to restrict the electron temperature. In particular, in the case of a tungsten vapor this temperature is restricted to 6000 K, and less than 10% of the atoms are ionized at this temperature. Hence, xenon is suitable as a buffer gas in this event.

4.3 Cluster radiation

Usage of clusters as radiators in a cluster plasma under consideration is advantageous due to the high radiative absorption cross section of clusters. The basis of the method for measuring the absorption cross section of metallic clusters is the concept of photo-induced evaporation [86]. According to this concept, the absorption of photons leads to the decay of a cluster and hence to variation in its mass. The cluster radiative absorption cross section follows from the measurement of the mass spectrum of a cluster ion as a function of the laser intensity. Below we shall use data for the radiative absorption cross sections of lithium [87], potassium [88, 89] and silver [90] clusters when the absorption cross section σ_{abs} can be approximated by the formula

$$\sigma_{abs}(\omega) = \sigma_{max}\,\frac{\Gamma^2}{\hbar^2(\omega-\omega_0)^2+\Gamma^2}\,. \qquad (4.26)$$

Table 9 contains the parameters of this formula. The data from this table will be used as a model for clusters of heat-resistant metals in order to analyze the radiative properties of the cluster plasma of a light source.

Table 9. Parameters of formula (4.26) for the radiative absorption cross section of metallic clusters [19].

Element	$\hbar\omega_0$, eV	Γ, eV	σ_{max}/n, 10^{-17} cm^2	Δn
Li	3.1 ± 0.1	1.12 ± 0.15	5.2 ± 0.8	139–1500
K	2.00 ± 0.05	0.26 ± 0.10	3.4 ± 0.6	9–900
Ag	3.9 ± 0.1	0.59 ± 0.03	9 ± 1	9–21

In addition to this information, various spectroscopic measurements [91–98] help us to understand individual aspects of radiative processes involving clusters, and the theory allows us to comprehend the details of these processes. Below we shall use the data of Table 9 as model parameters for radiation of hot metallic clusters. Within the accuracy of measurements and based on this dependence, the maximum cross section σ_{max} is proportional to the number n of cluster atoms. These data allow one to evaluate various parameters of a gas containing hot clusters. In particular, Table 10 gives the specific power of radiation and light output η for hot clusters with the radiative parameters of lithium, potassium and silver clusters presented in Table 9. It is seen that such clusters are more effective radiators than a black body due to a more advantageous spectrum of radiation.

Table 10. The specific power of cluster radiation expressed in 10^7 W g^{-1}, and the light efficiency η which is expressed in lm W^{-1} and is given in parentheses. The data of Table 9 are used when constructing a model for metallic clusters at high temperatures.

Element	T, 10^3 K		
	3.0	3.5	4.0
Li	2.0(51)	4.9(80)	10(102)
K	4.0(108)	8.6(141)	17(165)
Ag	0.71(51)	1.6(75)	3.5(88)
Black body	(22)	(39)	(57)

We consider the nature of cluster radiation as a result of the interaction of an electromagnetic wave and the electron subsystem of the metallic cluster. The dipole Mie resonance [99] and the model of free electrons may provide the basis of this interaction if we consider the cluster as a bulky particle. In this case, the resonance in the radiative absorption cross section of the cluster results from reflection of the electromagnetic wave from a particle boundary [100, 101]. The various theoretical versions of radiation absorption by metallic clusters [102–112] are developed from this concept. Considering the radiative process as a result of interaction of an electromagnetic wave and the cluster electron subsystem, one can represent two limiting versions of the theory. In the first case we neglect the interaction of electrons with the environment, so that the resonance in the radiative absorption cross section is due to a plasmon and results from the collective degrees of freedom of the electron subsystem. The other approximation for this process takes as a basis the interaction of a probe electron with a parent core that allows one to introduce an oscillator strength for radiative transitions [96] like that of free atoms. Then the total oscillator strength of the cluster is proportional to the total number of valent electrons, or to the number of cluster atoms. These approximations lead to different sum rules, and the analysis shows the validity of the second version [18, 113], while the plasmon approximation leads to contradiction with available experimental data [18, 113].

Useful information for radiation by hot clusters follows from measurements of the spectral power of radiation emitted by hot clusters [114–116]. In these experiments [114–116], spectra of radiation of Nb, Hf and W clusters were measured after irradiation of a cluster beam by a laser pulse. The resultant signal was accumulated during many pulses, which restricts the accuracy of measurements. From these measurements it follows that the radiation spectrum of clusters within a given time after a laser pulse is approximated by the blackbody spectrum with a certain radiation temperature. Figure 10 plots some spectra for the radiation of these clusters, and Fig. 11 gives these spectra for tungsten clusters at different delay times, i.e. at different radiation temperatures. The analysis [117] shows that the cooling of an

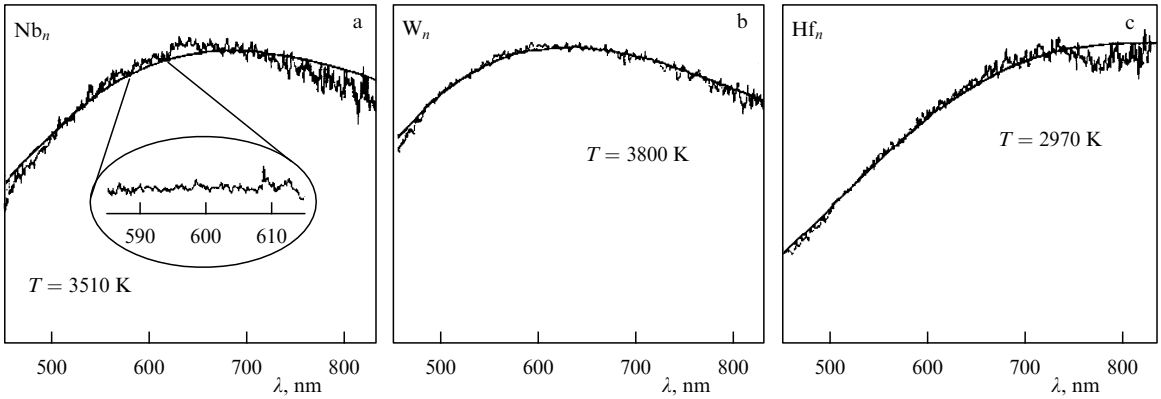

Figure 10. Radiation spectra of hot clusters of niobium (a), tungsten (b) and hafnium (c) [115, 116]. An appropriate radiation temperature is indicated, which follows from the spectrum.

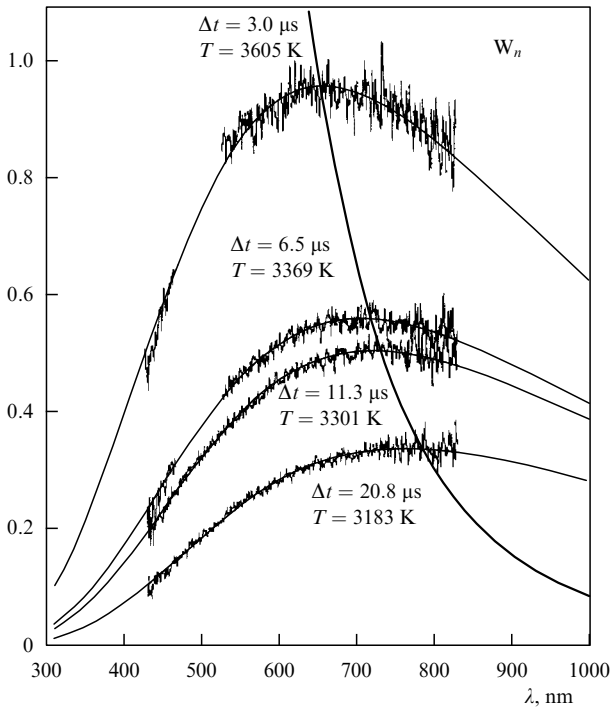

Figure 11. Radiation spectra of hot tungsten clusters [115] versus the delay time Δt with respect to the time of cluster heating by laser radiation. The radiation temperatures are indicated, which correspond to the spectra.

irradiated cluster is determined by its emission, and the rate of such cooling allows one to find the radiative absorption cross section of a hot cluster.

Treatment of these measurements under the assumption that the absorption cross section is independent of the photon frequency over some range of frequencies gives for the radiative absorption cross section per atom the value $(5 \pm 1) \times 10^{-18}$ cm^2 for tungsten clusters [117] if they emit radiation in the temperature range $T = 3170-3550$ K, which corresponds to the emission wavelengths $\lambda_{\max} = 0.68-0.76$ μm for the maximum spectral powers. In the case of niobium clusters, the absorption cross section per one atom is $(6 \pm 1) \times 10^{-18}$ cm^2 [117] under assumption that clusters emit radiation in the temperature range $T = 3200-3600$ K, which corresponds to the emission wavelengths $\lambda = 0.67-0.75$ μm for the maximum of the spectral power. These values of the specific absorption cross sections are less than those for the above cold clusters.

Clusters inserted into an arc plasma are effective radiators. Along with the above parameters characterizing the light efficiency of metallic clusters, we introduce also as this parameter the quantity

$$\xi = \int v_{\mathrm{ev}} \frac{\mathrm{d}E}{P_{\mathrm{rad}}} ,$$

where E is the binding energy of cluster atoms, and P_{rad} is the cluster radiation power, and v_{ev} is the evaporation rate. When inserted into a plasma of a given temperature in the absence of an atomic vapor, the cluster evaporates and emits radiation. The parameter ξ characterizes the efficiency of radiation of this cluster, and small values of this parameter correspond to a high efficiency of cluster radiation. Table 11 contains values of ξ for the initial tungsten cluster size $n = 1000$, and the data of Table 9 for the radiative absorption cross sections of Li, K, and Ag clusters were used in modelling the tungsten clusters at high temperatures. From the data of Table 11 it follows that the optimal temperature of tungsten clusters in the cluster plasma of a light source is about 4000 K.

Table 11. The efficiency ξ of cluster radiation in the course of evaporation [118].

Element	T, 10^3 K		
	3.5	4.0	4.5
Li	0.008	0.1	0.7
K	0.005	0.06	0.4
Ag	0.03	0.3	2

4.4 Heat equilibrium of clusters in plasmas

Metallic clusters under consideration are located in a plasma where the electron temperature T_{e} differs from the gaseous temperature T. The cluster temperature T_{cl} must lie between these values because it results from collisions of atoms and electrons with clusters. The cluster temperature refers to the motion of cluster atoms, and just this temperature determines the evaporation rate of cluster atoms and the rate of electron emission from the cluster's surface. In addition, the cluster temperature is responsible for radiation of hot clusters. Below we shall connect the temperature of a cluster located in an arc plasma with the gaseous and electron temperatures on the

basis of a simple model of collisions such that an atomic particle after collision with a cluster obtains the cluster's average thermal energy. This means that for $T_e > T$ an atom obtains on average the energy $(3/2)(T_{cl} - T)$ from the cluster, and an electron transfers on average to the cluster the energy $(3/2)(T_e - T_{cl})$ after each collision. Then the power which a cluster takes from electrons is $(3/2)(T_e - T_{cl})v_e N_e \sigma_e$, where v_e is the average electron velocity, N_e is the number density of electrons, and σ_e is the cross section of electron–cluster collisions. The power which atoms obtain from the cluster is equal to $(3/2)(T_{cl} - T)v_a N_a \sigma_a$, where v_a is the average velocity of atoms, N_a is the number density of atoms, and σ_a is the cross section of collisions of atoms with the cluster. The stationary condition combined with the use of formulas (2.2), (3.10) for the rate constants of collisions of atoms and electrons with clusters leads to the following expression for the cluster temperature T_{cl} [119]:

$$T_{cl} = \frac{T + \zeta T_e}{1 + \zeta}\,, \tag{4.27}$$

where for a positively charged cluster of charge Z one finds

$$\zeta = \sqrt{\frac{T_e M}{T m_e}} \left(1 + \frac{Ze^2}{r T_e}\right) \frac{N_e}{N_a}\,. \tag{4.28}$$

Here m_e and M are the electron and atom masses, respectively. On the basis of formula (3.10) one can find the temperature of a negatively charged cluster. It is seen that the cluster temperature can depend both on the cluster size and charge.

Because we are dealing with a three-temperature system, where the gaseous, electron and cluster temperatures are different, it is necessary in each case to ascertain which temperature should be used. In particular, formula (4.28) relates to a positively charged cluster, and its ionization is determined by the electron thermoemission which is connected with the cluster temperature. Therefore, the strongest dependence in formula (3.21) is governed by the cluster temperature, if an electron leaving the charged cluster core does not collide with plasma electrons. Hence, in the case $r \ll \lambda$, where r is the cluster radius, and λ is the mean free path of electrons in a plasma, formula (3.26) for the average charge of a large cluster has the form

$$\bar{Z} = \frac{r T_{cl}}{e^2} \ln\left[\frac{2}{N_e}\left(\frac{m_e T_{cl}}{2\pi\hbar^2}\right)^{3/2}\right] - \frac{rW}{e^2}\,, \tag{4.29}$$

so that the electron temperature in formula (3.26) is replaced by the cluster temperature. Correspondingly, the characteristic temperature T_* at which the ratio (3.28) of the densities of single-charged clusters equals unity, relates to the cluster temperature. In Table 6 the cluster temperature T_* is indicated, at which the average cluster charge is zero.

In the same manner, the two-temperature regime of an arc plasma can be taken into account for the cluster charge when it is negative. In the situation when the cluster charge is determined by attachment of electrons and positive ions to the cluster, we have the following equation for the cluster charge instead of (3.12):

$$x = \ln\left(\frac{1}{x}\sqrt{\frac{M T_e}{m_e T}}\right), \qquad |Z| = x\,\frac{r_W\, n^{1/3} T_e}{e^2}\,.$$

Practically, the two-temperature regime of the plasma is not of principal significance for the cluster charge in this case. For example, for argon as a buffer gas and atomic argon ions in the plasma, the solution of this equation yields $x = 4.17$ for $T_e = T$, and $x = 4.45$ for $T_e = 2T$.

4.5 Character of growth of charged clusters in plasma

The local equilibrium established between clusters and their atomic vapor is determined by the equality between the total rate of atomic attachment to clusters and the total evaporation rate of atoms. But this system is not stable because small clusters evaporate and large clusters grow, i.e. the size distribution function f_n of clusters varies in time. Normalizing the size distribution function to the number density of clusters N_{cl} by the relation $\int f_n\,\mathrm{d}n = N_{cl}$, we shall study the evolution of charged clusters in a plasma. If a typical cluster charge is large enough, one can neglect the coagulation process (4.1), and the cluster growth is determined by attachment and evaporation processes (1.1). Using the expressions (2.2) and (2.3) for the rate of atom attachment and atom evaporation, we obtain the following expression for the collision integral resulting from processes (1.1) [16, 35]:

$$I_{col}(f_n) = -\frac{\partial}{\partial n}\left\{k_0(T) n^{2/3} f_n \left[N - N_{sat}(T_{cl}) \exp\left(\frac{\Delta\varepsilon}{T_{cl} n^{1/3}}\right)\right]\right\}, \tag{4.30}$$

and we took into account here that the atom attachment process is governed by the gaseous temperature, whereas the cluster temperature determines the rate of the evaporation process. This form of the collision integral provides that small clusters evaporate, large clusters grow, and the critical size n_{cr}, at which the rates of attachment and evaporation processes are equalized, is determined by the relation

$$N = N_{sat}(T_{cl}) \exp\left(\frac{\Delta\varepsilon}{T_{cl} n_{cr}^{1/3}}\right). \tag{4.31}$$

Here, $\Delta\varepsilon = 2A/3$, and A is the specific surface energy of a liquid cluster, which is defined by formula (2.6), and Table 1 gives its values for some metals at the melting point. One can divide clusters into two groups by size whose boundary is $n = n_{cr}$. Denoting the number densities of bound atoms in clusters of the first and second group by N_1 and N_2, respectively, we have $N_1 + N_2 = N_b$. In the course of cluster size evolution, transitions of clusters from one group to the other group are absent.

Assuming local equilibrium, we neglect the inhomogeneity of this plasma and, correspondingly, the transport processes. Hence, in this approximation the evolution of the size distribution function of clusters is described by the kinetic equation

$$\frac{\partial f_n}{\partial t} = I_{col}(f_n)\,. \tag{4.32}$$

The additional relation follows from the conservation of the number density of free and bound atoms. In particular, we have

$$\frac{\mathrm{d}N_b}{\mathrm{d}t} = \sum_n n\,\frac{\partial f_n}{\partial t} = \int_0^\infty k_0(T) n^{2/3} f_n \times \left[N - N_{sat}(T_{cl}) \exp\left(\frac{\Delta\varepsilon}{T_{cl} n^{1/3}}\right)\right] \mathrm{d}n = 0\,, \tag{4.33}$$

where $T_{\rm cl}$ is the cluster temperature and, for simplicity, we below shall take it to be identical with the gaseous temperature T. Equation (4.33) accounts for the balance of attaching and evaporating atoms, thus establishing the connection between the equilibrium number density of free atoms N and the number density of free atoms $N_{\rm sat}(T)$ at saturation vapor pressure for a given temperature.

Let us analyze the evolution of the size distribution function f_n on the basis of equation (4.32) in the equilibrium conditions cited above. This distribution function tends to zero in the limits of small and large cluster sizes, so that we may approximate it by

$$f_n \sim \exp\left[-\left(\frac{n}{n_0}\right)^{\alpha} - \left(\frac{n_0}{n}\right)^{\alpha}\right], \tag{4.34}$$

where n_0, α are the parameters. Evidently, the critical cluster size $n_{\rm cr}$ and the average cluster size $\bar{n}$ are of order n_0. We assume this shape of the distribution function to be conserved during the cluster evolution when the parameter n_0 varies. Then the bound atom balance equation for clusters with $n < n_{\rm cr}$ has the form

$$\frac{{\rm d}N_1}{{\rm d}t} = n_{\rm cr} f(n_{\rm cr}) \frac{{\rm d}n_{\rm cr}}{{\rm d}t} - k_0(T) \times \int_0^{n_{\rm cr}} \left[N - N_{\rm sat}(T) \exp\left(\frac{\Delta\varepsilon}{Tn^{1/3}}\right)\right] n^{2/3} f_n \, {\rm d}n = 0 . \tag{4.35}$$

We obtain one more integral relation by multiplying Eqn (4.32) by n^2 and integrating the result over n. This gives

$$\frac{{\rm d}\overline{n^2}}{{\rm d}t} - \frac{\overline{n^2}}{\bar{n}} \frac{{\rm d}\bar{n}}{{\rm d}t} = \frac{2k_0(T)}{N_{\rm cl}} \int_0^{\infty} \left[N - N_{\rm sat}(T) \exp\left(a \frac{\bar{n}^{1/3}}{n^{1/3}}\right)\right] n^{5/3} f_n \, {\rm d}n , \tag{4.36}$$

where $a = \Delta\varepsilon / T\bar{n}^{1/3}$. From this it follows

$$\frac{{\rm d}\bar{n}}{{\rm d}t} = \gamma k_0 N_{\rm sat}(T) \bar{n}^{2/3} . \tag{4.37}$$

Assuming the quantities $x_{\rm cr} = n_{\rm cr}/n_0$, $\bar{x} = \bar{n}/n_0$ and $\overline{x^2} = \overline{n^2}/n_0^2$ to be conserved in time and denoting $x = n/n_0$, we obtain from formulas (4.35) and (4.36):

$$\gamma = \frac{\bar{x}^{1/3}}{x_{\rm cr}^2 f(x_{\rm cr})} \int_0^{x_{\rm cr}} \left[\frac{N}{N_{\rm sat}(T)} - \exp\left(a \frac{\bar{x}^{1/3}}{x^{1/3}}\right)\right] x^{2/3} f(x) \, {\rm d}x = \frac{2\bar{x}^{1/3}}{\overline{x^2} \int_0^{\infty} f(x) \, {\rm d}x} \int_0^{\infty} \left[\frac{N}{N_{\rm sat}(T)} - \exp\left(a \frac{\bar{x}^{1/3}}{x^{1/3}}\right)\right] x^{5/3} f(x) \, {\rm d}x , \tag{4.38}$$

with the quantity $N/N_{\rm sat}$ following from equation (4.33). Solution of Eqn (4.38) gives the parameter α of the distribution function (4.34) and the coefficient in formula (4.37) for the rate of cluster growth.

The character of cluster evolution depends on the parameter $a = \Delta\varepsilon/(T_{\rm cl}\bar{n}^{1/3})$. In particular, Fig. 12 plots the dependence of $n_{\rm cr}/\bar{n}$ and the portion s of bound atoms in evaporating clusters (i.e. among clusters of the first group) as a function of the parameter a. Next, if we introduce the reduced rates of evaporation $v_{\rm ev}$ and attachment $v_{\rm at}$ for clusters of the first group and denote these quantities for clusters of the second group by $\beta_{\rm ev}$ and $\beta_{\rm at}$, correspondingly,

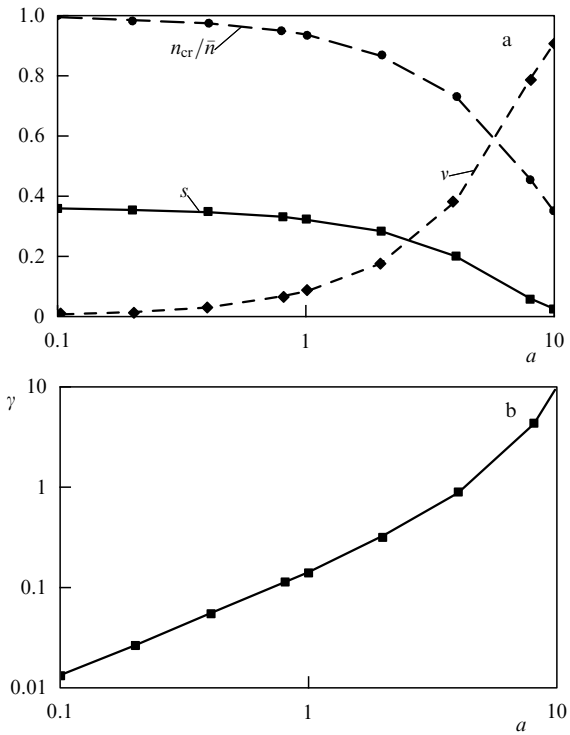

Figure 12. The parameters of an equilibrium of clusters with the parent atomic vapor versus the parameter a: $n_{\rm cr}/\bar{n}$ is the ratio of the cluster critical size to its average size; s is the portion of evaporating clusters, α is the ratio of the flux of atoms passing from evaporating clusters to growing ones to the total flux of evaporating atoms, and γ is the parameter entering equation (4.37).

we obtain

$$v_{\rm ev} + \beta_{\rm ev} = 1 , \qquad v_{\rm at} + \beta_{\rm at} = 1 , \qquad \frac{v_{\rm ev}}{v_{\rm at}} > 1 , \qquad \frac{\beta_{\rm ev}}{\beta_{\rm at}} < 1 . \tag{4.39}$$

Then, for the equilibrium conditions under consideration, the quantity

$$(v_{\rm ev} - v_{\rm at}) N k_0 \int n^{2/3} f_n \, {\rm d}n$$

is the number of bound atoms which change from clusters of the first group to clusters of the second group per unit time and volume. Figure 12a displays the dependence of the quantity $v = v_{\rm ev} - v_{\rm at}$ on the parameter a. In particular, for $a = 1$ we have $n_{\rm cr} = 0.94\bar{n}$, $s = N_1/N_{\rm b} = 0.32$, $v = 0.085$, and the dependence $\gamma(a)$ is given in Fig. 12b.

The general character of the process of cluster formation, when a gaseous compound of a heat-resistant metal is inserted into an arc plasma, was described in Section 2.2. The compound decomposes at temperatures $T > T_1$, and stable metallic clusters can be formed at temperatures $T < T_2$. Hence, clusters can exist in the temperature range (2.10): $T_1 < T < T_2$. Nucleation of an atomic vapor and cluster growth proceed according to processes (1.1) and (4.1). The cluster plasma exists if the number density $N_{\rm b}$ of bound atoms in clusters greatly exceeds the number density N of free atoms, which according to Eqn (4.33) is of the order of the saturated vapor number density $N_{\rm sat}(T)$ at a given temperature. At the

stage of cluster growth when clusters are neutral, they grow as a result of coagulation process (4.1). Then the average cluster size is determined by formula (4.6b), and from the latter it follows for the rate of cluster growth:

$$\frac{d\bar{n}}{dt} = 3.8 N_b k_0 \bar{n}^{0.2} . \quad (4.40)$$

This equation describes the growth of neutral clusters, while Eqn (4.37) relates to the growth of both neutral and charged clusters, provided that an equilibrium of a cluster with the parent atomic vapor occurs. One can see that the rates of cluster growth for the regimes which are given by formulas (4.37) and (4.40) are expressed in terms of different parameters. We emphasize the strong temperature dependence of the growth rate in the first regime, whereas the temperature dependence of the rate of the coagulation process (4.1) is weak.

Let us consider as an example the case when the WF_6 compound with a mean molecular number density 1×10^{16} cm^{-3} is introduced into a plasma. According to Table 2, tungsten clusters are formed in the temperature range between 2600 and 4100 K. For definiteness, we take a temperature of about 3700 K, as in the example of Section 2.3, and the average cluster size $\bar{n} = 1000$. At this temperature $N_{sat} = 6.4 \times 10^{13}$ cm^{-3}, and the equilibrium number density of free atoms is $N = 1.3 \times 10^{14}$ cm^{-3}. Under these conditions $a \approx 1$. Assuming that the other metal atoms in a plasma form clusters, we have for the number density of bound atoms $N_b = 1 \times 10^{16}$ cm^{-3}, which significantly exceeds the number density of free atoms. According to formulas (4.37), (4.40), the cluster growth rate $d\bar{n}/dt$ is equal to 1×10^5 and 1.6×10^7 s^{-1} in the first and second cases, correspondingly. When clusters get a charge, the coagulation process stops because of repulsion forces between identically charged clusters. Then the growth of clusters is determined by the first growth regime only, and the rate of the cluster growth process given by formula (4.37) decreases.

Transport processes involving free atoms promote cluster growth and redistribution of a metal over the tube cross section. The first type of transport processes corresponds to displacement of atoms to the region where clusters can grow. The other transport process results from the gradient of the equilibrium number densities of free atoms due to the temperature gradient. The first process proceeds during a typical time $\tau_{dif} \sim r_0^2/D_a \sim 0.1$ s, where r_0 is the tube radius, and D_a is the diffusion coefficient of metal atoms. The typical time of the second transport process resulting in collection of clusters in a narrow region is determined by formula (2.20) and is equal to $\tau \sim 1$ s.

One more transport process involving clusters takes place in an arc discharge due to transverse electric fields. Indeed, in hot regions of the plasma the clusters are positively charged due to the thermoemission process, while in cold regions of the plasma, where the cluster charge is determined by the attachment of electrons and ions to its surface, clusters have a negative charge, so that near the boundary of these regions at temperatures close to T_* clusters are neutral. Because under the action of transverse electric fields positive ions move to the walls, these fields cause motion of clusters to a region where clusters are neutral. The typical time of redistribution of clusters in space as a result of this effect is $\tau \sim \Delta x/(EK)$, where Δx is the size of the region occupied by clusters, $E \sim T_e/(er_0)$ is the typical transverse electric field strength, and K is the cluster mobility. For a typical cluster size $n \sim 10^3$, this estimate gives $\tau \sim 10-100$ s.

Thus, we observe a special type of equilibrium in a cluster plasma where transport processes are weak in comparison with kinetic processes. Various processes establish a local equilibrium between clusters and plasma, which is determined by the hierarchy of times characteristic for these processes.

4.6 Cluster plasma in light sources

Effective interaction of metallic clusters with light and the advantageous shape of the radiative absorption spectrum make metallic clusters effective radiators for a light source. Hence, starting from the Weber and Scholl paper [31] of 1992, several types of cluster light sources have been analyzed both by experimental and theoretical methods [18, 31–34, 119, 120]. In all the cases clusters were located in a plasma. The first scheme of a cluster light source by Weber and Scholl [31] used tungsten and rhenium clusters in a microwave discharge with a power of 100 W. An important element of this scheme is the regenerative chemical cycle which turns a metal into a gaseous compound at low temperatures, and into clusters at high temperatures. Within the framework of this scheme, the light efficiency of the cluster lamp, obtained in the tungsten case, was 56 lm W^{-1}, and in the rhenium case 62 lm W^{-1}. These values testify to the good prospects of the above experiments. This experimental research was later broadened [32–34]. The theoretical analysis of a cluster lamp is guided by an arc plasma [18, 119, 120]. We shall give below the basic peculiarities of this device which follow from the above analysis of the cluster plasma.

First, clusters are formed and exist at higher temperatures than solids, and because the efficiency of radiation increases with the temperature of radiators, cluster lamps are more efficient than incandescent lamps. Second, the cluster instability in cluster lamps, which leads to collection of a metal in an intermediate region of discharge in the form of clusters, promotes an increase in the efficiency of cluster lamps. Third, a cluster plasma is not stationary, and this is simultaneously a drawback and advantage of cluster plasma as a light source. Governing transport processes involving clusters when clusters move to hot regions of a discharge, one can increase the light efficiency of this system. Evidently, light efficiencies of the order of 100 lm W^{-1} are available for cluster lamps, and in the tungsten case the optimal temperature of radiating clusters falls in the range 3600–4200 K.

5. Cluster generation

5.1 Methods of cluster generation and applications

Methods of cluster generation use the fact that clusters are an intermediate state of matter in the course of transition from the gaseous state to a condensed state. Therefore, the transformation of a gas or vapor into a condensed phase is usually employed in these methods, and the process is stopped at a certain stage. In order to prevent subsequent coagulation of the forming clusters, they are taken in the form of a cluster beam. This beam is subsequently used for film deposition and cluster applications.

Table 12 lists the methods of cluster generation and some their peculiarities. Let us analyze them briefly. The first method of cluster formation is based on bombardment of a target with ions of keV energies [69, 121–130]. The fragment-clusters formed result from an ion impact and may have a

Table 12. Methods of generation of cluster beams and their peculiarities.

Method	Object	Peculiarities
Bombardment of a target with keV-ions	–	Small-size clusters
Free jet expansion of a vapor from an oven	Low-evaporated	Medium cluster size and intensity
Laser evaporation and free jet expansion	Heat-resistant	Low intensity
Stream from a cluster plasma	Heat-resistant	Large-size clusters, high intensity

charge. They are separated and accelerated. This method allows one to obtain a beam of small clusters of not high intensity. Usually this method is used for generation of selective beams of small clusters which are applied for research.

A cluster beam is formed as a result of the evolution of an expanding vapor. There are various methods for the formation of an expanding vapor depending on the cluster material and parameters of the output cluster beam. An oven is used for fusible metals, so that an atomic vapor forming in the oven expands through a nozzle into a vacuum together with a buffer gas. The cooling of this mixture during expansion causes nucleation of the vapor and formation of clusters. This method provides generation of fairly intense cluster beams, which are deposited onto a substrate for production of thin films [131 – 154]. In the case of heat-resistant metals, a laser beam is used to evaporate them and form free atoms [155 – 159]. The evaporating atoms are mixed with a flow of the buffer gas, and the subsequent expansion of the mixture leads to formation and growth of clusters.

Notice some peculiarities of these methods. The efficiency of vapor formation may be high if a vapor is to be formed from a condensed state. In particular, erosion of metals must be high during their transformation into a vapor which is to be used further for cluster production. We shall characterize the efficiency of evaporation by the ratio of the energy consumed to the number of atoms formed, that is by the energy cost of one atom. One can demonstrate it in the case of the vaporization of a tungsten wire which simultaneously loses energy as a result of light emission. In this situation the cost of one atom is $\varepsilon = 28$ keV at the wire temperature $T = 3300$ K, and $\varepsilon = 4.2$ keV at $T = 3600$ K [18]. The binding energy per one tungsten atom for these temperatures according to Table 1 is 8.5 eV. It is seen that this method of metal evaporation is characterized by a low efficiency. The sharp temperature dependence of the atomic energy cost is due to the exponential temperature dependence for the evaporating atomic flux and also due to the fact that the radiation from the surface determines the energy balance at these temperatures. For materials with a low temperature of evaporation, for example, for copper, a heated wire can be effective for generation of an atomic vapor.

Laser evaporation of surface atoms can provide highly efficient generation of atomic vapor of heat-resistant metals due to the nature of this process. In addition, gas discharge methods may be used for this purpose if a discharge provides high erosion of the materials. In particular, a magnetron discharge leads to a high erosion of the cathode and therefore it can provide the basis for an effective generator of cluster beams [160 – 163]. A hollow cathode discharge is characterized by even higher efficiency of cathode sputtering by ion currents and is also suitable for production of an atomic vapor which is converted further into clusters. The effectiveness of the method of atom formation in a vacuum is due to the explosive electron emission which takes place in a vacuum discharge [164, 165]. Then at the basic stage of the process, an ion current forms an atomic vapor by vaporization of the cathode and propagates through this vapor. Each evaporating atom is ionized further in a plasma, so that it generates one ion and one electron. If we suppose ions to be singly charged, this gives the relation $i = 2ej$ between the atom flux j and the discharge current density i, so that the atomic energy cost is equal to $\varepsilon = 2eV$, where V is the discharge voltage. Usually, V is of the order of the atomic ionization potential, i.e. $V \sim 10$ eV. Thus, this method of creation of an atomic vapor is rather effective.

The method of cluster generation depends on the sort of atoms or molecules constituting clusters. Figure 13 shows a layout of a cluster source for generation of molecular clusters [166, 167]. At the first stage of the process, clusters of rare gases (for example, argon clusters) are formed as a result of the adiabatic expansion of the gas through a small orifice (300 μm in diameter). These clusters pass through a scattering chamber where the material of resultant clusters (for example, NaCl) is evaporated in a resistively heated oven. Molecules are captured by rare gas clusters and finally evaporate them. As a result, molecular clusters are formed, which can contain rare gas atoms or not depending on the conditions of aggregation. This type of cluster generator is called the cluster aggregate source [167].

Clusters have a high reactivity so that contact of two clusters leads to their joining, and the properties of the incident clusters are lost in the resulting cluster. Therefore, clusters are used in the form of a beam where they are separated. There are various applications of cluster beams and we shall consider them briefly. The advantage of using a cluster beam for film deposition consists in the possibility to charge clusters and accelerate cluster ions. Fast cluster ions can be employed even in thermonuclear fusion reactions [168 – 172]. It is convenient to use cluster beams to make holes in foils [162]. Each fast cluster is like a bullet, and the ultimate hole size depends on the cluster size and energy, so that the density and size of holes on the resulting sieve can be adjusted. As a flux of energetic particles, a cluster beam is used for cleaning surfaces. The surface atoms then evaporate under the action of fast clusters [139, 140].

The main application of cluster beams is the production of so-called cluster-assembled materials which have specific properties and are nanostructures [173]. There are two methods for using cluster beams for the purpose. The first one, the 'ion cluster beam' method [175], involves a beam of charged liquid clusters which is used for fabrication of thin

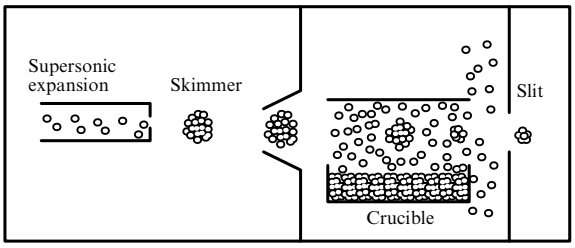

Figure 13. Scheme of the cluster aggregation source. A rare gas is found in a chamber, and its clusters are formed as a result of the supersonic expansion of a rare gas. Molecules evaporating in a crucible attach to clusters and substitute for atoms of rare gases in them [167].

films. In fact, this method is similar to the method of film deposition by atomic beams. The advantage of the ion cluster beam method consists in the possibility to govern the energy of charged clusters and also in the more technological regime of film formation. A drawback of the ion cluster beam method is the relatively low intensity of beams. For example, the maximum rate of silver deposition by the ion cluster beam method is 74 nm s^{-1} [137, 138]. This rate of film deposition corresponds to an atomic beam generated by a laser beam with intensity of the order of 1 W cm^{-2}. Because of the small intensity, the ion cluster beam method is only used for manufacturing small elements of microelectronics. The other method of application of cluster beams uses the low-energy cluster beam deposition (LECBD) technique and involves a beam of neutral solid clusters of small energy [175]. The advantage of this method is that the size distribution function of clusters in a beam is rather narrow because clusters with magic numbers are formed by this technique. Hence, this method allows one to create nanometer films with embedded clusters of identical sizes. It is impossible to produce such structures by other methods, and clusters of various materials and sizes can be used for this purpose (see, for example, Refs [175–179]).

5.2 Generation of clusters from a cluster plasma

Below we shall consider the method of cluster generation on the base of a high-pressure flowing afterglow plasma with a small admixture of a metal to the buffer gas. In standard methods for generation of a cluster beam, clusters are formed in the course of gas expansion in the nozzle region, and the typical time of this process is of order $\tau \sim 10^{-7}-10^{-6}$ s. The advantage of generation of clusters in a plasma [180, 181] is connected with the relatively high times of their growth. Therefore, this method is convenient for materials with a low saturation vapor pressure, namely, for refractory metals. One more advantage of this method is a high intensity of the resulting cluster beam because of a high density of the plasma used. Notice that the optimal parameters of a cluster plasma invoked for generation of clusters differ from those of cluster lamps. Indeed, a light source requires a high temperature of clusters and a high density of buffer gas in order to hamper transport processes. The cluster plasma in a cluster beam generator is characterized by a lower temperature and pressure of the buffer gas.

A general scheme for the cluster beam generator is given in Fig. 14. The generator of cluster beams under consideration includes three basic elements. The first is a plasma generator of low power (below 1 kW), and in the second part of this generator a narrow beam of molecules is directed along the axis of the flowing afterglow plasma. Molecules decompose in this region, and metallic clusters are formed. Metal atoms transported from all the plasma volume attach to clusters, so that the metal is collected near the flow axis in the form of clusters. In the last stage, the central part of a plasma flow containing clusters is extracted and directed into a vacuum where the atoms of the buffer gas are removed by pumping, and the cluster beam is governed by external electric fields.

Along with the cluster growth process, the charging of clusters takes place. Usually clusters obtain negative charge, which allows one to separate the cluster flow from the buffer gas and create a cluster beam. Under the conditions realized in this scheme, the cluster growth and cluster charging processes proceed in the afterglow plasma simultaneously with plasma relaxation. Below we shall analyze these processes in order to prove that this method of cluster generation is realistic. This method, along with generation of metallic clusters, allows one also to extract refractory metals from their gaseous or volatile compounds.

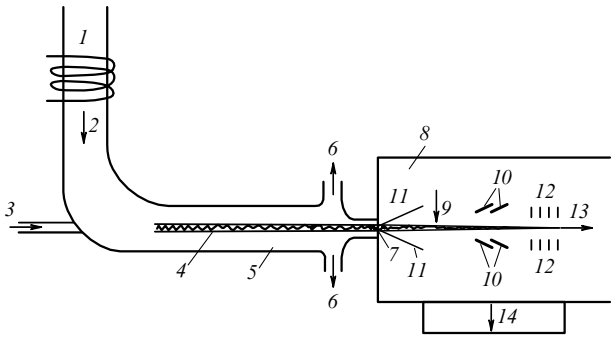

Figure 14. Scheme of a generator of clusters from an arc afterglow: *1* — plasma generator; *2* — plasma flow; *3* — introduction of a gaseous compound of a heat-resistant metal; *4* — cluster beam in a plasma flow; *5* — afterglow discharge tube; *6* — output plasma flow; *7* — nozzle for plasma expansion into a vacuum; *8* — vacuum camera; *9* — electron beam; *10* — skimmers; *11* — expanding buffer gas; *12* — electric field optics; *13* — cluster beam of a buffer gas; *14* — pumps.

In the case of refractory metals, it is convenient to combine generation of clusters with chemical regeneration [31–34] when a gaseous compound MX_k is introduced into a gas (M is a metal atom, X is a halogen atom). This simplifies the introduction of a refractory metal into a plasma and allows one to prevent attachment of metal atoms to the walls of the tube through which the plasma flows. A gaseous compound MX_k exists only at low temperatures. Starting from a temperature T_1, the compound MX_k decays, and the metal condensed phase becomes advantageous thermodynamically. At temperatures above T_2, the metal condensed phase consisting of clusters decays into an atomic metal vapor. Thus, clusters exist in the temperature range (2.10) if thermodynamic equilibrium is attained in this plasma. Table 2 contains these temperatures under typical conditions in this plasma.

The method of chemical regeneration [31] for introduction of metal atoms into a plasma allows us to attain a high density of metal atoms in a hot region, which leads to the high intensity of the resultant cluster beam. In standard methods of cluster generation on the basis of vaporization of atoms from a metal surface, the number density of atoms is restricted by the atom number density at the saturation vapor pressure complying with the surface temperature. Table 13 contains the values of this atom number density $N_{\mathrm{sat}}(T_{\mathrm{m}})$ at the melting point. It is seen that these values are less than those obtained by decomposition of gaseous or volatile compounds of these metals.

The diffusion coefficients of large clusters in a buffer gas are inversely proportional to their surface area: $D_n = D_0/n^{2/3}$. Within the framework of the liquid drop model for clusters, the parameter D_0 is determined by formula (2.15) and its values for refractory metals are collected in Table 3. From this, on the basis of the Einstein relation, one can find the cluster mobility K which is the ratio of the cluster drift velocity w in an external electric field to the field strength E. We have

$$K = \frac{ZeD}{T}\,, \tag{5.1}$$

Table 13. Parameters† of atomic metal vapors and characteristics of cluster scattering in argon.

Metal	$N_{\rm sat}(T_{\rm m})$, 10^{13} cm^{-3}	$Kn^{1/3}$, cm^2 (V s)$^{-1}$	$\theta n^{1/3}$
Ti	2.4	0.44	0.58
V	11	0.48	0.63
Fe	17	0.50	0.66
Co	3.5	0.51	0.67
Ni	2.1	0.52	0.67
Zr	0.005	0.40	0.52
Nb	0.39	0.44	0.58
Mo	13	0.46	0.61
Rh	1.9	0.48	0.63
Pd	22	0.47	0.62
Ta	2.3	0.44	0.59
W	13	0.46	0.61
Re	8.1	0.47	0.62
Os	9.6	0.48	0.63
Ir	3.2	0.47	0.62
Pt	0.081	0.46	0.61
Au	0.017	0.45	0.59
U	5.4×10^{-7}	0.39	0.55

† $N_{\rm sat}(T_{\rm m})$ is the number density of atoms at the melting point and saturation vapor pressure; K is the cluster mobility at a temperature of $T = 1000$ K and the atomic number density 2.69×10^{19} cm^{-3} in argon; n is the number of cluster atoms, and θ is the angle of cluster beam deflection.

where Z is the cluster charge. For definiteness, we consider the regime of cluster charging as a result of the attachment of electrons and ions to the cluster's surface, which proceeds according to the schemes

$$\mathrm{e} + \mathrm{M}_n^{-Z} \longleftrightarrow \mathrm{M}_n^{-Z-1}\,, \qquad \mathrm{A}^+ + \mathrm{M}_n^{-Z} \longleftrightarrow \mathrm{A} + \mathrm{M}_n^{-Z+1}\,, \tag{5.2}$$

where M is the metal atom, and A is the buffer gas atom. We have negatively charged clusters, and their charges are given in Table 6 together with the boundary temperatures T_* below which this regime of cluster charging takes place. One can see that the negative cluster charge depends weakly on the type of the heat-resistant metal, so that an average over the cluster materials of Table 6 yields for the cluster charge

$$\bar{Z} = (0.080 \pm 0.005)\left(\frac{T}{1000}\right)n^{1/3}\,, \tag{5.3}$$

where the temperature T is expressed in K.

For large clusters and an afterglow plasma of not high temperature, we can find the cluster charge on the basis of formula (3.12). Because $Z \sim T$ and $Z \sim n^{1/3}$, we have in this case $K \sim \sqrt{T}n^{-1/3}$. Table 13 contains values of the mobility of large metallic clusters in an argon plasma at temperature $T = 1000$ K. Averaging over the cluster materials of Table 13, we arrive at the following expression for the cluster mobility [in cm^2 (V s)$^{-1}$ at the normal number density of argon atoms]:

$$K = (0.46 \pm 0.03)n^{-1/3}\sqrt{\frac{T}{1000}}\,, \tag{5.4}$$

where the temperature is expressed in K. From this one can conclude that displacements of clusters in the plasma flow under the action of transverse electric fields are relatively small.

Since even in the regime (5.2) of cluster charging, which leads to a high cluster charge, the cluster displacement during the flow time is small, clusters conserve their locations with respect to the flow axis during the motion of the plasma. Hence, one can create a narrow cluster beam if clusters are formed close to the flow axis, as occurs when decay of molecules containing metal atoms proceeds near the flow axis.

Analyzing the character of formation and evolution of clusters in a plasma flow, we will be guided by two examples in order to ascertain the real parameters of this scheme of cluster beam generation. In the first case, a beam of iridium clusters results from the introduction of the compound IrF_6 with the average concentration of 0.1% into argon at a pressure of 100 Torr, so that the iridium clusters formed may be applied for fabrication of rhodium–iridium thermocouples. In the second example, molybdenum clusters are formed from MoF_6 introduced with an average concentration of 0.1% into argon at a pressure of 1 atm, and these clusters are deposited onto a target for fabrication of molybdenum mirrors [160]. According to Table 2, iridium clusters are produced at temperatures below $T_2 = 3200$ K, whereas IrF_6 molecules decompose at temperatures above $T_1 = 1300$ K. In the same way, we have that molybdenum clusters exist at temperatures below $T_2 = 3200$ K, whereas MoF_6 molecules decompose at temperatures above $T_1 = 2300$ K. The accuracy of these data is 100–200 K. We take an initial temperature of 3300 K at the flow center in both cases.

5.3 Gas-dynamic and heat processes in a plasma flow

Because of its small concentration, a metallic compound does not influence the gas-dynamic and thermal parameters of a plasma flow, and we take account of the buffer gas only. A noticeable variation in the temperature T over the cross section of the plasma flow is of importance and, for simplicity, we shall use the parabolic temperature profile

$$T(\rho) = T_0 - \frac{T_0 - T_{\rm w}}{r_0^2}\,\rho^2\,, \tag{5.5}$$

where ρ is the distance from the tube center, r_0 is the radius of the discharge tube, and T_0, $T_{\rm w}$ are the temperatures at the tube center and on the walls.

From the Navier–Stokes equation [182, 183] it follows that the distribution of the flow velocity u_z over the tube cross section is given by

$$u_z(\rho) = \frac{\mathrm{d}p}{\mathrm{d}z}\left[\ln\frac{r_0}{\rho}\int_0^{\rho}\frac{\rho'\,\mathrm{d}\rho'}{\eta(\rho')} + \int_{\rho}^{r_0}\ln\frac{r_0}{\rho'}\,\frac{\rho'\,\mathrm{d}\rho'}{\eta(\rho')}\right], \tag{5.6}$$

where the axis z is directed along the flow, η is the viscosity of the buffer gas, and p is the gas pressure. In reality, the coefficient of viscosity decreases by several times when we move from the tube center to walls, but it is convenient to connect the flow velocity with that in the case where the temperature is constant over the tube cross section. In this case we have [182, 183]

$$u(\rho) = u_0\left(1 - \frac{\rho^2}{r_0^2}\right), \qquad u_0 \equiv u(0) = \frac{r_0^2}{4\eta}\,\frac{\mathrm{d}p}{\mathrm{d}z}\,,$$

and the flow rate is equal to

$$G = \int N_{\rm a}u_z(\rho)2\pi\rho\,\mathrm{d}\rho = \frac{\pi r_0^2}{2}\,N_{\rm a}u_0\,,$$

where N_a is the number density of atoms of the buffer gas. When the gas temperature varies over the tube cross section, we introduce an effective temperature T_{eff}, such that the flow rate is equal to that at a constant temperature T_{eff} over the tube cross section, i.e.

$$G = \int N_a u_z(\rho) 2\pi\rho \, d\rho = \frac{\pi r_0^4 N_a(T_{eff})}{8\eta(T_{eff})} \frac{dp}{dz}$$
$$= N_a(T_{eff}) \frac{u_0(T_{eff})}{2} \pi r_0^2 . \quad (5.7)$$

The values of T_{eff} depending on T_0 (the temperature on the axis) are given in Table 14 for argon, where the temperature dependence for the coefficient of viscosity is $\eta(T) \sim T^{0.71}$[84], and the atomic number density is $N_a(T) \sim 1/T$. Usage of the effective gas temperature simplifies the analysis of the problem at hand.

Table 14. Effective temperature T_{eff} of argon flow in a cylindrical tube, and the ratio of the velocity on the axis $u_0(T_{eff})$ to that at room temperature over all the flow cross section and with the same pressure gradient.

T_0, 10^3 K	0.3	0.5	1	1.5	2	2.5	3	3.5	4
T_{eff}, 10^3 K	0.3	0.428	0.721	1.00	1.27	1.54	1.80	2.06	2.32
T', 10^3 K	0.3	0.429	0.731	1.02	1.31	1.59	1.87	2.15	2.43
$\frac{u_0(T_{eff})}{u_0(T_w)}$	1	0.755	0.501	0.390	0.324	0.281	0.249	0.225	0.206

Another effective temperature corresponds to the power transferred by the flow. Neglecting the contribution of the flow kinetic energy to its enthalpy because of the small flow velocity in comparison with the sound speed, we have for enthalpy per unit volume: $h = c_p T(\rho) N_a(\rho) = c_p p$, where $c_p = 5/2$ is the heat capacity per one atom for an atomic gas, and we used the equation of state $p = N_a T$ for an ideal gas. From this we have for the power P which is transported by the flow:

$$P = \int h u_z(\rho) 2\pi\rho \, d\rho = h \frac{u_0(T')}{2} \pi r_0^2 ,$$

where T' is the effective temperature for this process, and its values are given in Table 14. It follows from the data of this table that the effective temperatures for the flow rate T_{eff} and transferred energy T' practically coincide, and this allows us to connect the transport parameters of interest:

$$P = c_p T_{eff} G . \quad (5.8)$$

Assuming heat transport to be determined by the thermal conductivity of the buffer gas, we obtain the heat balance equation of the flow:

$$\frac{dP}{dz} = 2\pi r_0 \kappa(T_w) \frac{dT}{d\rho}(r_0) = 4\pi\kappa(T_w)\Delta T ,$$

where $\kappa(T_w)$ is the thermal conductivity of the buffer gas near the walls, and $\Delta T = T_0 - T_w$ is the temperature difference between the flow center and the walls. From this it follows for this quantity along the flow:

$$\Delta T = C \exp\left(-\frac{z}{l}\right) , \qquad l = \alpha G . \quad (5.9)$$

It follows from Table 14 that the quantity $(T_{eff} - T_w)/\Delta T = 0.57 \pm 0.01$ in the region of interest for this analysis. Table 15 gives values of the coefficient α for various buffer gases when the walls of the flow tube are at room temperature. It follows from the analysis that the flow rate must be not small in order to provide this regime of plasma relaxation. Parameters of the plasma flow in the examples of iridium and molybdenum clusters under consideration are collected in Table 16. In particular, the tube length l which provides a decrease in the buffer gas temperature in a tube of constant radius up to the temperature T_1 is large in comparison with a typical laboratory size. One can decrease this length by using an expanding tube.

Table 15. The coefficient α in formula (5.9).

Buffer gas	He	Ne	Ar	Kr	Xe	N_2	O_2
α, 10^{-21} cm s	1.0	3.2	8.8	16	27	6.0	5.9

Table 16 contains also the values of the Reynolds number of the flow for the examples under consideration. We introduce the Reynolds number as

$$\mathrm{Re} = u_0 r_0 m_a \frac{N_a(T_{eff})}{\eta(T_{eff})} ,$$

where m_a is the atomic mass, r_0 is the tube radius. Under these Reynolds numbers the flow is laminar, and the thermal conductivity mechanism determines heat transport. The values of the pressure gradient dp/dz follow from formula (5.7). Because this quantity is relatively small, $p = \mathrm{const}$ downstream.

When gaseous molecules containing a refractory metal atom are introduced into a plasma, they decay in collisions

Table 16. Parameters of the plasma flow and processes in the plasma for the iridium and molybdenum clusters under consideration.

Parameter	Ir	Mo	Parameter	Ir	Mo
p, atm	0.13	1	δT, K	60	100
T_0, K	3300	3300	ρ_h, cm	0.1	1
u_0, 10^3 cm s^{-1}	12	6	A	1×10^5	2×10^4
G_{Ar}, g s^{-1}	0.7	2	t_{max}, 10^{-5} s	9	5
τ_{ch}, 10^{-3} s	0,1	2	$N(t_{max})$, 10^{15} cm^{-3}	6	5
D, cm^2 s^{-1}	50	7	N_{cl}, 10^{12} cm^{-3}	1	3
χ, cm^2 s^{-1}	90	15	$n(t_{max})$, 10^3	6	2
l, cm	60	260	$n(\tau_{ch})$, 10^3	7	70
dp/dz, atm cm^{-1}	3×10^{-6}	2×10^{-5}	n	7×10^3	1×10^6
Re	300	1000	ρ_0, cm	0.2	0.1
G_M, mg s^{-1}	3	5	τ_{at}, s	2×10^{-5}	2×10^{-6}
j_M, mg (cm^2 s)$^{-1}$	20	100	N_e, cm^{-3}	3×10^{12}	4×10^{12}
I, A	3×10^{-4}	3×10^{-5}	N_e', cm^{-3}	1×10^{10}	2×10^{10}

with buffer gas atoms. The condition for molecules to decay while located in the central region of the flow has the form

$$\frac{1}{\tau_{\rm ch}} = k_{\rm g} N_{\rm a} \exp\left(-\frac{\varepsilon_{\rm ch}}{T}\right) > \frac{1}{\tau_0}\,, \tag{5.10}$$

where $k_g \sim 10^{-10}$ cm^3 s^{-1} is the gas-kinetic rate constant, $\varepsilon_{\rm ch}$ is the binding energy for a halogen atom in the molecule, τ_0 is a typical transport time of the molecule leaving the central region of the tube, where $\Delta T \sim T^2/\varepsilon_{\rm ch}$, i.e. the rate of the chemical process has the same order of magnitude there as at the center. The width of this region for the temperature profile (5.5) and $T_0 \gg T_{\rm w}$ takes the form $\rho \sim r_0\sqrt{T_0/\varepsilon_{\rm ch}}$. Because the formed metal atoms quickly join to clusters, we require the relation (5.10) to be valid at the temperature T_2 (see Table 2) below which clusters exist. In particular, in the MoF_6 case, when $\varepsilon_{\rm ch} \approx 4$ eV, the criterion (5.10) is valid at pressures $p > 0.1$ atm. In addition, a size ρ of the region where molecules decay effectively is more than the typical size of the region where clusters are formed. This follows from the subsequent estimates.

Next, the decomposition of molecules leads to a decrease in the buffer gas temperature. Table 16 contains the values of the decrease in the buffer gas temperature δT for the examples under consideration, if the average molecule concentration is 10^{-3} and the temperature profile (5.5) is conserved after the temperature decrease. In reality, the temperature decrease may be higher than that of Table 16, because during the time of molecular decay the heat propagates a restricted distance $\rho_{\rm h} \sim 6\chi\tau_{\rm ch}$. This allows one to use a more high temperature in the beginning of the process at the flow center.

5.4 Nucleation processes in afterglow plasmas

Formation of clusters from metal atoms can proceed according to the regimes described by formulas (4.10) and (4.11). Indeed, if the time $\tau_{\rm ch}$ of decay of molecules is small compared to the typical time τ of transformation of an atomic vapor into a gas of clusters, the system develops according to the first scheme with the parameters (4.10). In the opposite limiting case, the parameters of the clusters formed are determined by formulas (4.11). In the iridium example under consideration we have $\tau_{\rm ch} \sim \tau$, and in the molybdenum case $\tau_{\rm ch} \gg \tau$. Therefore, we will keep the second regime for the data of Table 16. Notice that the delay in the nucleation process is due to the formation of diatomic molecules in three-body collisions. In the next phase of this process, diatomic molecules are nuclei of condensation, and cluster growth proceeds faster than formation of diatomic molecules. Hence, when transformation of an atomic metal vapor into clusters finishes, the clusters are large.

Table 16 contains the parameters of cluster growth which include: $t_{\rm max}$ — the maximum lifetime of atoms with respect to attachment to clusters; the number density of free metal atoms $N(t_{\rm max})$ and the typical cluster size $n(t_{\rm max})$ reached at this moment; the number density $N_{\rm cl}$ of clusters which is attained by the time $t_{\rm max}$ and later varies weakly, and, finally, the typical cluster size $n(\tau_{\rm ch})$ when all the atoms are transformed into clusters. In the beginning we consider molecules to be located at the flow axis, so that they propagate across the flow as a result of diffusion along with metal atoms formed. But, because of their low mobility, the clusters that form conserve their positions with respect to the flow center during the plasma evolution.

An arising metal atom attaches to a cluster, and the characteristic lifetime of this process is

$$\tau_{\rm a} \sim \frac{n^{1/3}}{k_0 N_{\rm b}}\,, \tag{5.11}$$

where $N_{\rm b}$ is the number density of bound atoms. The maximum in the number density of free metal atoms is reached by the time $t_{\rm max}$ during which clusters are formed. Hence, the width of the resultant cluster beam is determined by the distance that molecules and atoms pass during time $t_{\rm max}$. The atoms which are formed later attach to clusters located in the region of size $\rho_0 = \sqrt{6Dt_{\rm max}}$, which is small in comparison with the tube radius r_0. If an atom is formed outside a region occupied by clusters, it returns and attaches to clusters. Only a small part of atoms can reach the tube walls because

$$r_0 \gg \rho_0\,. \tag{5.12}$$

Thus, the tube radius r_0 is an arbitrary parameter of the problem, which must satisfy the condition (5.12) only.

When all the molecules decayed and atoms formed were transformed into clusters, the subsequent cluster growth proceeds via coagulation of clusters (4.1). We assume clusters to be neutral and use formula (4.6b) for the average cluster size. The values of this parameter at the exit of the afterglow tube for the examples under consideration are given in Table 16 where the tube length was set equal to 30 cm. Note that the final cluster size depends greatly on the initial number density of metal atoms.

5.5 Relaxation of an afterglow cluster plasma

Because an afterglow plasma is not supported by an external power source, the temperature and density of electrons and ions in this plasma decrease with time. We now analyze the character of plasma relaxation, assuming this plasma to be in equilibrium in the beginning. At the first stage of plasma evolution, the number densities of electrons and ions unambiguously correspond to the plasma temperature, which is assumed to be identical for electrons and the buffer gas. Below a particular temperature $T_{\rm eq}$, evolution of the electron number density is controlled by the rate of plasma cooling, which we describe by the parameter $\mathrm{d}T/\mathrm{d}t$. In addition, the electron number density in the course of this regime of plasma relaxation is determined by the processes

$$\mathrm{e} + \mathrm{A} \longleftrightarrow 2\mathrm{e} + \mathrm{A}^+\,, \tag{5.13}$$

and the balance equation for the electron number density $N_{\rm e}$ has the form [184, 185]

$$\frac{\mathrm{d}N_{\rm e}}{\mathrm{d}t} = K_e\left[N_S^2(T) - N_{\rm e}^2\right]N_{\rm e}\,, \tag{5.14}$$

where K_e is the rate constant of three-body electron – ion recombination (see formula (4.14)), $N_S(T)$ is the equilibrium number density of electrons under ionization equilibrium. We used the principle of detailed balancing to obtain the rate constant of atomic ionization by electron impact. It follows from this equation that at slow cooling $N_{\rm e} = N_S(T)$, i.e. ionization equilibrium is supported, and the temperature $T_{\rm eq}$ at which this equilibrium is violated is given by the relation-

ship [184, 185]

$$K_e(T_{eq})N_S^2(T_{eq}) = \frac{e^C}{2}\frac{I}{T_{eq}^2}\frac{dT}{dt}, \quad (5.15)$$

where $C = 0.577$ is the Euler constant, and I is the ionization potential of a buffer gas atom. At temperatures below T_{eq}, the solution of equation (5.13) in the case $dT/dt = \text{const}$ has the form

$$\frac{1}{N_e^2(t)} = \frac{4TK_e}{7\,dT/dt}, \qquad T \ll T_{eq}, \quad (5.16)$$

where T is the current temperature at instant t. It is convenient to rewrite this formula in the form

$$N_e = N_0\sqrt{\frac{dT}{dt}}\left(\frac{T}{1000}\right)^{7/4}, \quad (5.17)$$

where $N_0 = 1.6 \times 10^9$ cm^{-3}, the temperature is expressed in K, and dT/dt in K s^{-1}.

It follows from the relation (5.15) and the Saha formula (3.21) for the electron number density that the boundary temperature is determined by the combination of parameters

$$\frac{1}{N_a}\frac{dT}{dt},$$

where N_a is the number density of the buffer gas atoms. Table 17 gives the values of the boundary temperature T_{eq} as a function of this product for plasma relaxation in argon and xenon. Comparing this temperature with a typical range of temperatures (2.10) for cluster growth (see Table 2), one can see that nucleation processes proceed in a nonequilibrium plasma.

Table 17. The boundary temperature T_{eq} of an equilibrium plasma for plasma relaxation in argon and xenon according to formula (5.15).

$\frac{1}{N_a}\frac{dT}{dt}$, K cm^3 s^{-1}		10^{-16}	10^{-15}	10^{-14}	10^{-13}	10^{-12}
T_{eq}, 10^3 K	Ar	4.8	5.2	5.6	6.0	6.5
	Xe	3.7	3.9	4.2	4.5	4.9

The above character of plasma relaxation takes place in the absence of clusters in the plasma. Attachment of electrons and ions to clusters leads to cluster charging and recombination of plasma electrons and ions according to the scheme (5.2). As a result, the number density of electrons and ions drops with the typical rate of this process following from formulas (3.11):

$$\frac{1}{\tau_{at}} = \frac{k_0 x N_b}{n^{1/3}}, \quad (5.18)$$

where x is the solution of equation (3.12) (see Table 5). When clusters are forming, attachment of electrons and ions to clusters proceeds fast (see Table 16 for the examples under consideration). Hence, the number density of electrons and ions in the region occupied by clusters drops sharply, and later it is determined by transport of a plasma from regions free from clusters.

Let ρ_0 be the radius of a region containing clusters, N_e' be the electron number density in this region, and N_e be the electron number density in other regions where clusters are absent. Because of this character of the equilibrium, we have the following balance equation for plasma transport and decay:

$$\rho_0^2\frac{N_e'}{\tau_a} \sim D_a N_e, \quad (5.19)$$

where D_a is the ambipolar diffusion coefficient of the plasma. Table 16 presents the number density of electrons and ions N_e' at the exit of the afterglow discharge tube in the case when this quantity is determined by transport of electrons and ions from plasma regions which are free from clusters for the examples under consideration.

5.6 Charging of clusters

When clusters are formed, attachment of electrons and ions to the cluster surface as a result of processes (5.2) governs the negative cluster charge. This charge is equal approximately to $Z = 0.08n^{1/3}$ for clusters of heat-resistant metals at $T = 1000$ K. Let us introduce a typical time τ_{rel} of decrease of the plasma density. The criterion for charging of clusters on the basis of processes (5.2) is such that the rate of electron thermoemission from the cluster surface varies faster than the number density of electrons. This gives

$$\frac{1}{\tau_{rel}} \ll \frac{dT}{dt}\frac{W}{T^2}, \quad (5.20)$$

where W is the metal work function, which coincides with the ionization potential of a large cluster. The right-hand side of this criterion is equal to 1×10^4 s^{-1} in the iridium case at the exit of the afterglow discharge tube ($T = 1200$ K), and 3×10^3 s^{-1} in the molybdenum case ($T = 2200$ K at the exit of the afterglow discharge tube). The rates of electron and ion attachment to clusters are significantly greater than the term in the right-hand side of this formula, and hence at the first stage of evolution of an afterglow plasma the processes (5.2) of plasma recombination and cluster charging become dominant. The cluster charge is given in Table 6 for this regime of cluster charging, which lasts a short time.

When the number density of electrons and ions drops significantly, i.e. $T > T_*$ (T_* is the temperature of the cluster neutrality, see Table 6), clusters get a positive charge. But because the number density of clusters is high and released electrons remain in the cluster region, this charge is small, so that clusters are practically neutral. Indeed, the equilibrium establishes in this case:

$$M_n \longleftrightarrow M_n^+ + e, \quad (5.21)$$

and the average cluster charge Z follows from the balance of rates of these processes. Then we have

$$Z = \frac{\nu_{em}}{N_{cl}k_e n^{2/3}}, \quad (5.22)$$

where $\nu_{em}(T)$ is the rate of electron thermoemission, N_{cl} is the number density of clusters, k_e is the reduced rate constant for electron collisions with a cluster ($k_e = 2.4 \times 10^{-8}$ cm^3 s^{-1} at $T = 2200$ K). We used the relation $N_e = ZN_{cl}$ for the electron number density, i.e. we neglected the transport of released electrons from the cluster-occupied region. In particular, in the molybdenum case at the exit of the afterglow discharge tube ($T = 2200$ K) we have near the flow axis $Z \sim 0.1$. The

Table 18. The neutrality temperature T_* and the rate of electron thermoemission for large iridium and molybdenum clusters.

N_e, cm^{-3}		10^8	10^9	10^{10}	10^{11}	10^{12}	10^{13}	10^{14}	10^{15}
Ir	T_*, 10^3 K	1.85	2.00	2.19	2.41	2.69	3.03	3.47	4.07
	$v_{em}/n^{2/3}$, s^{-1}	1.2	13	170	2.0×10^3	2.6×10^4	3.3×10^5	4.2×10^6	5.9×10^7
Mo	T_*, 10^3 K	1.59	1.71	1.86	2.04	2.25	2.51	2.84	3.26
	$v_{em}/n^{2/3}$, s^{-1}	0.059	0.68	8.1	96	1.2×10^3	1.5×10^4	1.9×10^5	2.5×10^6

rates $v_{em}(T)$ of electron thermoemission are given in Table 18 for iridium and molybdenum clusters together with the number densities of electrons which provide cluster neutrality at a temperature indicated.

The next stage of cluster charging is due to transport of electrons and ions to the cluster region. The relaxation time in this case is $\tau_{rel} \sim r_0^2/(6D_a) \sim 0.1$ s, and the criterion (5.20) is valid, but the time of establishment of the equilibrium (5.2) turns out to be large [this time equals $\sim 1/v_{em}(T)$ for a given temperature]. As a result, clusters are charged negatively, but their charge is less than that in the equilibrium case (5.2).

5.7 Processes in expanding afterglow plasma with clusters

At the last stage of plasma evolution, the central part of a plasma flow, which contains clusters, can be separated from the plasma flow, and this flow part sets off to a vacuum. Thereafter atoms of the buffer gas are extracted by pumping, and the beam of charged clusters is governed by external transverse and longitudinal electric fields. This is possible at small pressures of the buffer gas. At this stage, it is possible to give clusters an additional charge, if the cluster beam is crossed by an electron beam or passes through a region of a glow discharge. If the cluster charge is determined by processes (5.2), the charging currents I for the examples under consideration are given in Table 16. The mobility of charged clusters reduced to the normal density of argon atoms is determined by formula (5.4) and is shown in Table 13 at $T = 1000$ K. This is an excessive value, because the regime of cluster charging (5.2) is established partially, and we use it for estimates. On the basis of these values one can see that transport of charged clusters is negligible in a plasma flow and can be noticeable, when the gas pressure becomes small. Then the cluster beam can be focused and accelerated.

A cluster beam moving in a longitudinal electric field in the flux of a cluster plasma is dispersed as a result of collisions with atoms of the buffer gas. Let us introduce the typical angle θ of disassembly of a cluster beam in a buffer gas. We take it as

$$\theta = \frac{\Delta x}{wt} = \frac{\sqrt{2Dt}}{wt} ,$$

where $\Delta x^2 = 2Dt$ is the beam disassembly squared in a time t, the cluster drift velocity in an electric field of strength E is $w = KE$, and this formula gives

$$\theta = \frac{\Delta x}{wt} = \frac{2D}{EK\Delta x} . \qquad (5.23)$$

This deflection angle does not depend on the number density of atoms N_a and gas temperature T, and $\theta \sim n^{-1/3}$. Table 13 lists the values of this deflection angle in argon for $\Delta x = 0.5$ cm, and $E = 10$ V cm^{-1}. These values confirm the possibility to control a beam of charged clusters.

It is necessary to keep in mind that cluster charges set up high electric fields, which lead to additional dispersion of the cluster beam. Table 16 contains the charging currents I which provide the cluster charge under conditions of reactions (5.2). On separation of the cluster beam from a plasma, a noncompensated negative charge of $3 \times 10^{10}e$ cm^{-1} and $4 \times 10^9 e$ cm^{-1} arises for the iridium and molybdenum cases under consideration if the cluster beam moves with the sound speed of argon. This charge establishes large electric fields on the beam surface, which lead to its dispersion. Therefore, in reality a cluster charge proves to be lower than that during the charging regime (5.2)

Above we neglected the presence of halogen atoms in the plasma flow. Indeed, at high temperatures ($T > T_1$) the halogen atoms do not react with clusters, and at low temperatures these atoms are pumped after passing the nozzle. Nevertheless, the presence of halogen atoms and molecules in the plasma creates a technological problem and requires a special material for the walls and a careful purification of the buffer gas pumped. Interaction of clusters with electrons removes halogen atoms from the cluster surface in the form of negative ions. In addition, attachment of electrons to halogen atoms, if it proceeds effectively, produces a plasma consisting of positive and negative ions, which changes the character of cluster charging. Thus, the presence of halogen atoms in the plasma can influence the character of physical processes in it, which requires additional analysis.

When the afterglow plasma with clusters flows out of the nozzle and expands into the vacuum, atomic particles are scattered and pumped from the plasma stream, whereas collisions of clusters with atoms of the buffer gas do not create a noticeable transverse momentum for an individual cluster because of its large mass. Hence, buffer gas atoms are removed from the plasma flow as a result of their scattering. Pumping allows one to remove the atoms which move towards the walls. As a result, after a while the plasma stream is transformed into a beam of clusters. It is of importance in this method that clusters collect near the center of the discharge tube, which permits us to use only the central part of the plasma flow for generation of a cluster beam.

It follows from the above analysis that the plasma method of cluster generation provides a high-intensity cluster beam. Indeed, the maximum specific intensity of cluster flux is 80 μg (cm^2 s)$^{-1}$ [137, 138] for the standard method and silver clusters, whereas the cluster outward flux intensity G_M in the plasma method exceeds this value by two-three orders of magnitude (see Table 16). Chemical regeneration [31] is significant for this method since it provides a high number density of metal atoms. If they result from vaporization of the metal surface, the number density of atoms cannot exceed that at the saturation vapor pressure at the melting point (see Table 13), which leads to a low-intensity cluster beam. Nevertheless, such a method of producing metal atoms can be successfully employed because of its technological simpli-

city. In addition, the gathering of clusters near the flow axis simplifies the extraction of clusters from the plasma flow in this method, and the size of clusters is adjusted by the buffer gas pressure. Therefore, this method for generation of cluster beams of heat-resistant metals provides high yield parameters for the cluster beams.

Concluding, generation of a cluster beam from a plasma is determined by competition between several processes and is possible in a narrow range of plasma parameters. In particular, at the first stage of the process, on the one hand, plasma parameters on the flow axis must provide a fast decomposition of molecules with formation of metal atoms and, on the other hand, a fast nucleation of metal atoms must proceed in this region. The method under consideration allows us to concentrate clusters in the central part of the plasma flow, which increases the density of the resultant cluster beam and simplifies further extraction of clusters. Though the competition of various processes in a plasma means that this method requires a special analysis for each particular case, it can be used for generating cluster beams of various heat-resistant metals. Because all the atomic vapor in this method is transformed into clusters, this technique of generation of cluster beams can provide the same rate of deposition of atoms on targets as that in the case of beams of atoms or atomic ions. But, due to their large mass, charged clusters are more easily focussed and controlled than atomic ions. This means that the cluster technology of film deposition of heat-resistant metals has advantages over the employment of neutral atomic beams and atomic ion beams.

6. Conclusions

A cluster plasma is a specific physical object where clusters can grow and evaporate in a dense ionized gas. Though this plasma is found in local thermodynamic and ionization equilibria due to the weakness of transport processes, such a system is nonequilibrium with respect to processes of cluster growth and cluster evaporation. The processes of cluster growth are combined with the processes of charging of clusters and, depending on the conditions, this system may evolve in different ways. Cluster plasma can be used for light sources and for generation of cluster beams, which are applied for deposition and fabrication of nanostructure materials. In addition, generation of cluster beams may be employed for extraction of heat-resistant metals from their compounds. Therefore, a cluster plasma can form the basis of a high technology having to do with nanostructure materials.

The author thanks V P Kraĭnov for valuable discussions. This study was supported in part by RFBR grant #99-02-16094.

References

1. Reist P C *Introduction to Aerosol Science* (New York: Macmillan Publ. Comp., 1984)
2. Smirnov B M *Physics of Ionized Gases* (New York: Wiley, 2000)
3. Kaplan S A, Pikel'ner S B *Interstellar Medium* (Cambridge: Cambridge Univ. Press, 1982)
4. Tsytovich V N *Usp. Fiz. Nauk* **167** 57 (1997) [*Phys. Usp.* **40** 53 (1997)]
5. Morfill G E et al. *Phys. Plasma* **6** 1 (1999)
6. Tsytovich V N *Aust. J. Phys.* **51** 763 (1998)
7. Chu J H, Lin I *Phys. Rev. Lett.* **72** 4009 (1994)
8. Thomas H et al. *Phys. Rev. Lett.* **73** 652 (1994)
9. Hayashi Y, Tachibana K *Jpn. J. Appl. Phys.* **33** L804 (1994)
10. Melzer A, Trottenberg T, Piel A *Phys. Lett. A* **191** 301 (1994)
11. Trottenberg T, Melzer A, Piel A *Plasma Sources Sci. Technol.* **4** 450 (1995)
12. Morfill G E, Thomas H *J. Vac. Sci. Technol. A* **14** 490 (1996)
13. Fortov V E et al. *Pis'ma Zh. Eksp. Teor. Fiz.* **63** 176 (1996) [*JETP Lett.* **63** 187 (1996)]
14. Fortov V E et al. *Pis'ma Zh. Eksp. Teor. Fiz.* **64** 86 (1996) [*JETP Lett.* **64** 92 (1996)]
15. Nefedov A P, Petrov O F, Fortov V E *Usp. Fiz. Nauk* **167** 1215 (1997) [*Phys. Usp.* **40** 1163 (1997)]
16. Ishimaru K *Phys. Rep.* **34** 1 (1982)
17. Fortov V E, Yakubov I T *Neideal'naya Plazma* (Nonideal Plasma) (Moscow: Energoatomizdat, 1994)
18. Smirnov B M *Usp. Fiz. Nauk* **167** 1169 (1997) [*Phys. Usp.* **40** 1117 (1997)]
19. Smirnov B M *Usp. Fiz. Nauk* **164** 665 (1994) [*Phys. Usp.* **37** 621 (1994)]
20. Smirnov B M *Plasma Chem. Plasma Process.* **13** 673 (1993)
21. Lide D R (Ed.) *Handbook of Chemistry and Physics* 79th ed. (London: CRC Press, 1998 – 1999)
22. Echt O, Sattler K, Recknagel E *Phys. Rev. Lett.* **47** 1121 (1981)
23. Knight W D et al. *Phys. Rev. Lett.* **52** 2141 (1984)
24. Harris I A, Kidwell R S, Northby J A *Phys. Rev. Lett.* **53** 2390 (1984)
25. Zel'dovich Ya B *Zh. Eksp. Teor. Fiz.* **12** 525 (1942)
26. Frenkel Ja I *Kinetic Theory of Liquids* (Oxford: Oxford University Press, 1946)
27. Abraham F F *Homogeneous Nucleation Theory* (New York: Academic Press, 1974)
28. Landau L D, Lifshitz E M *Statisticheskaya Fizika* Vol. 2 (Statistical Physics) (Moscow: Nauka, 1978) [Translated into English (Oxford: Pergamon Press, 1980)
29. Martin T P et al. *J. Chem. Phys.* **100** 2322 (1994)
30. Martin T P *Phys. Rep.* **273** 199 (1996)
31. Weber B, Scholl R *J. Illum. Eng. Soc.* (Summer) 93 (1992)
32. Scholl R, Weber B, in *Physics and Chemistry of Finite Systems: from Clusters to Crystals* Vol. 2 (Eds P Jena, S N Khana, B K Rao) (Dordrecht: Kluwer Academic Publ., 1992) p. 1275
33. Weber B, Scholl R *J. Appl. Phys.* **74** 607 (1993)
34. Scholl R, Natour G, in *Phenomena in Ionized Gases* (Eds K H Becker, W E Carr, E E Kunhardt) (Woodbury: AIP Press, 1996) p. 373
35. Smirnov B M *Phys. Scripta* **58** 363 (1998)
36. Chapman S, Cowling T G *The Mathematical Theory of Non-Uniform Gases* (Cambridge: Cambridge Univ. Press, 1952)
37. Ferziger J H, Kaper H G *Mathematical Theory of Transport Processes in Gases* (Amsterdam: North-Holland, 1972)
38. Landau L D, Lifshitz E M *Elektrodinamika Sploshnykh Sred* (Electrodynamics of Continuous Media) (Moscow: Nauka, 1982) [Translated into English (Oxford: Pergamon Press, 1984)]
39. Ding A, Hesslich J *Chem. Phys. Lett.* **94** 54 (1983)
40. Echt O et al. *Phys. Rev. A* **38** 3286 (1988)
41. Schreier P, Märk T D *J. Chem. Phys.* **87** 1456 (1987)
42. Schreier P, Stamatovic A, Märk T D *J. Chem. Phys.* **89** 2956 (1988)
43. Lezius M et al. *J. Chem. Phys.* **91** 3240 (1989)
44. Smirnov B M, in *Proc. 12 Symp. Application of Plasma Processes* (Eds J D Skalny, M Cernak) (Slovakia: Liptovsky Jan, 1999) p. 45
45. Smirnov B M *Clusters and Small Particles in Gases and Plasmas* (New York: Springer-Verlag, 2000)
46. Langevin P *Ann. Chem. Phys.* **8** 245 (1905)
47. Landau L D, Lifshitz E M *Mekhanika* (Mechanics) (Moscow: Nauka, 1973) [Translated into English (Oxford: Pergamon Press, 1980)]
48. Smirnov B M, in *Atomic Physics with Heavy Ions* (Eds H F Beyer, V P Shevelko) (Berlin: Springer-Verlag, 1999)
49. Landau L D, Lifshitz E M *Statisticheskaya Fizika* Vol. 1 (Statistical Physics) (Moscow: Nauka, 1976) [Translated into English (Oxford: Pergamon Press, 1980)]
50. Cini M *J. Catalysis* **37** 187 (1975)
51. Beck D E *Solid State Commun.* **49** 381 (1984)
52. Perdew J P *Phys. Rev. B* **37** 6175 (1988)
53. Makov G, Nitzan A, Brus L E *J. Chem. Phys.* **88** 5076 (1988)
54. Smith J M *Am. Inst. Aeronaut. Astronaut. J.* **3** 648 (1965)
55. Wood D M *Phys. Rev. Lett.* **46** 749 (1981)
56. Van Staveren M P J et al. *Phys. Rev. B* **35** 7749 (1987)

57. Bréchignac C et al. *J. Chem. Soc. Faraday Trans.* **86** 2525 (1990)
58. Leopold D G, Ho J H, Lineberger W C *J. Chem. Phys.* **86** 1715 (1987)
59. Ganteför G et al. *Faraday Discuss. Chem. Soc.* **86** 197 (1988)
60. Gausa M et al. *Int. J. Mass Spectrom. Ion Proc.* **102** 227 (1990)
61. Seidl M, Meiwes-Broer K H, Brack M *J. Chem. Phys.* **95** 1295 (1991)
62. Cobine J D *Gaseous Conductors* (New York: Dover, 1958)
63. Weidele H *Verzögerte Electronenemission Negativ Geladener Wolframcluster* (Konstanz: Hartung-Gorre Verlag, 1995)
64. Weidele H et al. *Chem. Phys. Lett.* **237** 425 (1995)
65. Cheshnovsky O et al. *Chem. Phys. Lett.* **138** 119 (1987)
66. Pettiette C L et al. *J. Chem. Phys.* **88** 5377 (1988)
67. Taylor K J et al. *Chem. Phys. Lett.* **152** 347 (1988)
68. Ganteför G et al. *Z. Phys. D* **12** 405 (1989)
69. Ganteför G et al. *J. Chem. Soc. Faraday Trans.* **86** 2483 (1990)
70. Smoluchowski M V *Z. Phys.* **17** 585 (1916)
71. Smirnov B M *Usp. Fiz. Nauk* **149** 177 (1986) [*Sov. Phys. Usp.* **29** 481 (1986)]
72. Smirnov B M *Phys. Rep.* **188** 1 (1990); *Fizika Fraktal'nykh Klasterov* (Physics of Fractal Clusters) (Moscow: Nauka, 1991)
73. Green H L, Lane W R *Particulate Clouds: Dust, Smokes and Mists* (Princeton: Van Nostrand, 1964)
74. Rao B K, Smirnov B M *Phys. Scripta* **56** 588 (1997)
75. Biberman L M, Vorob'ev V S, Yakubov I T *Kinetika Neravnovesnoĭ Nizkotemperaturnoĭ Plazmy* (Kinetics of Nonequilibrium Low-Temperature Plasmas) (Moscow: Nauka, 1982) [Translated into English (New York: Cons. Bureau, 1987)]
76. Smirnov B M *Teplofiz. Vys. Temp.* **24** 239 (1986) [*High Temp.* **24** 176 (1986)]
77. Gilardini A L *Low-Electron Collisions in Gases* (New York: Wiley, 1972)
78. Huxley L G, Crompton R W *The Diffusion and Drift of Electrons in Gases* (New York: Wiley, 1974)
79. Smirnov B M *Physics of Weakly Ionized Gases* (Moscow: Mir Publ., 1981)
80. Smirnov B M, Smirnov M B *Phys. Scripta* **56** 302 (1997)
81. Hoyaux M F *Arc Physics* (New York: Springer-Verlag, 1968)
82. Neuman W *The Mechanism of the Thermoemitting Arc Cathode* (Berlin: Academic-Verlag, 1987)
83. Eletskiĭ A V, Smirnov B M *Usp. Fiz. Nauk* **166** 1197 (1996) [*Phys. Usp.* **39** 1137 (1996)]
84. Vargaftik N B *Tablitsy po Teplofizicheskim Svoĭstvam Zhidkosteĭ i Gazov* (Tables of Thermophysical Properties of Liquids and Gases) (Moscow: Nauka, 1972) [Translated into English (New York: Halsted Press, 1975)]
85. Asinovskiĭ É I, Kirillin A V, Nizovskiĭ V L *Stabil'nye Elektricheskie Dugi i Ikh Primenenie v Teplofizicheskom Eksperimente* (Stabilized Electric Arcs and Their Application in Thermophysical Experiment) (Moscow: Nauka, 1992)
86. Alexander M L et al. *Phys. Rev. Lett.* **57** 976 (1986)
87. Bréchignac C et al. *Phys. Rev. Lett.* **70** 2036 (1993)
88. Bréchignac C et al. *Chem. Phys. Lett.* **164** 433 (1989)
89. Bréchignac C et al. *Phys. Rev. Lett.* **68** 3916 (1992)
90. Tiggesbumker J et al. *Chem. Phys. Lett.* **190** 42 (1992)
91. Haberland H et al. *Phys. Rev. Lett.* **69** 3212 (1992)
92. Haberland H et al. *Z. Phys. D* **26** 8 (1993)
93. Hövel H et al. *Phys. Rev. B* **48** 18178 (1993)
94. Ellert C et al. *Phys. Rev. Lett.* **75** 1731 (1995)
95. Haberland H, von Issendorff B *Phys. Rev. Lett.* **76** 1445 (1996)
96. Ellert C et al. *Z. Phys. D* **39** 317 (1997)
97. Klein-Wiele J-H, Simon P, Rubahn H-G *Phys. Rev. Lett.* **80** 45 (1998)
98. Schmidt M, Haberland H *Eur. Phys. J. D* **6** 109 (1999)
99. Mie G *Ann. Phys.* (Leipzig) **25** 377 (1908)
100. Born M, Wolf E *Principles of Optics* (Oxford: Pergamon Press, 1964)
101. Bohren C F, Huffman D R *Absorption and Scattering of Light by Small Particles* (New York: Wiley, 1983)
102. Ekardt W *Phys. Rev. B* **31** 6360 (1985)
103. Kresin V *Phys. Rev. B* **38** 3741 (1988); **39** 3042 (1989); **40** 12507 (1989); **42** 3247 (1990)
104. Kresin V *Phys. Rep.* **220** 1 (1992)
105. Kreibig U, Genzel L *Surf. Sci.* **156** 678 (1985)
106. Yannouleas C et al. *Phys. Rev. Lett.* **63** 255 (1989)
107. Serra L et al. *Phys. Rev. B* **39** 8247 (1989)
108. Bonacic-Kountecky V, Fantucci P, Kountecky J *J. Chem. Phys.* **93** 3802 (1990)
109. Ekardt W, Penzar Z *Phys. Rev. B* **43** 1322 (1991)
110. Selby K et al. *Z. Phys. D* **19** 41 (1991)
111. Kresin V, Volmer M *Optical Properties of Metallic Clusters* (Berlin: Springer-Verlag, 1995)
112. Fomichev S V, Zaretsky D F *J. Phys. B* **32** 5083 (1999)
113. Smirnov B M, Weidele H *Zh. Eksp. Teor. Fiz.* **116** 1903 (1999) [*JETP* **89** 1030 (1999)]
114. Frenzel U et al. *Surf. Rev. Lett.* **3** 505 (1996)
115. Frenzel U et al. *Z. Phys. D* **40** 108 (1997)
116. Frenzel U *Schwarzkörperstrahlung von Metallclustern* (Konstanz: Hartung-Gorre Verlag, 1996)
117. Smirnov B M, Weidele H *Pis'ma Zh. Eksp. Teor. Fiz.* **69** 453 (1999) [*JETP Lett.* **69** 490 (1999)]
118. Smirnov B M, in *Physics of Clusters* (Eds V D Lakhno, G N Chuev) (Singapore: World Scientific, 1998) p. 56
119. Smirnov B M *Phys. Scripta* **53** 608 (1996)
120. Smirnov B M *Phys. Scripta* **51** 380 (1995)
121. Begemann W et al. *Z. Phys. D* **3** 183 (1986)
122. Ganteför G et al. *Z. Phys. D* **9** 253 (1988)
123. Lutz H O, Meiwes-Broer K H *Nucl. Instrum. Methods Phys. Res. B* **59** 395 (1991)
124. Barlak T M et al. *J.Phys. Chem.* **85** 3840 (1981)
125. Barlak T M et al. *J. Am. Phys. Soc.* **104** 1212 (1982)
126. Ens W, Beavis R, Standing K G *Phys. Rev. Lett.* **50** 27 (1983)
127. Martin T P *Phys. Rep.* **95** 167 (1983)
128. Martin T P *Ber. Bunsenges. Phys. Chem.* **88** 300 (1984)
129. Fayet P, Woste J *Z. Phys. D* **3** 177 (1986)
130. Begemann W et al. *Z. Phys. D* **12** 229 (1989)
131. Hagena O F, in *Molecular Beams and Low Density Gas Dynamics* (Ed. P P Wegener) (New York: Dekker, 1974) p. 93
132. Takagi T *Pure Appl. Chem.* **60** 781 (1988)
133. Becker E W *Laser Part. Beams* **7** 743 (1989)
134. Hagena O F *Rev. Sci. Instrum.* **36** 2374 (1992)
135. Takagi T *J. Vac. Sci. Technol. A* **2** 382 (1984)
136. Gspann J, in *Physics and Chemistry of Finite Systems: From Clusters to Crystals* Vol. 2 (Eds P Jena, R K Rao, S N Khanna) (Dordrecht: Kluwer Acad. Publ., 1992) p. 1115
137. Hagena O F, Knop G, Ries R *KfK Nachr.* **23** 136 (1991)
138. Hagena O F, Knop G, Linker G, in *Physics and Chemistry of Finite Systems: From Clusters to Crystals* Vol. 2 (Eds P Jena, B K Rao, S N Khanna) (Dordrecht: Kluwer Acad. Publ., 1992) p.1233
139. Henkes P R W, Klingelhofer R *J. Phys.* (Paris) **50** 159 (1989)
140. Henkes P R W, Klingelhofer R *Vacuum* **39** 541 (1989)
141. Gspann J *Z. Phys. D* **26** 174 (1993)
142. Hagena O F *Surf. Sci.* **106** 101 (1981)
143. Hagena O F, Knop G, in *Proc. 18th RGD Symposium* (Vancouver, Canada, 1992)
144. Hagena O F *Z. Phys. D* **4** 291 (1987)
145. Hagena O F *Z. Phys. D* **17** 157 (1990)
146. Hagena O F *Z. Phys. D* **20** 425 (1991)
147. Hagena O F, Obert W *J. Chem. Phys.* **56** 1793 (1972)
148. Gspann J *Z. Phys. D* **3** 143 (1986)
149. Gspann J *Z. Phys. D* **20** 421 (1991)
150. Sattler K, Muhlbach J, Recknagel E *Phys. Rev. Lett.* **45** 821 (1980)
151. Kappes M M, Kunz R W, Schumacher E *Chem. Phys. Lett.* **91** 413 (1982)
152. Knight W D et al. *Phys. Rev. Lett.* **52** 2141 (1984)
153. Martin T P *J. Chem. Phys.* **81** 4426 (1984)
154. Castleman A W, Keesee R G *Z. Phys. D* **3** 167 (1986)
155. Smalley R E *Laser Chem.* **2** 167 (1983)
156. Hopkins J P et al. *J. Chem. Phys.* **78** 1627 (1984)
157. Liu Y et al. *J. Chem. Phys.* **85** 7434 (1986)
158. Milani P, de Heer W A *Rev. Sci. Instrum.* **61** 1835 (1990)
159. Cheshnovsky O et al. *Chem. Phys. Lett.* **139** 233 (1987); *Rev. Sci. Instrum.* **58** 2131 (1987)
160. Haberland H et al. *J. Vac. Sci. Technol. A* **10** 3266 (1992)
161. Haberland H et al. *Mater. Sci. Engin. B* **19** 31 (1993)
162. Haberland H et al. *J. Vac. Sci. Technol. A* **12** 2925 (1994)
163. Haberland H et al. *Surf. Rev. Lett.* **9** 887 (1993)

164. Mesyats G A *Ektony* (Ectons) (Ekaterinburg: Nauka, 1993)
165. Mesyats G A *Usp. Fiz. Nauk* **166** 601 (1995) [*Phys. Usp.* **38** 567 (1995)]
166. Balnc G et al. *J. Chem. Phys.* **192** 680 (1995)
167. Nowak C et al. *J. Electron Spectrosc. Relat. Phenom.* **101 – 103** 199 (1999)
168. Beuler R, Friedman L *Chem. Rev.* **86** 521 (1986)
169. Matthew M W et al. *J. Phys. Chem.* **90** 3152 (1986)
170. Beuler R J, Friedlander G, Friedman L *Phys. Rev. Lett.* **63** 1289 (1989)
171. Leonas V B *Usp. Fiz. Nauk* **160** (11) 135 (1990) [*Sov. Phys. Usp.* **33** 956 (1990)]
172. Beuler R J et al. *Phys. Rev. Lett.* **67** 473 (1991)
173. Gleiter H *Nanostruct. Mater.* **6** 3 (1995)
174. Takagi T *Cluster Beam Deposition and Epitaxy* (Parker Ridge, N.J.: Noyes Publications, 1988)
175. Perez A et al. *J. Phys. D* **30** 709 (1997)
176. Perlarin M et al. *Chem. Phys. Lett.* **277** 96 (1997)
177. Melinon P et al. *J. Chem. Phys.* **107** 10278 (1997)
178. Palpant B et al. *Phys. Rev. B* **57** 1963 (1998)
179. Ray C et al. *Phys. Rev. Lett.* **80** 5365 (1998)
180. Smirnov B M *Pis'ma Zh. Eksp. Teor. Fiz.* **68** 741 (1998) [*JETP Lett.* **68** 779 (1998)]
181. Smirnov B M *J. Phys. B* **33** 115 (2000)
182. Landau L D, Lifshitz E M *Gidrodinamika* (Fluid Mechanics) (Moscow: Nauka, (1988) [Translated into English (Oxford: Pergamon Press, 1986)]
183. Krainov V P *Qualitative Methods in Physical Kinetics and Gasdynamics* (New York: American Institute of Physics, 1992)
184. Smirnov B M *Plasma Chem. Plasma Process.* **12** 177 (1992)
185. Smirnov B M *Teplofiz. Vys. Temp.* **29** 418 (1991) [*High Temp.* **29** 318 (1991)]